LOW NOISE DISTRIBUTED AMPLIFIERS IN BROADBAND COMMUNICATION SYSTEMS

A Dissertation

Presented to the Faculty of the Graduate School

of Cornell University

In Partial Fulfillment of the Requirements for the Degree of

Doctor of Philosophy

by

Anthony Kopa

January 2011

LOW NOISE DISTRIBUTED AMPLIFIERS IN BROADBAND COMMUNICATION SYSTEMS

Anthony Kopa, Ph. D.

Cornell University 2011

Distributed amplifiers have long been utilized to extract useful gain from an active device technology over extreme bandwidths. The distributed topology is well suited to delivering gain over larger bandwidths than other circuit techniques by breaking the gain-bandwidth tradeoff and replacing it with a gain-delay tradeoff. For bandwidths approaching the transition frequency (f_T) of the active device technology employed, the distributed amplifier has lower noise figure than alternative techniques. This dissertation explores the region of the design space where distributed amplifiers are the best choice and reveals several new techniques for achieving improved noise and gain compared with conventional distributed techniques. The blue-noise active termination (BNAT) is a hybrid active-passive low-noise termination uniquely tailored to exploit the bi-directional propagation characteristic of the distributed amplifier to remove the effect of one of the amplifier's primary noise sources. This results in significant improvement in low frequency noise figure. Also, π–type filter sections are shown to be superior to conventional T-type sections as the building blocks of monolithically integrated distributed amplifiers. π–type sections give higher gain and lower noise in less area for the same bandwidth than would be possible using T-type sections. Finally, enhancement of the distributed amplifier's dispersion characteristic is demonstrated which opens the door for applications as a dispersive delay line in analog signal processing and time-domain communication schemes.

BIOGRAPHICAL SKETCH

Anthony Kopa was born in Honesdale, PA in 1982 and soon after moved to Fort Pierce, FL where he grew up. He began his college education at Indian River Community College in 1999, graduating with an AA in 2001 and gaining admission to the University of Florida. There he studied electrical engineering and worked in the Biomedical MEMS Research Lab under Dr. Huikai Xie, graduating with a BS *summa cum laude* in 2003, and MS in 2004.

He was admitted to Cornell University and joined the Apsel Lab, under the advisement of Dr. Alyssa B. Apsel, in 2004. There he explored many topics including optoelectronic receivers, integrated microwave photonics, and ultimately broadband distributed amplification culminating in this dissertation. In 2008, he was honored as an *Analog Devices Outstanding Student Designer*.

Anthony is now with Raytheon Integrated Defense Systems in Andover, MA where he works on reconfigurable, adaptable, and heterogeneous RFIC and MMIC technologies.

In loving memory of my mother

ACKNOWLEDGMENTS

I owe my deepest gratitude to the most influential teachers in my life: my parents for supporting and encouraging me at every step and my advisor Alyssa for being a guide, role model, and source of motivation and wisdom on this long journey.

I'm thankful for the many other teachers who have shaped my life – Dr. Xie, for giving me my first opportunity at research and design; Dr. Srivastava, for letting me teach his class; Dr. Ramaswamy, for guidance and wisdom; Dr. Zheng, for sparking my interest in electromagnetism; and Anand Pappu and Zhongtao Fu, my big brothers, for generously sharing all they learned ahead of me.

It has been a pleasure to work with Bo Xiang, thank you for being a great research partner, and all my other labmates for helping me see problems from so many different perspectives, teaching me so much about the wider world, and never actually needing to learn to configure Cadence.

My friends have shaped my life outside the classroom and laboratory and I would never have made it this far without you all. My sister, Marisa, you are my oldest friend and I love you very much. "The crew:" Andy, Ryan, Matt, Matt, Dennis, Marie, Sarah, Ania, Julia, Jenny, and so many more - Fridays haven't been the same without you. Barbara, I learned so much about myself and the world with you.

TABLE OF CONTENTS

LIST OF FIGURES

LIST OF TABLES

Chapter 1

Broadband Amplifier Overview

The low noise amplifier (LNA) is a critical element in virtually all communication systems, as it serves the dual role of amplifying small received signals up to useful levels as well as easing the noise requirements of other circuits and signal processing down the receiver chain [1]. As with all interesting engineering problems, there are tradeoffs when attempting to achieve several performance metrics simultaneously. With the emergence of broadband communication systems including ultra-wideband (UWB) [2] and software-define radio (SDR) [15], noise and bandwidth in particular are in direct contention making the development and maturation of broadband LNAs challenging. In the most strict and fundamental definition, a broadband LNA must have broadband impedance matching, broadband gain, and low noise. Of course, "broad" bandwidth and "low" noise are relative to the application. In addition there are other critical performance metrics for an amplifier such as linearity, power consumption, and power efficiency. All such performance metrics must be considered in the context of a complete system, but this work will deal primarily with noise and bandwidth improvement techniques at the circuit level.

There is a growing portion of the LNA design space where the designer is forced to choose the distributed amplifier (DA) topology to simultaneously achieve high bandwidth and low noise characteristics. This is because the DA is uniquely able to overcome gain and bandwidth tradeoffs inherent to all other amplifiers, while maintaining low noise levels [1]. The critical role of the LNA in communication

systems motivates finding a deeper understanding of the potentials and limitations of the DA.

1.1 Introduction to the Distributed Amplifier

The DA was first introduced in a patent by William S. Percival in 1936 and was first published by Ginzton, et al. in 1948 [7]. The original implementation was with vacuum tubes, but the topology has subsequently been monolithically integrated using III-V FETs [8][9], silicon bipolar transistors, and finally in CMOS [10] as each technology has matured. The DA is uniquely capable of achieving higher bandwidth than other amplifier topologies because its fundamental limitation is gain-delay tradeoff rather than the more common gain-bandwidth tradeoff. In this section, I will introduce the fundamentals of DA operation and explain how and why it is capable of achieving such high bandwidths compared to alternative circuits.

1.1.1 How does it work?

Fundamentally, a distributed amplifier is a traveling wave circuit. Like ripples traveling across the surface of a pond, an electrical signal applied to a DA takes a long time (compared to the fundamental frequency components of the signal) to propagate through the circuit. As this signal propagates through the circuit, it is periodically sensed by active gain elements. The outputs of those several gain elements are added up with the appropriate phase relation to make an amplified copy of the original signal. Figure 1.1 is one example of a distributed amplifier formed by two *LC* ladders, also known as artificial transmission lines, and FETs. The inductors are shown explicitly in the schematic and the capacitors are the parasitic capacitances associated with the FETs. The *LC* ladder serves several purposes, but the most important is to

establish a roughly lossless path for signals to propagate from one transistor to the next. Let us follow the signal through the circuit to understand how it works.

Assume some small signal disturbance at the input of the circuit. The input signal takes some time to reach the first FET gate, more time to reach the second FET gate, and so on until it is absorbed in the termination resistor at the end of the input line. Each FET will produce a current at its drain proportional to the input signal. That drain current is divided evenly, half traveling along the output line to the left and half travelling to the right. The portions traveling to the left are absorbed in the termination resistor at the beginning of the output line, so we will ignore these. If the delay from drain to drain is the same as the delay from gate to gate, the portions travelling to the right will add up in-phase and leave the amplifier through the output port. Since the current contribution from each transistor *adds* to the total, this amplifier can provide gain even if each individual transistor is only providing a gain less than unity. This is

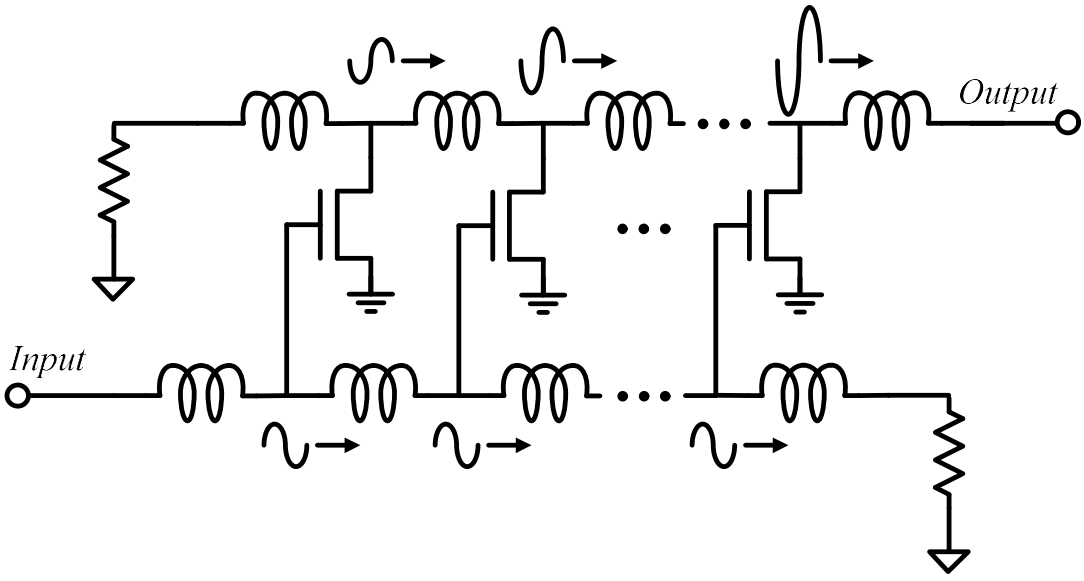

Figure 1.1 Basic distributed amplifier. Input and output signal traveling at the same rate from left to right experience additive gain from the several gain cells.

distinctly different from the case of a cascade of amplifiers, where *multiplying* gains less than unity results in tremendous loss. The power gain, G, can be roughly approximated by

$$G = \left(\frac{1}{2} g_m R_L N \right)^2 \tag{1.1}$$

where g_m is the transconductance of each individual transistor, R_L is the load resistance, and N is the number of transistors in the amplifier [7]. If all these elements are truly lossless, then this structure can be repeated indefinitely (infinite N), trading more delay for more gain, with an arbitrarily high bandwidth.

Naturally, none of the elements of this circuit can be truly lossless. Loss from the inductors, gate resistance, non-quasi-static effects, and output conductance all contribute significant loss to the propagating signals. In contrast to the additive gain, the loss is multiplicative. Each additional section dissipates the same percentage of power [7]. This means that loss has an exponential growth with increasing N. At some point, extending the structure by one more unit cell (a transistor and associated inductors) will introduce more multiplicative loss than additive gain. This point is the optimum length of the DA, where either increasing or decreasing its size will give lower gain. What is so special about this arrangement compared to other broadband circuit topologies is that the high frequency performance is limited solely by second-order effects like *loss* in the active and passive elements and not by the *capacitance* of the transistors used. Thus the performance of a DA is determined more by the quality of the passive devices and interconnects than by the feature size or material system of the transistors.

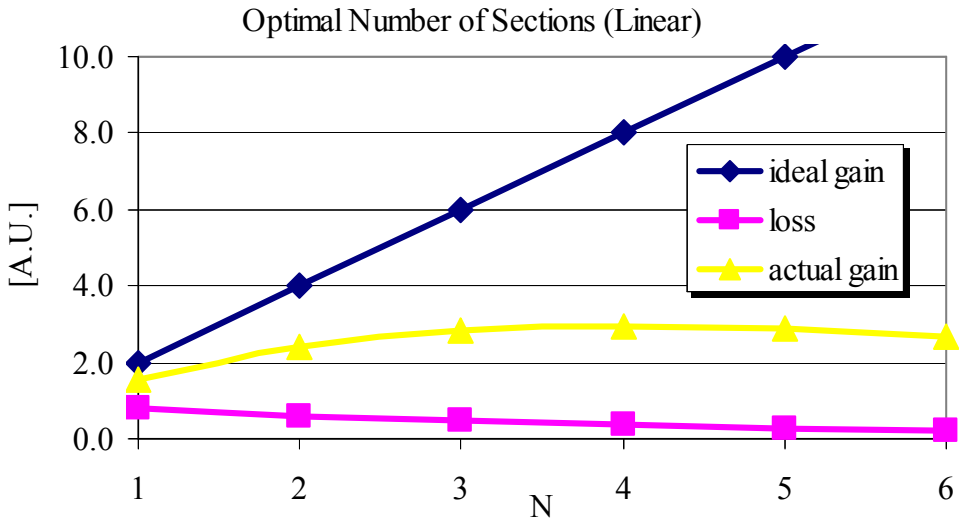

(a)

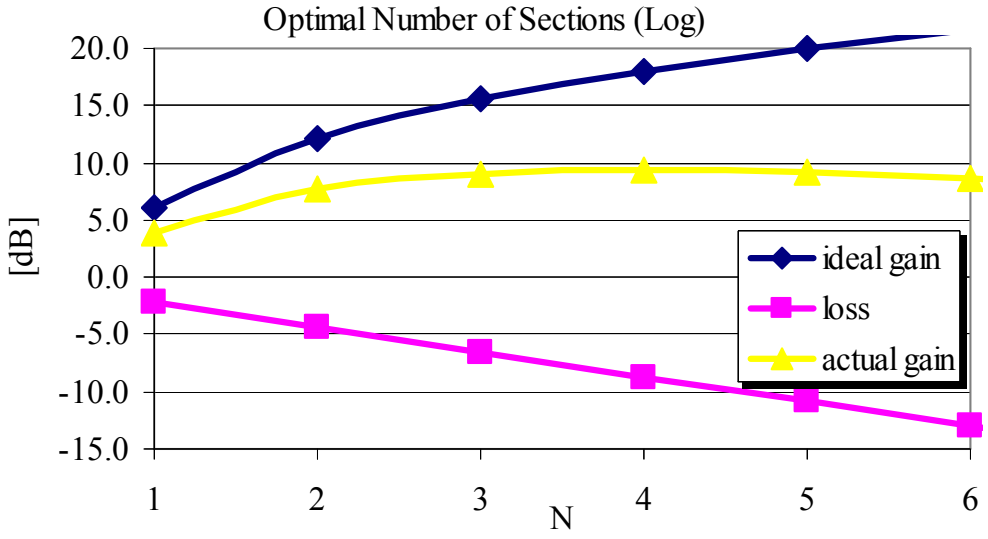

(b)

Figure 1.2 Example illustrating the optimal number of sections, *N*, for a typical DA. Clearly, (a) gain grows linearly with *N* and (b) loss grows exponentially with *N*. *N*=4 is the optimum in this example.

1.1.2 Why CMOS?

The DA is primarily selected for amplifiers operating at microwave frequencies and above, while CMOS technology has only recently produced MOSFETs capable of operating in that range. Thus for most of their respective history's CMOS and distributed amplifiers were incompatible. Figure 1.3 shows f_T and minimum noise figure, the critical metrics for a microwave transistor, for various CMOS technology nodes. It has been a long climb for CMOS, from digital baseband circuits, to low/medium frequency analog circuits, and finally to RF and microwave circuits. The circuit level similarity between all field effect transistors - whether JFET, MESFET, HEMT, MOSFET, or otherwise – allowed quick translation of standard microwave circuits into silicon as CMOS feature sizes decreased and f_T's increased. Achieving satisfactory transistor quality is only half of the battle of high frequency design, with passive devices being of equal importance. The fundamental difference between passive device design in Si and traditional materials such as GaAs is that GaAs is an excellent dielectric while Si is relatively lossy. This limits silicon passives to the thin metal stack encased in SiO_2 above the substrate, while GaAs processes allow for much thicker metals and lower capacitance by using the full thickness of the substrate as an insulator/dielectric. This is not all bad for Si though, as the forced small form factors are complementary to the desire for smaller area circuits.

1.1.3 CMOS Distributed Amplifiers

The research and innovations presented in this dissertation are not targeted at any particular application; rather they are topological improvements to the DA as it could be used in many applications or processes. However, it is still valuable to take a brief look at the state of the art of CMOS distributed amplifiers to know how and why my

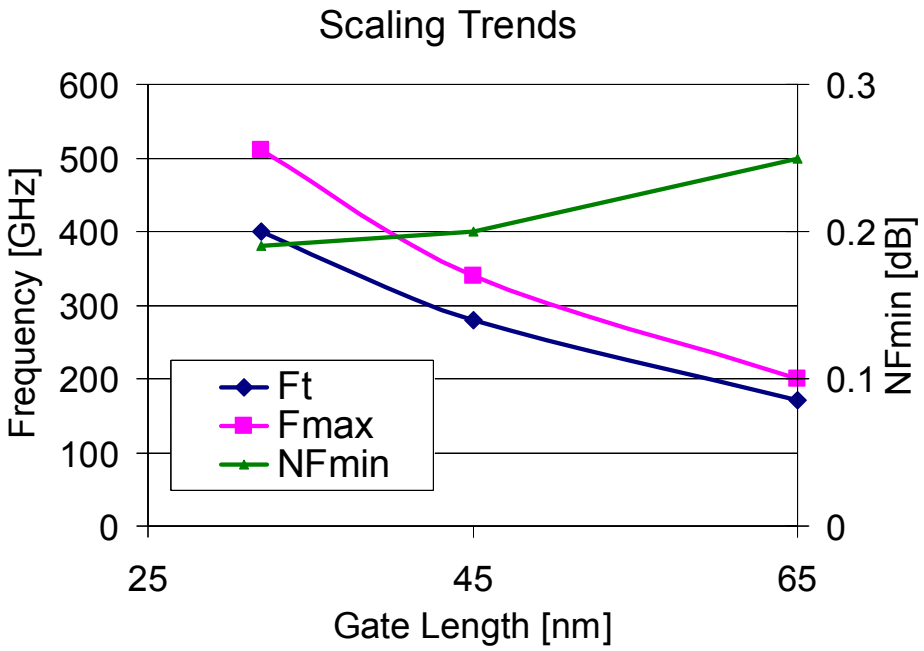

Figure 1.3 Effect of Scaling on RF properties of CMOS, from ITRS 2007 [11].

research will benefit present and future systems. Gain-bandwidth, noise, and area are all driving factors within the research community.

As mentioned above, the gain-delay tradeoff of the DA allows gain-bandwidth products (GBP) far in excess of other circuit topologies. Designers have invented further modifications to the DA to take this advantage to another level. Top numbers to date in CMOS include 120GHz GBP following a fairly standard circuit design, but using a high quality 120nm SOI process [12]. Introducing cascaded amplifiers inside each gain cell [13] has produced GBP of 394GHz in 180nm CMOS. Internal feedback, leveraging the bi-direction nature of the DA [14] has shown the best performance ever in Si, with a GBP of 660GHz in 90nm. These all demonstrate the power of the DA to far exceed the f_T of its process.

With maturation of UWB radio, DAs covering the 3.1-10.6GHz range have become increasingly prevalent in the literature, with hundreds of publications in just

the past few years. Of particular note are examples using innovative inductor structures to reduce area such as mutual inductance coupling [6] and multilayer spirals [21]. These developments illustrate the critical role area plays in a technology's viability.

A general understanding of the noise properties of the DA was sufficient for many, many years, as the DA faced little competition from other circuits in the same bandwidth range. After the scaling of recent years, we now have several circuit topologies capable of covering the UWB band and designers are motivated to search for every last scrap of performance from their circuits, as well as to better understand when to choose one approach over another. This has spurred much more theoretical attention to the noise of the DA, with researchers seeking to expand upon the seminal treatment in [22]. Of particular note are two new analytical techniques, one more conventional but insightful [3] and a more radical approach which treats the DA as an FIR filter [6]. Still others have sought to target and systematically remove dominant noise sources altogether [4],[5].

1.2 Broadband Low Noise Amplifiers

We can understand the need specifically for the DA by comparing it to alternative circuits. Choosing a circuit topology for an application is a complicated balancing act,

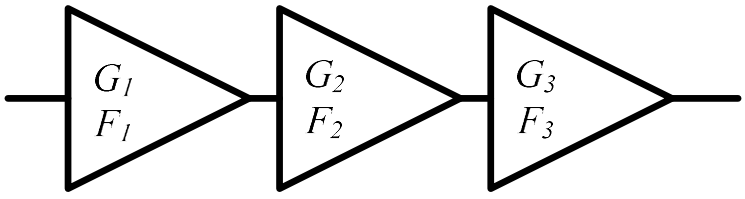

Figure 1.4 Cascade of three amplifiers (or other RF elements) characterized by a gain, G_x, and a noise figure, F_x.

relating several specifications and tradeoffs. I do not seek to provide a comprehensive method of selecting one LNA over another, but do wish to establish a portion of the design space where DAs are common or even requisite.

1.2.1 Why use an LNA?

The basic requirement of an LNA is that it provide matching, gain, and low noise over a given bandwidth. Matching is not strictly required, but the LNA is generally the first component in a receiver chain and bears the burden of interacting with the feed line and thus should be impedance matched to the feed line. Gain, perhaps obviously, amplifies the incoming signal, but why do we need the amplification? And how low is "low noise"?

Friis' Formula [23] is an expression which quantifies the total noise figure of a cascade of elements as shown in Figure 1.4. The r^{th} element in the chain is characterized by a gain, G_r, and a noise figure, F_r. The total noise figure for the chain is then

$$F = F_1 + \frac{F_2 - 1}{G_1} + \frac{F_3 - 1}{G_1 G_2} + \cdots . \tag{1.2}$$

Clearly, if G_1 is made large, then the total noise is dominated by F_1, the noise of the first element. In this way, the LNA's gain and noise figure together determine the overall noise of the system. The system level noise requirement translates almost directly to the LNA noise requirement, unless there is a particularly noisy or lossy element downstream.

Beyond its effect of masking the noise of the rest of the system, the gain of the LNA is needed simply to amplify the received signal. This may seem somewhat obvious to anyone familiar with analog receivers, but the issue remains even as receiver architectures become more and more digital. Consider an idealized, Mitola-

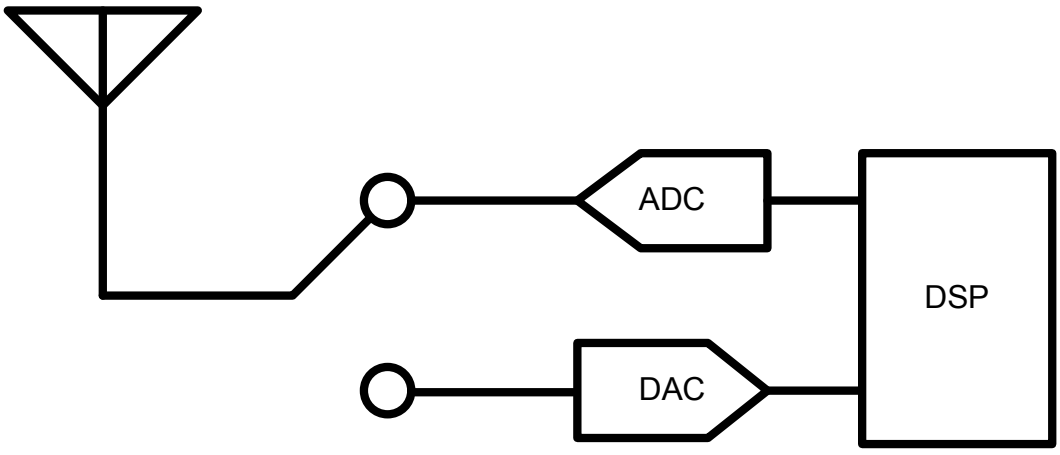

Figure 1.5 The ideal, Mitola-style software defined radio contains no analog elements. The realities of modern data converters leave this type of radio a dream for the future.

style software defined radio (SDR) [15] as depicted in Figure 1.5, which is a theoretical 100% digital transceiver. An 11GSample/s 12-bit ADC would be sufficient to Nyquist sample the commercialized radio spectrum (0-5.5GHz) [16]. If such an ADC could be built in CMOS (which it cannot today) and had a full scale voltage of 1.2V, then the LSB is approximately 0.3mV (1.2V divided by 2^{12}=4096). This corresponds to a -60dBm signal received from a 50Ω transmission line or antenna. That is a relatively large signal in terms of wireless communication and yet is barely large enough to register 1bit of response from the 12bit ADC. Gain is required to bring realistically sized signals up to a reasonable fraction of the ADC full scale range. In fact, a single amplifier is rarely enough gain and several more amplifiers will be used in various parts of a receiver, often with automatic gain control to best utilize a large dynamic range. It is extremely unlikely that an ADC will recover broadband signals without the aid of amplifiers any time soon.

1.2.2 Broad-Tuning vs. Broadband

Different applications use the term "broadband" in different ways. Some systems, such as non-Mitola-style software defined radio (SDR), seek to pass a relatively narrow frequency slice at a time, but require the ability to select that narrow channel from a wide range of the radio spectrum. Such systems may be characterized as "broad-tuning," because they are fundamentally narrowband, wideband, or even ultra-wideband (the lesser of 500MHz or 20% bandwidth) in nature.

There have been some very interesting advances in broad-tuning systems in recent years, including designs which have no explicit LNA. There are several points in a typical narrowband receiver chain where gain can be introduced. Traditionally, some gain is introduced at RF, though only a limited amount of gain is possible at such high frequency. The narrowband channel is mixed down to an intermediate frequency (IF) where gain is more plentiful than at RF, but flicker noise is significantly lower than at baseband. There have been promising developments of receivers with bandwidths on the order of 25MHz or more which can down-mix signals up to 2GHz [21]. Such systems down-mix the desired band to IF or baseband, low-pass filter, and provide gain only at the lower frequency. The noise figure and dynamic range of some passive mixing techniques have gotten low enough that no preceding gain is required. Other approaches retain high frequency gain, but incorporate LNA and mixer into a single circuit [20]. These systems can be tuned to cover wide ranges of frequency spectrum, but ultimately only pass a narrow bandwidth at a time. Thus, these types of receivers are broad in tuning range, but not in instantaneous bandwidth.

In contrast, a truly broadband system covers a large instantaneous bandwidth, often several decades of bandwidth at a time. In the case of gigabit digital communication, this range extends from near DC to microwave frequencies. Emerging

military systems seek to cover all the electronic warfare (EW) bands (50MHz to 18GHz and higher) simultaneously for real-time spectrum analysis [24]. UWB radio standards allow for only a portion of the full 3.1-10.6GHz allocated band to be used at a time, usually with narrowband-like radio architectures. On the contrary, impulse based UWB radios seek to use that entire 7.5GHz bandwidth at once [25].

1.2.3 Basic LNA Topologies

There is a relatively short list of broadband LNAs, each with its advantages and limitations. To be considered a broadband amplifier in this context, the circuit must preserve a wide bandwidth in two ways. First, the gain bandwidth (not to be confused with gain-bandwidth product) is the frequency where the gain falls by 3dB from its low frequency value. The matching bandwidth is the frequency at which the input return loss, or S_{11}, increases above -10dB. We can compare the different topologies analytically to roughly sketch the shortcomings of each in terms of noise figure and gain-bandwidth product. I will conduct a brief analysis of the most popular LNA topologies, including the DA, and compare the noise figure each can achieve in a given bandwidth.

The following analyses will have some common assumptions. First, I'll assume all transistors have infinite output resistance, no feedback capacitance, and no gate resistance to make the analyses simple. No additional loading at the output of the amplifier is considered. In addition, I'll omit gate induced noise current, which only becomes significant very near f_T. It is most instructive to write the noise figure expressions in terms of universal circuit and device parameters such as bandwidth, BW; unity gain frequency, f_T; source resistance, R_S; and the process and bias dependant excess noise parameter, γ. Detailed derivations for each of these analyses are available in the Appendix.

1.2.3.1 Common-Gate Amplifier

A typical common-gate amplifier is shown in Figure 1.6(a). The impedance looking into the source, $1/g_m$, provides the real impedance for matching and the gate-source capacitance will limit the matching bandwidth. This is a valid assumption as long as no inductors are included for bandwidth extension. Certainly, bandwidth extension techniques are helpful in boosting performance of many circuits, but the variety of techniques clouds the deductions to be taken from this analysis. For now, let us assume the simplest case. We can calculate the maximum allowed input capacitance of an RC matched circuit from the formula

$$C_{in} = \frac{1}{\pi R_S BW}\sqrt{\frac{|\Gamma|^2}{1-|\Gamma|^2}} \tag{1.3}$$

where $|\Gamma|^2$=0.1 corresponds to -10dB return loss. Substituting this value, (1.3) becomes

$$C_{in} = \frac{1}{3\pi R_S BW}. \tag{1.4}$$

If this capacitance limits the -10dB matching bandwidth it cannot also limits the 3dB gain bandwidth. Thus, the drain capacitance is assumed to limit the gain bandwidth.

Calculating the noise figure,

$$F_{CG} = 1+\gamma+\frac{4}{3}, \tag{1.5}$$

we see that it is constant over any bandwidth. The first term is from the source, the second from the transistor and the final term is from the load (this is omitted in many publications). Of course this is only a rough approximation.

A common modification to the common-gate topology is called g_m-boosting. An additional amplifier is introduced between the source and gate of the main FET to exaggerate the transconductance. This allows the use of a smaller transistor and serves to reduce the effect of the main transistor's noise by a factor of the boosting gain, A,

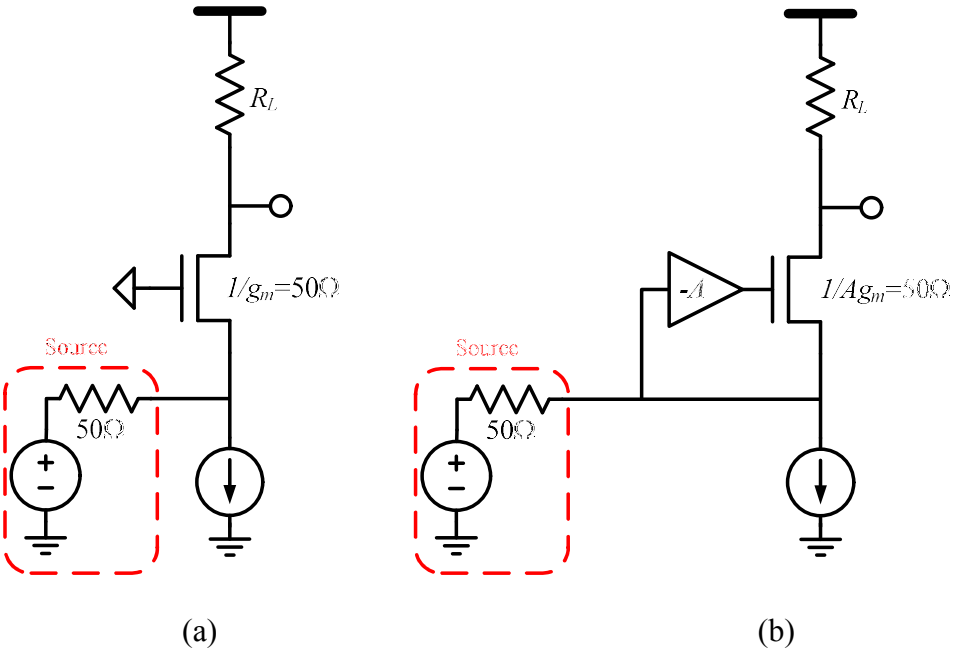

Figure 1.6 (a) Common-gate and (b) g_m-boosted Common-gate LNAs.

$$F_{CG} = 1 + \frac{\gamma}{A} + \frac{4}{3} \tag{1.6}$$

as well as extending the bandwidth. This can be implemented as simply as shown in Figure 1.6(b) or can be achieved by capacitively cross-coupling two common-gate amplifiers in a quasi-differential configuration.

1.2.3.2 Shunt Feedback Amplifier

Figure 1.7 shows a basic shunt feedback amplifier. The noise figure of this circuit can be expressed as

$$F_{FB} = 1 + \frac{1}{2}\left(\frac{BW}{f_T}\right) + 6\gamma\left(\frac{BW}{f_T}\right) + 3\left(\frac{BW}{f_T}\right)^2 \tag{1.7}$$

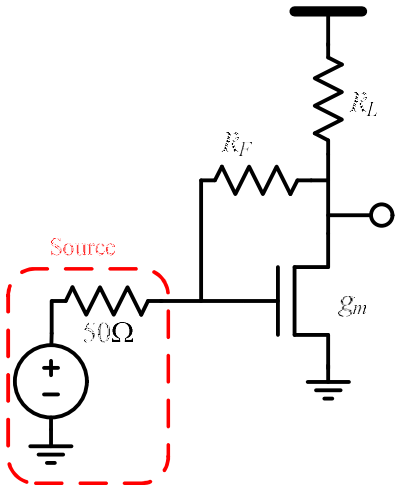

Figure 1.7 Shunt Feedback Amplifier utilizing resistive feedback.

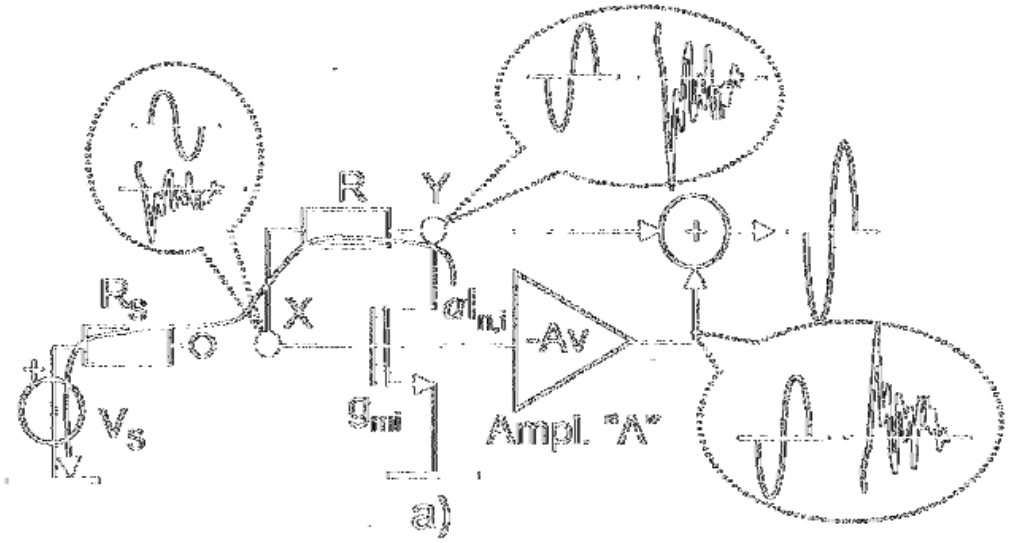

Figure 1.8 Illustration of the noise cancelling concept. The signal is inverted between nodes X and Y while the dominant noise source is not, allowing the noise to be canceled while the signal is reinforced [15].

using the same matching calculation from (1.4). Here the first term is from the source resistance, the second is from the feedback resistor, the third is from the transistor, and

the final term is from the load. Since all but the first term are frequency dependant, this circuit can have very low noise figure at low bandwidths, eventually losing out to the common-gate LNA at higher bandwidths.

1.2.3.3 Noise Cancelling Circuits

A technique to cancel part of the noise in a LNA was introduced in 2004 [17] and been receiving much attention since. The noise cancelling technique operates on the principle that the input signal and dominant noise source originate from different parts of the circuit. This allows a secondary amplifier to copy the input signal with the same polarity as the main amplifier, but the noise of the main amplifier is inverted. When the contributions of the primary and secondary amplifiers are combined, part of the noise from the primary amplifier is canceled out. This works well over high bandwidths because it is a fully feed-forward cancellation, rather than relying on feedback. This technique has been applied to both common-gate [18] and shunt feedback LNAs [17]. A general analysis of the technique is difficult and less instructive than for the previous circuits, but it has been shown to reduce noise figure on the order of 1-2dB in circuits of moderately broad bandwidth. The technique shows promise, but is relatively immature and is unlikely to extend to bandwidths of 10's of gigahertz.

1.2.3.4 Distributed Amplifier

A simple DA with N stages is shown to in Figure 1.9. The matching condition from (1.3) and (1.4) does not apply to the DA because it has a sharp matching cutoff created by the artificial transmission lines, not a slow RC degradation like the other circuits. This effect with be discussed in more detail in Chapter 2. The rigorous noise analysis of a DA is more cumbersome than for other circuits because there are many noise

sources which are copied by the many gain cells, however a cursory analysis yields a lower bound for noise figure of

$$F_{DA} = 1 + \frac{1}{N} + \frac{4\gamma}{N}\left(\frac{BW}{f_T}\right) + \frac{2}{N^2}\left(\frac{BW}{f_T}\right)^2. \tag{1.8}$$

Here the first term is from the source resistance, the second term is from the input line termination, the third term is from the N uncorrelated transistors, and the final term is from the output termination and load resistors. The key to the DA's low noise properties is that the noise is spread out over several uncorrelated transistors instead of a single transistor. Thus, the noise contributed is proportional to N while the gain is proportional to N^2. In practice, the noise figure of a broadband DA can approach the noise figure of a narrowband inductive degeneration common-source amplifier [22].

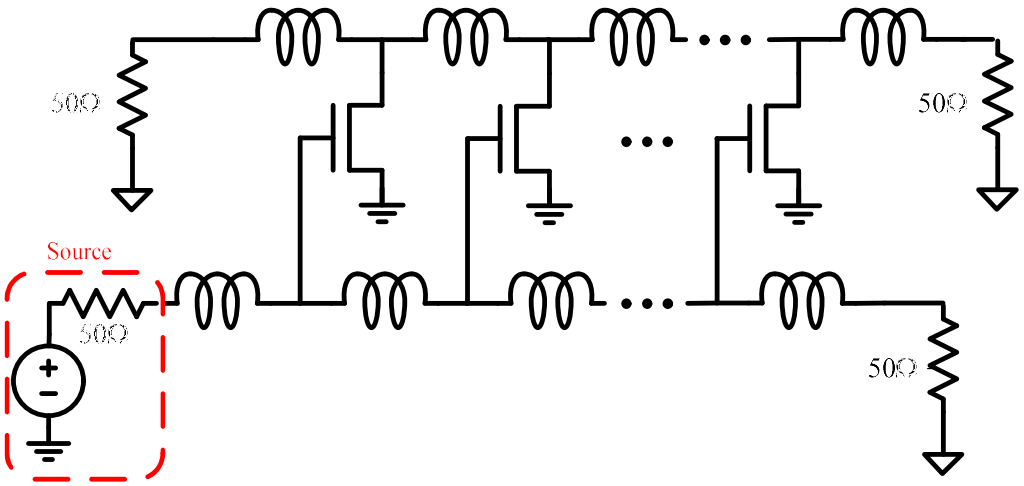

Figure 1.9 Simple distributed amplifier

1.2.3.5 Comparison of Broadband LNA Topologies

Figure 1.10 illustrates curves corresponding to equations (1.5)-(1.8), showing noise figure vs. bandwidth (normalized by f_T). The g_m-boosted common-gate amplifier always outperforms a simple common-gate amplifier and for bandwidths beyond about 25% of f_T it is lower than shunt feedback as well. Notice though, that a short (N=3) distributed amplifier is better than g_m-boosted common-gate below 60% of f_T and a medium-long (N=6) distributed amplifier is the best choice in all cases. Naturally, this comparison is based on a cursory analysis, but it shows that based on noise figure alone, the DA is a good candidate LNA at any bandwidth. Other considerations, such as relatively high power consumption and very high gain-

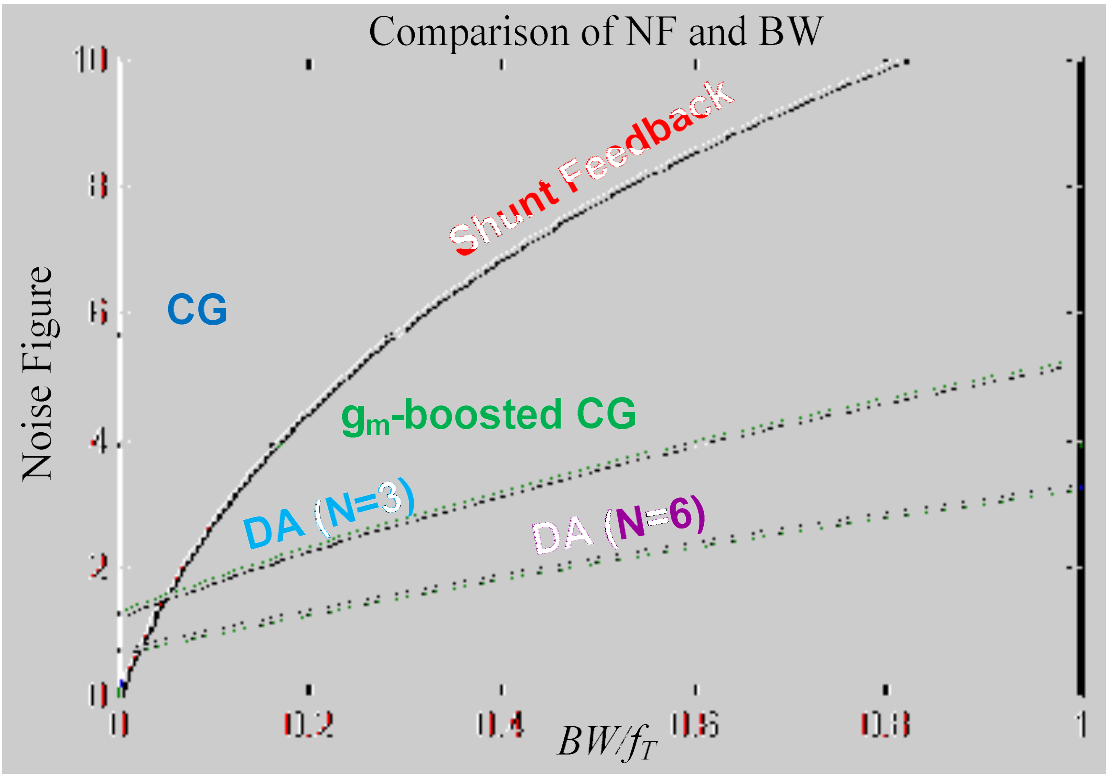

Figure 1.10 Comparison of various broadband LNA topologies' minimum attainable noise figure as a function of bandwidth normalized by f_T.

bandwidth product, ultimately relegate the DA to applications from about 30% of f_T and up. This is why we find DAs in the literature from the UWB range up through the farthest reaches of mm-wave, but rarely to never in the more common wireless communication bands. In lower bandwidth applications it may have desirable noise figure, but is much larger and more power hungry than the alternatives.

1.3 Broadband Techniques Beyond Amplification

The early radios of Marconi and his contemporaries were impulse radios, but the technology was abandoned for communication long ago in favor of the heterodyne radio [1]. Impulse radio is more than simply a broadband radio; it shifts the communication scheme from being primarily narrow-frequency "power signals" to narrow-time "energy signals." This shift will eventually necessitate the ability to manipulate temporal pulses as deftly as we manipulate frequency bands in common radios today. Since the frequency spectrum is scarce, but is only used a fraction of the time, the new temporal paradigm has the potential to open the airwaves to many more simultaneous users [15]. The physics and radar communities have long been interested in the manipulation of short pulses so we can learn much from them, but wireless communication carries with it the requirement that all components be small and relatively low power.

Dispersion is one of the primary effects scientists and engineers use to manipulate short pulses. I will show later in this dissertation that a small, low power dispersive element does not exist at present, but the DA is a promising candidate for dispersion engineering at the chip scale. I will introduce the dispersion enhanced artificial transmission line and use it to construct a DA capable of stretching and compressing short pulses. This demonstration is a stepping stone opening the

distributed amplifier to wider application, making it an enabling technology for a new (or rather old) breed of communication schemes.

1.4 This Dissertation

My objective is to present improvements and innovations upon the classical distributed amplifier which benefit its application to modern and future communication systems. The remainder of the dissertation is organized as follows.

Chapter 2 deals with techniques to increase the gain and reduce the area of CMOS distributed amplifiers, which this introduction has established as critical criteria for broadband LNA design. I present the bisected-π matching section as a new and improved matching section for a DA. Using the bisected-π section allows more gain, and thus higher gain-bandwidth product, to be achieved in a given process. The new topology also offers lower noise figure, fewer unique inductor sizes, and smaller total area than DAs with conventional matching sections. Combining increased gain and reduced area provides greatly increased gain per unit area which is generally considered a shortcoming of the DA. A full analytical and experimental gain and noise figure comparison of the novel and conventional circuits prove that the bisected-π matching section is a superior choice on all counts.

Chapter 3 concerns another critical issue in the design of broadband LNA front ends. Noise performance across a broad range of frequencies is, as established above, a critical metric for efficient and wide dynamic range amplifiers. In Chapter 3, I offer the Blue Noise Active Termination (BNAT) as a solution to a problem as old as the DA itself. The very rough noise analysis which produced equation (1.8) fails to capture the excess noise of a DA at low frequency. The source of that additional low frequency noise was isolated many years ago and various researchers have addressed the problem by creating tradeoffs with gain or matching. The BNAT solves the low

frequency noise issue by trading off area and power while leaving the gain and matching of the DA, the fundamental LNA metrics, undisturbed. The elimination of this noise source makes equation (1.8) much closer to reality and the deductions made in section 1.2.3.5 more valid.

Chapter 4, begins a discussion of the concept of temporal imaging and short pulse manipulation. From here I show how modification of the DA can produce a dispersive medium for emerging broadband communication systems. I introduce the new dispersion-enhanced DA with a very high dispersion per unit length. I use this dispersion-enhanced DA experimentally to coarsely stretch and compress high bandwidth microwave pulses. This demonstration is the first system to stretch and compress broadband pulses on-chip.

Chapter 2

Distributed Amplifier with π-type Matching Sections

The distributed amplifier (DA) is most notable for achieving gain-bandwidth products far above those possible with other topologies. Chapter 1 showed that for a sufficiently large bandwidth (relative to f_T) the DA becomes the best choice for an LNA. Next we will explore some of the history of the DA, including a rigorous analysis of the gain and noise, and develop an improvement upon the most common DA topology which better harnesses the gain and noise performance available from a given technology.

The distributed amplifier was originally introduced in the 1940's for vacuum tube amplifiers [26], but was a relative novelty until applied to III-V devices in the 1980's and then silicon technologies in the 1990's [7]. In the last decade, the DA has been fully integrated in mainstream commercial bulk CMOS [27]. Applications in ultra-wideband radio, digital data links, and other broadband systems keep the DA relevant and drive further development and improvements, particularly in low cost silicon. Cost drives analog circuitry into ever more complex and highly integrated chips in which not only performance, but design complexity and area efficiency are increasingly important [28]-[30].

The DA can be understood as a cascade of filter sections which absorb the parasitic capacitance of several active devices allowing broadband operation. These filter sections form artificial transmission lines allowing the current contributions of the many low gain elements to add in-phase for a large overall gain, depicted by the traveling signals in Figure 2.1. The input signal takes time to propagate from one gate

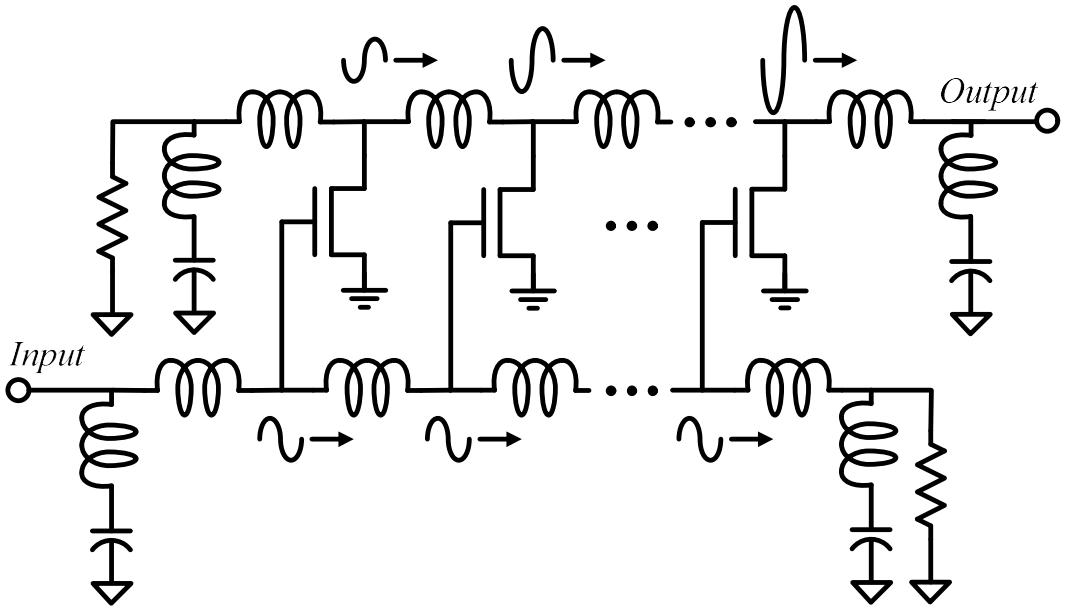

Figure 2.1 Conventional distributed amplifier constructed of T-type filter sections. As the input signal propagates down the input line, each successive transistor adds its contribution to the output line, with the input and output signals propagating in-phase from left to right.

to the next, while the output signal propagates from drain to drain at the same rate. The currents contributed by each transistor add linearly and in-phase, delivering an amplified copy of the input to the output. Virtually any lossless filter section can be employed to form the artificial transmission lines depending on the desired amplifier characteristics. As far back as the inaugural DA paper [26], Ginzton proposed using some common filter sections such as constant-k (k-sections), *m*-derived (m-sections), and bridged-T to make up the DA. Each of these filter types, individually and in various permutations, has been demonstrated in DAs over the years. The most common implementation in silicon is constant-k gain sections, often with *m*-derived termination sections. Invariably, designers have chosen T-type k-sections as the unit cell and the bisected-T m-section for matching. Figure 2.1 is a basic example of such a

configuration, where each transistor is of equal size. The prevalence of the T-type sections is likely a relic from an era before monolithic integration, when transistors came in discrete packages (thus equal capacitance for each transistor) and transmission line lengths (effectively inductors) were a trivial design parameter. This chapter will show that other configurations, which have not been demonstrated before, have clear advantages over the dominant design paradigm.

In today's mainstream CMOS processes, with low resistivity substrates and thin metal layers, simple transmission line structures are too lossy for practical use and the burden of DA design has shifted almost entirely to designing high quality spiral inductors [28] or low-loss, high-Z transmission lines [29]. In these processes inductor design is inaccurate, cumbersome, and time-consuming while transistor sizing is relatively trivial. The importance of area savings in integrated distributed amplifiers has driven some recent DAs to omit matching sections entirely, relying on bandwidth overdesign to achieve their matching and gain flatness specifications [30], [31].

In this chapter, I challenge the conventional wisdom for integrated DA's and propose an improved topology for increased gain and reduced area based on the less common π-type k-section and m-section, which better utilize the strengths and mitigate the weaknesses of modern integrated processes. The bisected-π m-section is briefly mentioned as a possible termination for an artificial transmission line in [32], but to my knowledge this termination has never been used in a monolithic DA nor have its advantages over the conventional design ever been explored. I will show that the bisected-π m-section can be used to provide gain, while the conventional bisected-T m-section cannot. A rigorous analysis of the impact of this modification on DA performance is followed by a confirmation of the predicted improvements via direct comparison in 130nm CMOS. A gain advantage of 1.2dB (32%) and an average noise figure reduction of 0.25dB across the 21.5GHz bandwidth demonstrates that my π-

based design paradigm is superior to the old T-based circuit. This increased performance comes with 17% smaller area and fewer unique inductor sizes for reduced cost and design effort. While the T-based DA is well suited to conventional microwave circuit platforms, the π-based DA is better suited to monolithic integrated designs. Improved gain and noise, without the sacrifice of bandwidth or impedance match, make this approach well suited for a distributed amplifier as a low-noise amplifier.

2.1 Synthesis of a Distributed Amplifier from Filter Sections

In order to understand the similarities and differences between the T-based and π-based distributed amplifiers, it is instructive to briefly review the characteristics of the applicable filter sections and how we form artificial transmission lines. Detailed treatments are available in [26], [32], and elsewhere throughout the literature.

2.1.1 Constant-k Sections

The simplest lossless low pass filter is the constant-k filter, or k-section. Figure 2.2 shows the k-section in both T and π varieties, named for their semblance to the "T" and "π" characters. Their image impedances are given by

$$Z_T(\omega) = \sqrt{\frac{L}{C}\left(1-\left(\frac{\omega}{\omega_c}\right)^2\right)} \tag{2.1}$$

and

$$Z_\Pi(\omega) = \sqrt{\frac{L}{C}\left(1-\left(\frac{\omega}{\omega_c}\right)^2\right)^{-1}} \tag{2.2}$$

respectively, where ω_c is the cutoff frequency

$$\omega_c = \frac{2}{\sqrt{LC}}. \tag{2.3}$$

Below the cutoff frequency, the image impedance is purely real so multiple copies of the same k-section are conjugate matched to each other. In other words, a cascade of k-sections is internally transparent with no reflections below cutoff. Beyond cutoff, the image impedance changes abruptly to purely imaginary and the sections are not conjugate matched to each other. There is a significant impedance mismatch between a cascade of k-sections and a standard 50Ω source as the frequency approaches cutoff and nearly total reflection beyond cutoff. Such a cascade of identical filter sections is called an artificial transmission line, where the image impedance is analogous to frequency dependent characteristic impedance. The poor matching near cutoff wastes valuable bandwidth.

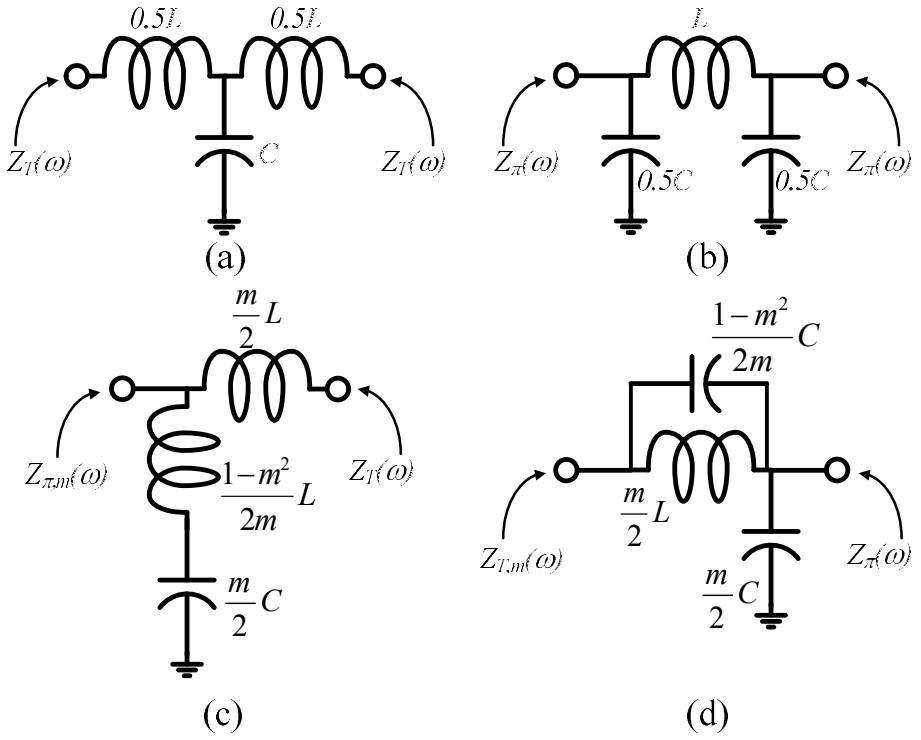

Figure 2.2 Filter sections including (a) T-type and (b) π-type k-sections and (c) bisected-T and (d) bisected-π m-sections, using the naming convention from [31].

2.1.2 m-Derived Sections

The m-derived section, or m-section, comes in T and π forms as well. It can be used to improve the matching between a cascade of k-sections and a real source or load near cutoff. The image impedance of a full T or π m-section is the same as a k-section given the same values of *L* and *C*. The full sections are not of interest here, however, let us bisect a T-type section through the shunt branch and look at the mid-shunt image impedance as in Figure 2.2(c),

$$Z_{\Pi,m}(\omega) = \sqrt{\frac{L}{C}} \frac{1-\left(\frac{\omega}{\omega_0}\right)^2}{\sqrt{1-\left(\frac{\omega}{\omega_c}\right)^2}} \tag{2.4}$$

where ω_c is the same as in (2.3) and ω_0 is the resonant frequency of the series tank

$$\omega_0 = \frac{\omega_c}{\sqrt{1-m^2}}. \tag{2.5}$$

Here we see the mid-shunt impedance is a function of the parameter *m* and it is well known that for *m*=0.6 this impedance very closely approximates a constant, real resistance up to cutoff [32]. Thus a bisected-T m-section can be used to couple power from a real 50Ω source into a cascade of T-type k-sections with minimal reflections from DC up to the cutoff frequency. Similarly, the bisected-π section of Figure 2.2(d) can match a cascade of π-type k-sections to 50Ω. An artificial transmission line formed of either T or π sections and terminated in the appropriate bisected m-section, is approximately transparent from a real source into a real load from DC to cutoff. This enables an amplifier designed for a desired cutoff frequency and wideband characteristic to be matched to the impedance of an off-chip signal source such as a wideband antenna.

2.1.3 Application to Distributed Amplifiers

Figure 2.3(a) shows a breakdown of an artificial transmission line formed from T-type sections as it is used in the DA of Figure 2.1. The capacitor in each k-section unit cell is the gate (or drain) parasitic capacitance of a transistor. Each unit cell contains one transistor whose transconductance is proportional to its capacitance. The matching sections at the beginning and end of the artificial transmission line perform the appropriate impedance transformation, but they do not directly influence the gain. They only contribute a phase shift as the signal propagates through.

For ideal lossless elements, such an artificial transmission line can be made infinitely long and thus the gain of a DA infinitely large. However, since all real

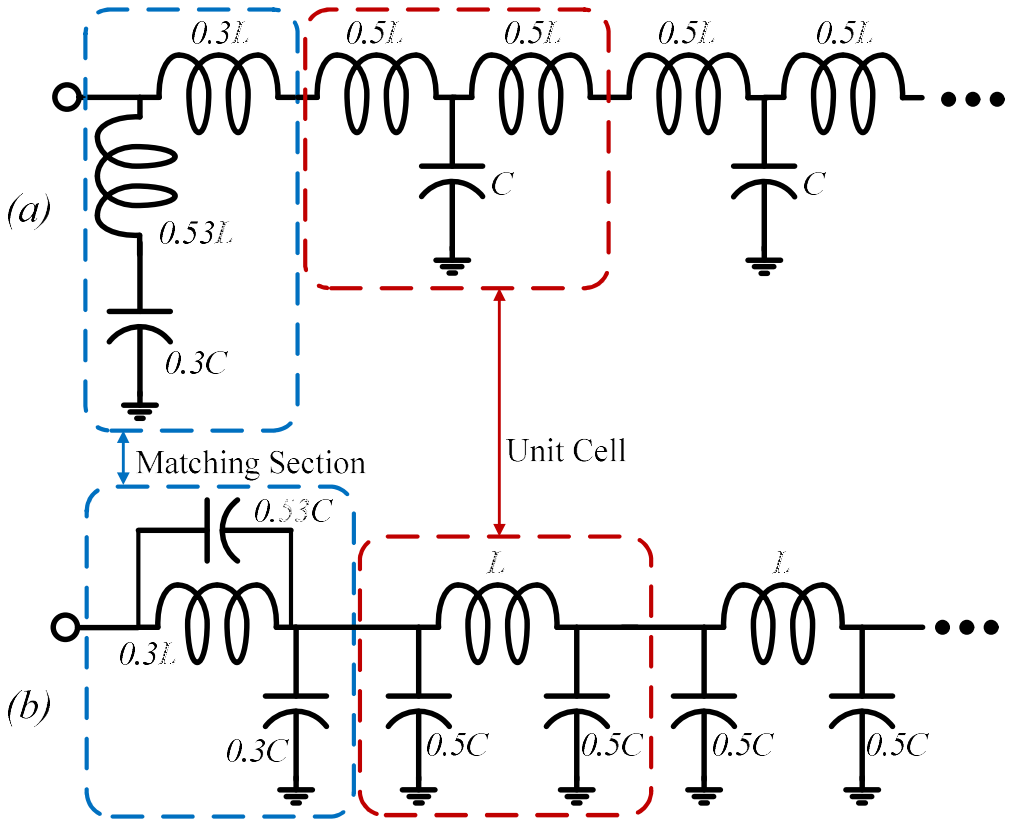

Figure 2.3 (a) Conventional and (b) proposed artificial transmission lines. For any value of *N*, the two lines have nearly identical s-parameters.

elements have some loss, there is a maximum number of unit cells, N_{max}, beyond which adding one more cell will introduce more loss than gain, providing no benefit. In other words, N_{max} is a measure of the optimal electrical length of the DA to give maximum gain. The value of N_{max} for a particular design is set by the process and desired bandwidth. Typical values of N_{max} for monolithic DAs range from 3-8, although higher numbers are occasionally reported. Refer to Figure 1.2 to see an illustration of why there is an optimal value of N.

Swapping all T-type sections for equivalent π-type sections, we have the artificial transmission line of Figure 2.3(b). Notice that one unit cell contains the same total capacitance, and thus transconductance, as in the T-based case. The primary difference in this new configuration is that the matching section contains an additional parallel capacitor to ground. This additional capacitor can be implemented by a transistor. The capacitor to ground in the matching section is in parallel with the left capacitor of the first k-section. These capacitors can be added together and implemented by a single transistor, which is 4/5 of the size of a full gain cell. As a result, a DA using N_{max} π-type k-sections and the bisected-π m-section roughly resembles a T-based DA containing N_{max}+1 transistors. This seeming contradiction is made possible because the new π-based DA adds extra gain from the m-sections without adding electrical length, a characteristic not available with the T-type matching section.

2.2 DA With Alternative Matching Section

Based on the above observation, it is clear that use of a π-based section as the primary building block of a DA will enable the use of a matching section with a gain element. Using this type of section, as opposed to the traditional T-type architecture, should provide advantages for monolithic integrated DA designs in terms of increased gain

and improved noise figure. In this section, we will calculate the forward available gain, reverse available gain, and intrinsic noise figure of this new DA configuration to show that for the same process and bandwidth (i.e. the same N_{max}) the π-based circuit outperforms the familiar T-based circuit. We will consider the FET-based DA in Figure 2.4, although the benefits of the π-architecture will also apply to non-FET DA's. For simplicity, we will assume lossless input and output artificial transmission lines with the same impedance and propagation constant, β.

2.2.1 Forward Available Gain

We calculate the forward available gain by finding the current contribution from each transistor to the load due to the input signal. Figure 2.4 shows each small signal FET, including noise generators, separated by inductors. A π-based DA with N k-sections actually contains N+1 transistors, which we number from left to right as 1, 2, … , N+1. For the r-th transistor, we define a gate voltage, V_r, and a drain current, I_r. As illustrated explicitly in Fig 3b, the first and last transistors are shared by an m-section and adjacent k-section and have width only 4/5 of the width of the interior transistors. The input line is lossless, so the voltages at the gate of each transistor have same

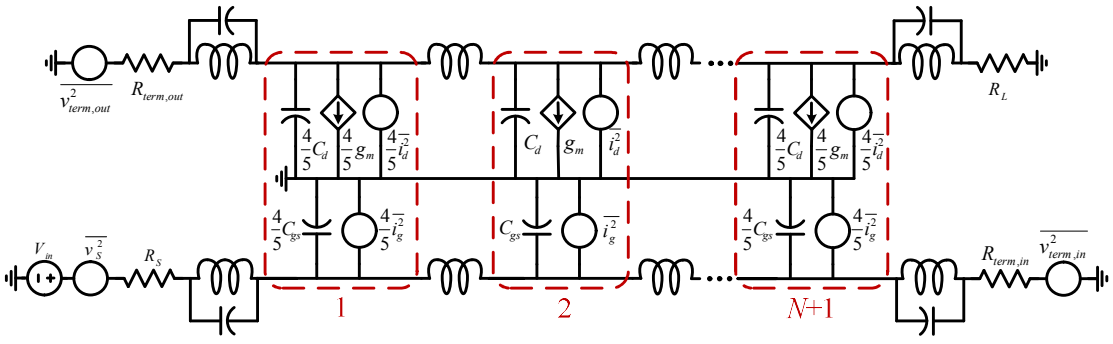

Figure 2.4 Small signal and noise model of a π-based DA, including input source resistant, R_S. Transistors are numbered from 1 to N+1 for a DA with N k-sections.

magnitude but differ by a phase factor given by

$$V_1 = V_{in}e^{-j\beta}, V_2 = V_{in}e^{-j2\beta}, \ldots, V_{N+1} = V_{in}e^{-j(N+1)\beta}. \tag{2.6}$$

If we say the transconductance of the interior transistors is g_m then the transconductance of the first and last transistors is 4/5 g_m. Using this convention, the drain current of each transistor is

$$I_1 = \frac{4}{5}g_m V_{in}e^{-j\beta}, I_2 = g_m V_{in}e^{-j2\beta}, \ldots, I_{N+1} = \frac{4}{5}g_m V_{in}e^{-j(N+1)\beta}. \tag{2.7}$$

These drain currents see equal impedance in both directions on the output line, so the forward (left to right) propagating half of each drain current adds on the load at the right end of output line as one current, I_{fwd}. The equal phase accumulation through the different signal paths means that they add in-phase at the output load as

$$\begin{aligned} I_{fwd} &= I_1 e^{-jN\beta} + I_2 e^{-j(N-1)\beta} + \ldots + I_{N+1}e^{-j\beta} \\ &= \frac{1}{2}g_m V_{in}\left(\frac{4}{5}e^{-j(N+1)\beta} + e^{-j(N+1)\beta} + \ldots + \frac{4}{5}e^{-j(N+1)\beta}\right) \end{aligned} \tag{2.8}$$

and the magnitude of this current is

$$\left|I_{fwd}\right| = \frac{1}{2}g_m\left(N + \frac{3}{5}\right)V_{in}. \tag{2.9}$$

The forward gain for this amplifier, from a source with impedance R_S into a load of impedance R_L is

$$G_{\pi,fwd} = \frac{1}{4}g_m^2 R_S R_L\left(N + \frac{3}{5}\right)^2. \tag{2.10}$$

The same analysis applied to the conventional T-based circuit yields

$$G_{T,fwd} = \frac{1}{4}g_m^2 R_S R_L N^2, \tag{2.11}$$

which is similar to the result in [33]. As we expected, the π-based circuit has higher gain for all N and since both circuits have the same N_{max}, the π-based circuit can

Table 2.1

Gain Boost for Different DA Sizes

N	*Gain Boost*
3	1.6dB
4	1.2dB
6	0.8dB
8	0.6dB

deliver higher gain in a given process. Table 2.1 shows the gain boost that can be expected for typical values of *N*. This boost to gain increases the ability of an LNA to mask the noise of other components in the receiver chain, improving the overall noise figure of a receiver.

2.2.2 Reverse Available Gain

The reverse gain of a distributed amplifier is due to the reverse propagating (right to left) current on the output line, which flows as I_{rev} into the left side termination of the output line. In essence, we treat the left side termination as if it were another output of the amplifier, though in practice the power delivered to this pseudo-output is wasted in the termination. This should not be confused with the reverse isolation of the amplifier (commonly referred to as S_{12}). This is not a critical performance metric for the amplifier, but is needed primarily to calculate the noise figure. These reverse propagating currents see different path lengths and thus add with mismatched phases at the left side termination as

$$\begin{aligned} I_{rev} &= I_1 e^{-j\beta} + I_2 e^{-j2\beta} + \ldots + I_{N+1} e^{-j(N+1)\beta} \\ &= \frac{1}{2} g_m V_{in} \left(\frac{4}{5} e^{-j2\beta} + e^{-j4\beta} + \ldots + \frac{4}{5} e^{-j2(N+1)\beta} \right). \end{aligned} \tag{2.12}$$

After grouping terms and taking the magnitude, we find this series reduces to

$$|I_{rev}| = \frac{1}{2} g_m V_{in} \left(\frac{\sin(N+1)\beta}{\sin\beta} - \frac{2}{5}\cos N\beta \right) \tag{2.13}$$

with the reverse available gain of a π-based DA given by

$$G_{\pi,rev} = \frac{1}{4} g_m^2 R_S R_L \left(\frac{\sin(N+1)\beta}{\sin\beta} - \frac{2}{5}\cos N\beta \right)^2 . \tag{2.14}$$

The same analysis for the T-based circuit gives

$$G_{T,rev} = \frac{1}{4} g_m^2 R_S R_L \left(\frac{\sin N\beta}{\sin\beta} \right)^2 . \tag{2.15}$$

For any appreciable value of N, (2.14) and (2.15) are similar in that they are approximately zero except when $N\beta$ is near 0 or π, corresponding to DC and the cutoff frequency, respectively. At those points each function is equal to its corresponding forward gain.

2.2.3 Noise Figure

Since we are evaluating the DA as an LNA, we would like to quantify its noise figure as a function of frequency over its broad bandwidth. Intuitively we expect that the improved gain of the π-based amplifier will provide some benefit in signal to noise ratio (and thus noise figure), however, to rigorously compare the noise of the two architectures we perform a full noise analysis. Noise sources considered in this analysis are illustrated in Figure 2.4 and include the source resistance, the transmission line termination resistors, and the transistors' thermal noise. We will calculate the contribution of each source to the total noise power at the load and then calculate the noise figure.

2.2.3.6 Source and Termination Resistors

For any amplifier, the noise power at the load due to the source is simply

$$P_{n,source} = kTBG_{fwd}\,, \tag{2.16}$$

where k is Boltzmann's constant, T is the standard noise temperature, and B is the bandwidth. Since the distributed amplifier is symmetric, the noise contribution due to the input line termination resistor, $R_{term,in}$, follows the same path as was calculated for the reverse available gain. Thus the input termination noise contribution to the output is

$$P_{n,term,in} = kTBG_{rev}\,. \tag{2.17}$$

And finally, since we have assumed lossless components the output line termination resistor, $R_{term,out}$, contributes directly to the output

$$P_{n,term,out} = kTB\,. \tag{2.18}$$

2.2.3.7 FETs

In this lossless analysis, we consider only the thermal channel noise and it's accompanying induced gate noise, which are given by

$$\overline{i_d^2} = 4kTBg_m\gamma \tag{2.19}$$

and

$$\overline{i_g^2} = 4kTB\delta\frac{\omega^2 C_{gs}^2}{g_m}, \tag{2.20}$$

where γ and δ are process and bias dependant parameters. These two sources are correlated, but we treat them independently and sum their power contributions at the load like uncorrelated sources. The distributed nature of the circuit limits this error to a few percent of the total noise.

The drain current noise generator of each transistor produces a forward and backward traveling wave on the output line. The forward traveling mean square noise current from each interior transistor is

$$\frac{1}{4}\overline{i_d^2} \tag{2.21}$$

and from the first and last transistors is the scaled value,

$$\frac{1}{4}\left(\frac{4}{5}\overline{i_d^2}\right). \tag{2.22}$$

We can combine these at the output by summing powers without regard for phase relation because each source is uncorrelated. The power at the load due to drain current noise is

$$P_{n,drain} = \frac{1}{4}\left(\frac{4}{5}\overline{i_d^2} + \overline{i_d^2} + \cdots + \frac{4}{5}\overline{i_d^2}\right)R_L = \frac{1}{4}\left(N + \frac{3}{5}\right)\overline{i_d^2}R_L\,. \tag{2.23}$$

The total noise from gate induced noise is considerably more cumbersome to calculate because the noise propagates in both directions on the gate line and all the transistors produce correlated copies of each independent noise source. To ease the difficult task of this calculation for a non-uniform DA, we will consider only the forward propagating components as those components add strictly in-phase and should account for most of the noise power. The forward propagating mean square current on the input line originating from the first transistor only is

$$\frac{1}{4}\left(\frac{4}{5}\overline{i_g^2}\right), \tag{2.24}$$

which develops a mean square voltage

$$\frac{1}{4}\left(\frac{4}{5}\overline{i_g^2}\right)Z_{\pi g}^2 \tag{2.25}$$

at the gate of every transistor, where $Z_{\pi g}$ is the mid-shunt image impedance of the artificial transmission line. Following the same procedure used for calculating the forward gain, we add the resulting drain currents in-phase giving a power at the load of

$$P_{n,gate,1} = \frac{1}{16}\overline{i_g^2} Z_{\pi g}^2 g_m^2 R_L \left[\frac{4}{5}\left(N + \frac{3}{5} \right)^2 \right]. \tag{2.26}$$

For the noise originating from the second transistor and propagating forward only, there is an amplified contribution from each transistor except the first, so the power at the load is

$$P_{n,gate,2} = \frac{1}{16}\overline{i_g^2} Z_{\pi g}^2 g_m^2 R_L \left(N - \frac{1}{5} \right)^2. \tag{2.27}$$

For all the transistors after the second and before the last the output noise power is

$$P_{n,gate,3-N} = \frac{1}{16}\overline{i_g^2} Z_{\pi g}^2 g_m^2 R_L \sum_{r=3}^{N} \left(N + \frac{9}{5} - r \right)^2. \tag{2.28}$$

Finally, the last transistor contributes

$$P_{n,gate,N+1} = \frac{1}{16}\overline{i_g^2} Z_{\pi g}^2 g_m^2 R_L \left(\frac{4}{5} \right)^3. \tag{2.29}$$

Summing (2.26), (2.27), (2.28), and (2.29), the total power due to the gate induced noise current is

$$P_{n,gate} = \frac{1}{16}\overline{i_g^2} Z_{\pi g}^2 g_m^2 \left(\frac{N^3}{3} + \frac{11N^2}{10} + \frac{29N}{30} + \frac{4}{25} \right) R_L. \tag{2.30}$$

With only a few percent error for N>1, this expression can be approximated by

$$P_{n,gate} = \frac{1}{48}\overline{i_g^2} Z_{\pi g}^2 g_m^2 (N+1)^3 R_L. \tag{2.31}$$

2.2.3.8 *Total Noise Figure*

Combining (2.16), (2.17), (2.18), (2.23), and (2.31) the total output noise is

$$P_{n,total} = kTBG_{fwd} + kTBG_{rev} + kTB + \frac{1}{4}\left(N+\frac{3}{5}\right)\overline{i_d^2}R_L + \frac{1}{48}\overline{i_g^2}Z_{\pi g}^2 g_m^2 (N+1)^3 R_L \quad (2.32)$$

.

Dividing by $kTBG_{fwd}$ gives the intrinsic noise figure of the π-based DA

$$F_\pi = 1 + \left[\left(\frac{1}{N+\frac{3}{5}}\right)\left(\frac{\sin(N+1)\beta}{\sin\beta} - \frac{2}{5}\cos N\beta\right)\right]^2 + \frac{4}{g_m^2 R_S R_L\left(N+\frac{3}{5}\right)^2} + \frac{4\gamma}{g_m R_S\left(N+\frac{3}{5}\right)} + \frac{\omega^2 C_{gs}^2 Z_{\pi g}^2 \delta (N+1)^3}{3 g_m R_S\left(N+\frac{3}{5}\right)^2}. \quad (2.33)$$

We approximate the final term for $N>1$ by dividing out the polynomials of N and dropping terms containing negative powers of N so that (2.33) becomes

$$F_\pi = 1 + \left[\left(\frac{1}{N+\frac{3}{5}}\right)\left(\frac{\sin(N+1)\beta}{\sin\beta} - \frac{2}{5}\cos N\beta\right)\right]^2 + \frac{4}{g_m^2 R_S R_L\left(N+\frac{3}{5}\right)^2} + \frac{4\gamma}{g_m R_S\left(N+\frac{3}{5}\right)} + \frac{\omega^2 C_{gs}^2 Z_{\pi g}^2 \delta\left(N+\frac{9}{5}\right)}{3 g_m R_S}. \quad (2.34)$$

Applying the same assumptions and procedure, the noise figure of the conventional T-based DA is

$$F_T = 1 + \left(\frac{\sin N\beta}{N\sin\beta}\right)^2 + \frac{4}{g_m^2 R_S R_L N^2} + \frac{4\gamma}{g_m R_S N} + \frac{\omega^2 C_{gs}^2 Z_{\pi g}^2 \delta \sum_{r=1}^{N}(N+1-r)}{g_m R_S N^2} \quad (2.35)$$

And similarly approximating the final term gives

$$F_T = 1 + \left(\frac{\sin N\beta}{N\sin\beta}\right)^2 + \frac{4}{g_m^2 R_S R_L N^2} + \frac{4\gamma}{g_m R_S N} + \frac{\omega^2 C_{gs}^2 Z_{\pi g}^2 \delta\left(N+\frac{3}{2}\right)}{3 g_m R_S}. \quad (2.36)$$

Now we compare (2.34) and (2.36) term by term. The second term of each arises from the input termination and is approximately zero except at DC and cutoff, where both reach a maximum of 1. The third and fourth terms are from the output termination and drain currents, respectively, and we clearly see the additional gain of the π-based circuit suppresses the noise sources at the output just as we would expect. The final term, due to gate induced noise, is slightly larger for the π-based circuit. The difference is unlikely to prove significant because for large *N*, both (2.34) and (2.36) approach the same value

$$F = 1 + \frac{4\gamma}{g_m R_S N} + \frac{\omega^2 C_{gs}^2 Z_{\pi g}^2 \delta N}{3 g_m R_S}. \tag{2.37}$$

It bears noting the difference between (2.36) and the result obtained in [33]. In his analysis, the author assumed the frequency dependant impedance $Z_{\pi g}$ to be the source impedance and similarly $Z_{\pi d}$ to be the load. This is valid because such frequency dependant impedances are easily approximated using m-sections. Here however, we include the detail of the m-sections in the intrinsic analysis, hence the slight discrepancy in the cancellation of factors. Also, our approximation in the last term from (2.35) to (2.36) is slightly more precise than in [33], to capture more accurately the subtle difference we are illustrating.

2.2.3.9 Other Advantages

In addition to better performance, the π-based topology has a variety of other advantages due to inductor sizing and placement. The proposed topology has only two unique inductor sizes (*L* and *0.3L*), increasing to four if the input and output lines are not identical. The conventional topology has three unique inductor sizes (*L, 0.53L,* and *0.8L*), increasing to six if the input and output need different values. Since inductors are generally difficult to model, especially in the 10's of gigahertz and upward, use of

fewer distinct inductors simplifies the design. This can have a significant impact on the design time as inductor design and layout are the most cumbersome portions of integrated DA design. Another advantage of the new topology is reduced inductor area. The proposed circuit uses two fewer total inductors for any value of *N* compared to the conventional circuit.

2.3 Design Example

To evaluate the performance difference between the conventional and proposed topologies, I designed and fabricated each circuit in 130nm CMOS. Figure 2.5 shows the schematics of both amplifiers. I selected a simple DA to highlight the differences between the two approaches; however more complex techniques such as tapered transmission lines [34] or cascaded gain cells [35] can use the bisected-π matching section as well.

I employ cascode gain cells to provide low output conductance, as is common in CMOS DAs. The cascode transistor does not add significantly to the circuit noise, so the above analysis with a simple FET is still reasonably valid. In each gain cell, the common-source transistor's drain couples to the common-gate transistor's source via a short length of transmission line to flatten the effective gate capacitance over the 20GHz target bandwidth. Both the common-source and common-gate transistors in each gain cell are minimum length with 40x2.5um fingers for low input resistance. For the bisected-π sections at the left and right ends of Figure 2.5(b), the transistors are scaled by 4/5 to 32x2.5um. Spiral inductors with metal ground shields form the artificial transmission lines and I add enough additional capacitance at the drain of each common-gate transistor to equal the common-source gate capacitance. I use interdigitated metal stack capacitors both types of matching sections. According to simulation, N_{max}=4 is the optimal number of gain cells for this process and bandwidth

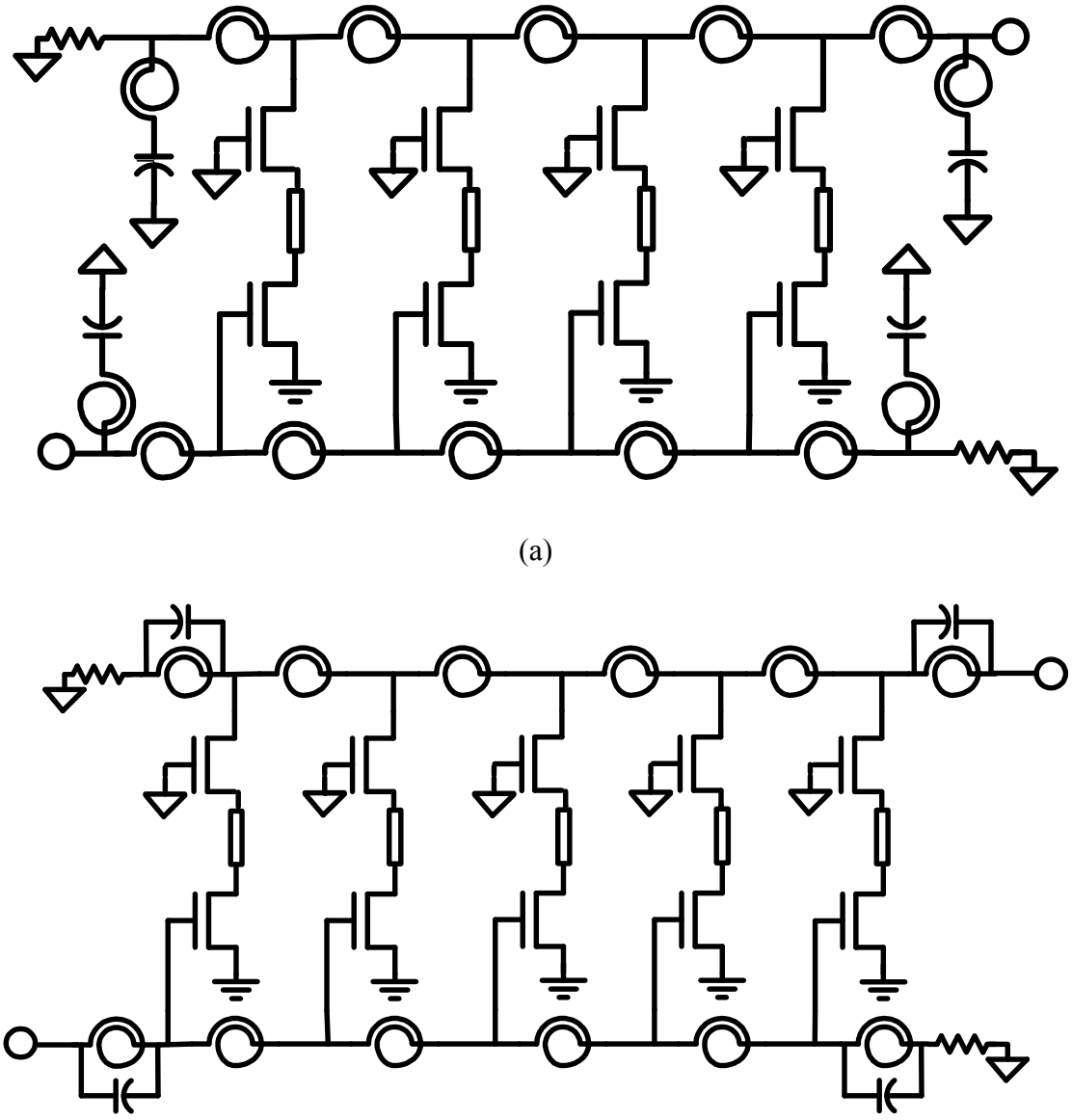

Figure 2.5 (a) Conventional T-based and (b) new π-based DA, both with N=4.

target. Biasing the transistors for maximum f_T, the T-based circuit consumes 30.0mA while the π-based circuit consumes 34.5mA. The additional current consumption is proportional to the additional active device area.

2.4 Measurement Results

Measured gain and noise figure are shown in Figure 2.6. The gain of the π–based circuit is larger than the T-based circuit over the full bandwidth by approximately 1.2dB as predicted in Table 2.1 for N=4. Figure 2.7 shows the gain difference growing larger than 1.2dB near the cutoff frequency. This can be explained by poor matching near cutoff for the T circuit. This poor matching is not inherent to the circuit and is a result of poor modeling or layout of the matching section. Matching and gain flatness theoretically should be the same for both circuits. However, the measured cutoff frequencies are equal at 21.5GHz showing clearly that the gain-bandwidth product is higher for the π-based circuit.

Figure 2.6 and Figure 2.7 also show that the π-based circuit has lower noise across the full bandwidth. This is a function of both the calculated difference in intrinsic noise figure and the smaller inductor, and thus reduced loss, at the input of the π-based circuit. Again I attribute the large difference near cutoff to mismatch in

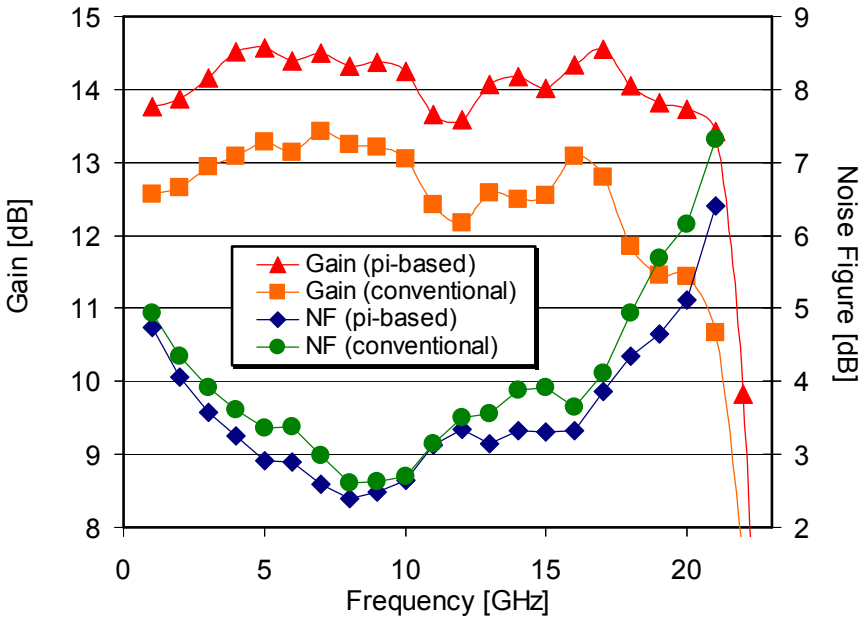

Figure 2.6 Measured gain and noise figure for both circuits.

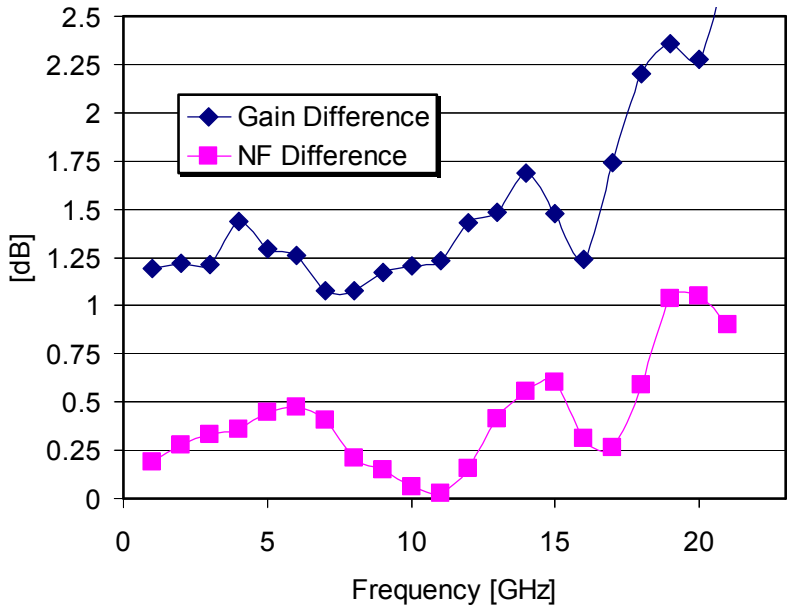

Figure 2.7 Performance difference between both circuits.

the T-based circuit. Die photos in Figure 2.8 illustrate an area reduction of 14%, from 800x1800µm to 800x1550µm including pad area. Without bias pads, as the circuit might appear in an integrated application, the area reduction is even greater at 17%.

These results show conclusively that our new π-based distributed amplifier delivers greater gain in less area in a given process than is possible with conventional

Table 2.2

Performance of Alternative Distributed Amplifiers

	π–based	T-based
Avg. Gain	14.1dB	12.9dB
Gain Ripple	$\pm$0.5dB	$\pm$0.5dB
Bandwidth	21.5GHz	21.5GHz
NF	See Fig. 6	See Fig. 6
DC Power	30.0mA @ 1.2V	34.5mA @ 1.2V
Area	1.24mm^2	1.44mm^2
Technology	IBM 8RF (130nm)	

DA design. This is made possible by utilizing a matching section which performs the appropriate impedance transformation as well as providing additional gain. The π-based DA demonstrated here is a more effective and efficient utilization of monolithic integrated circuit technology. To the best of my knowledge, this is the first demonstration of such a topology in an integrated CMOS distributed amplifier, as well as the first conclusive evaluation of its many benefits for such an application.

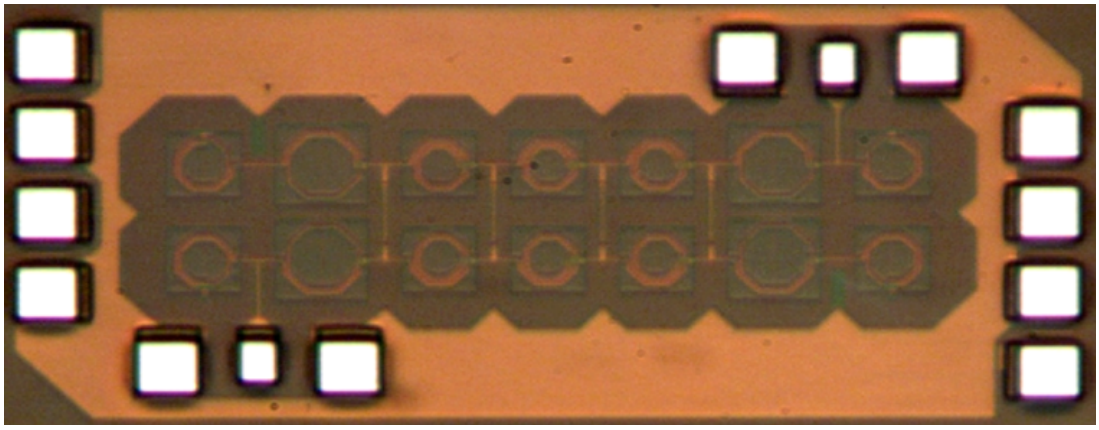

(a)

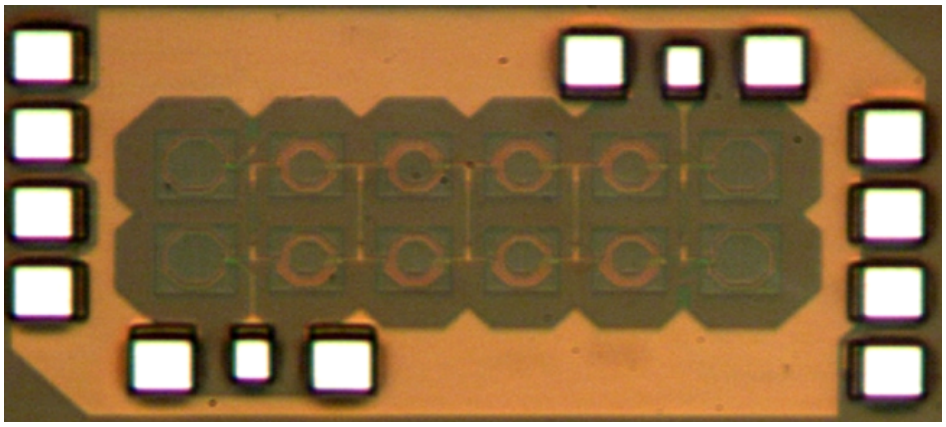

(b)

Figure 2.8 Equal scale die photos of the (a) conventional T-based and the (b) new π-based circuit

2.5 Conclusion

In this chapter, I have proposed and compared a new termination network for an integrated distributed amplifier to the conventional method. The π-based circuit provides increased gain and reduced noise figure over the conventional scheme with the same bandwidth and matching. In addition, a smaller area footprint and use of fewer inductors reduce the cost and design time of the circuit. The only significant tradeoff for the circuit is an increase in power consumption needed to generate the increased gain. This topology is especially well suited to monolithically integrated DA's, in both silicon and III-V technologies.

With demonstrated results which correspond very well with the theoretical prediction, I conclude that this new π-based distributed amplifier is superior to the old T-based topology. Virtually any design employing an *m*-derived matching section will benefit from choosing the π-based circuit. Also, the reduced area may allow some designs to use matching sections which would otherwise have to forgo them. With the flexibility offered in modern integrated processes, the π-based design can be used by designers to best capture the gain and noise performance of a DA as a broadband LNA.

Chapter 3

Blue Noise Active Termination

In Chapter 2, I identified each of the noise sources intrinsic to the distributed amplifier (DA) and quantified their individual contributions to the overall noise figure. One such source, the input line termination resistor, is a significant noise source which can potentially be avoided. In this chapter, I review the methods applied in the past for III-V material systems and more recent methods in silicon CMOS. Each of these has some short coming in terms of gain or matching, trading critical LNA metrics in exchange for the noise reduction. I continue by presenting a novel solution to the input termination noise problem. The technique, called Blue Noise Active Termination (BNAT), combines an active termination for low frequencies and a passive termination for high frequencies, to provide good matching and low noise over the full bandwidth of the DA while only sacrificing power and area. By removing the noise contribution of the input termination resistor, the broadband DA can truly approach minimum noise figure and compete with narrowband techniques like inductive degeneration as predicted by Aitchison in his seminal work on DA noise.

3.1 Input Line Termination Resistor Noise Contribution

Figure 3.1 shows a simple distributed amplifier to illustrate the noise contribution from the input line termination. As the input signal travels along the input transmission line of a distributed amplifier, each of the N gain cells making up the amplifier generates a forward and backward traveling current on the output line. The forward traveling currents are summed in-phase at the output port to produce a signal

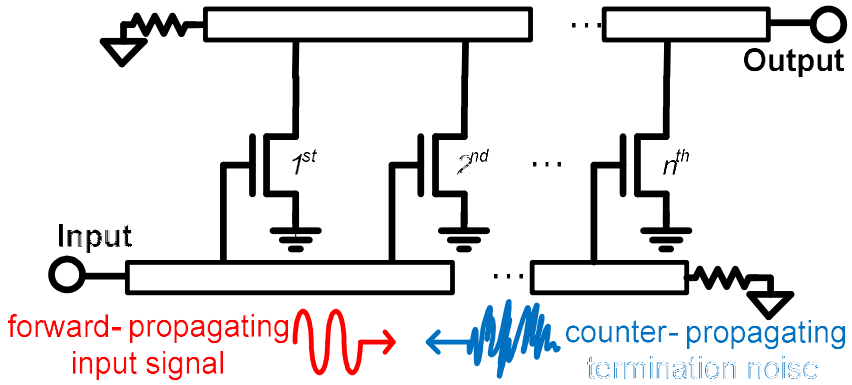

Figure 3.1 Distributed amplifier illustrating the difference between the intended signal and the input line termination noise

larger than any single gain cell could have produced. For a signal originating at the end of the input line, propagating in the opposite direction of the intended signal, the amplified copies from each gain cell will add with mismatched phases at the output. The amount of phase mismatch is a function of frequency, with greater mismatch at higher frequencies.

If we examine the intrinsic noise factor expression ignoring all terms except that originating from the input line termination we have

$$F = \ldots + \left(\frac{\sin(N \cdot \beta)}{N \cdot \sin(\beta)} \right)^2 + \ldots \tag{3.1}$$

where β is the phase constant per section of artificial transmission line and N is the number of sections (gain cells). As shown in Figure 3.2(a), this function is close to unity at DC and near the cutoff frequency of the amplifier and near zero in-between. Practically, non-ideal effects such as skin effect and dielectric loss diminish the high frequency lobe from this expression creating a low-pass rather than band-stop shape, as in Figure 3.2(b). Therefore a low noise termination for a distributed amplifier need only have reduced noise for lowest $1/N^{th}$ of the distributed amplifier bandwidth to eliminate most of the termination noise contribution.

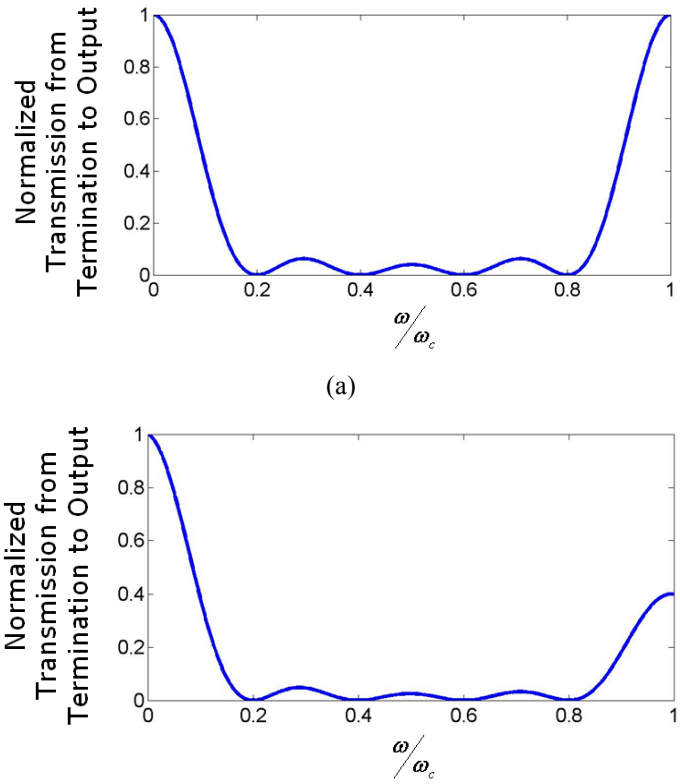

Figure 3.2 (a) Ideal transfer function from input termination to output for N=5 and (b) a more realistic transfer function taking into account skin effect losses. Only the lowest $1/N^{th}$ of the bandwidth sees a significant contribution.

3.1.1 Prior Solutions

This problem of reducing the low frequency noise has been tackled several times over the years, but the effectiveness of different approaches is process and application dependant. The issue was successfully solved for GaAs with an active termination over a decade ago, but a recent surge in interest in CMOS distributed amplifiers has inspired at least three distinct approaches in CMOS over the past two years, including the method presented later in this chapter.

3.1.1.10 Diode Connected FET

Reducing the impact of input termination noise on overall noise figure has been addressed in the past in III-V systems by using a diode connected FET to terminate the input transmission line instead of an ohmic resistor [37]. The FET offers a noise temperature below room temperature, as low as 160K, while maintaining an impedance of 50Ω over the operating bandwidth of the amplifier.

shows how this termination scheme was implemented in GaAs where the noise temperature of a diode connected FET is indeed below 290K. The transistor required some passives to bias it and ensure stability, but the impedance of the termination comes predominantly from the transistor alone. The low frequency noise lobe from the termination is greatly reduced with the active termination compared to an ohmic resistor with minimal impact on gain or matching.

(b) shows exactly the characteristic that I sought to implement in silicon CMOS. Although the source of the effect is disputed, many researchers have shown that the channel noise of sub-micron MOSFETs is enhanced beyond what is predicted by the long-channel theory [38]. In other words, the excess noise factor, γ, is greater than unity in modern CMOS FETs, making the noise temperature of a diode connected MOSFET close to or higher than room temperature and rendering this approach inapplicable to CMOS distributed amplifier design.

3.1.1.11 Frequency Dependant Passives

A recent technique developed by researchers at the University of Waterloo, Ontario, Canada in 2008 for silicon UWB applications is to use an all passive, frequency dependant termination [39]. This termination has high impedance at low frequency to give low noise, and lower impedance at high frequency to improve

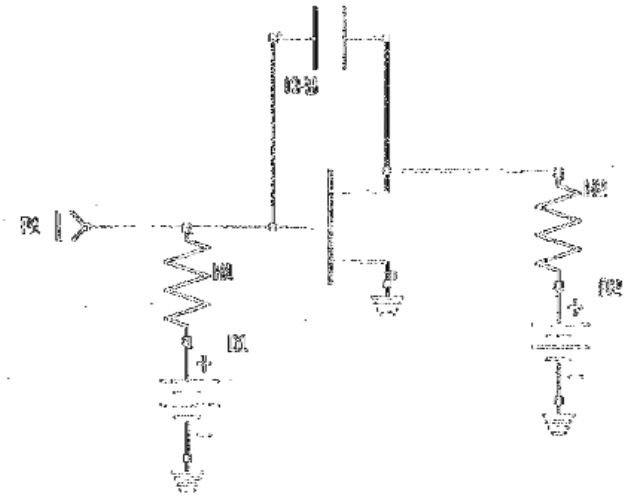

(a)

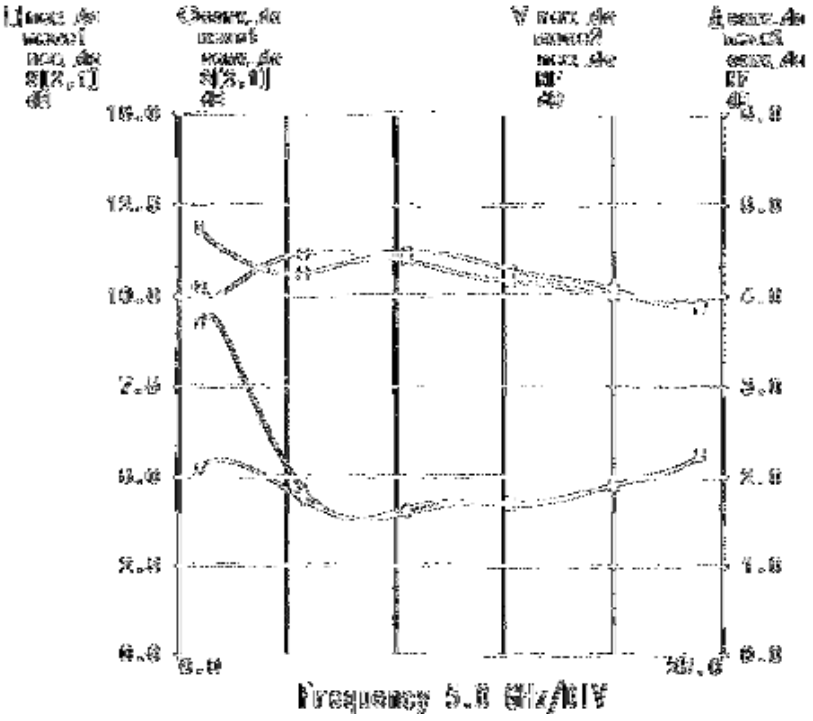

(b)

Figure 3.3 (a) Diode connected GaAs pHEMT active termination, (b) gain and noise figure comparison of a DA with and without active termination, (c) matching with and without active termination [37].

Figure 3.3 (Continued)

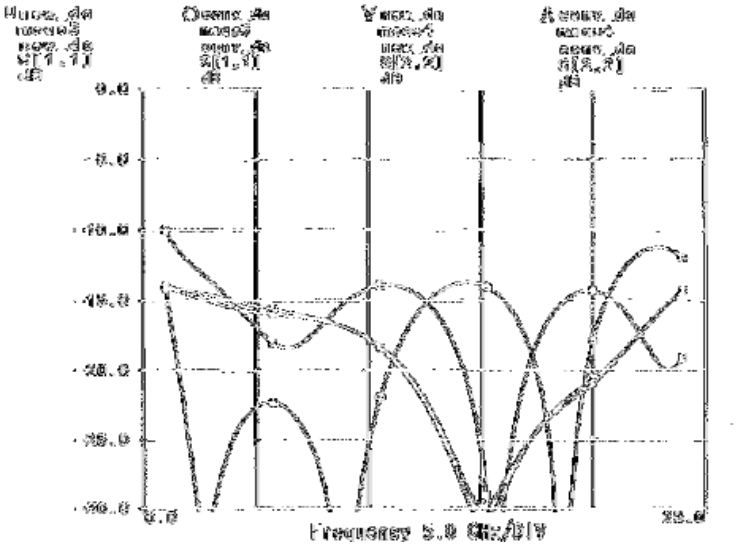

(c)

matching. This is achieved by introducing an inductor which shorts part of a >50Ω resistor at high frequency as shown in Figure 3.4(a). The low frequency degradation of matching was allowed to be as bad as -10dB which corresponded to a noise figure reduction of about 1dB over half of the target bandwidth. While this approach gave a significant noise figure reduction, it did not fundamentally alter the shape of the noise figure curve as profoundly as was possible for an active termination in III-V systems [37].

3.1.1.12 Tapered Input Line

Engineers at BAE Systems developed another solution to this problem for a DA covering the electronic warfare frequency band [5] in 2007. A tapered artificial

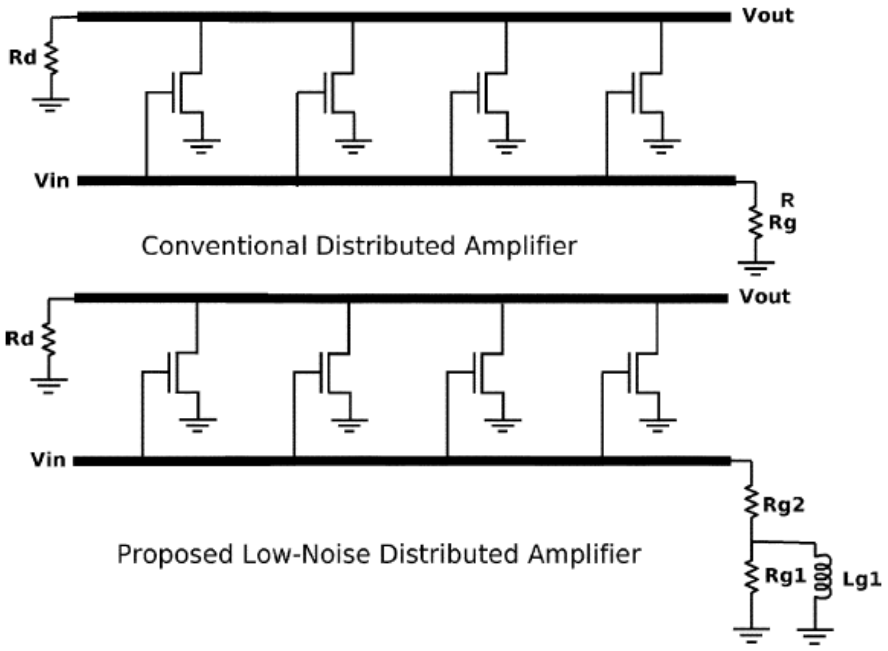

(a)

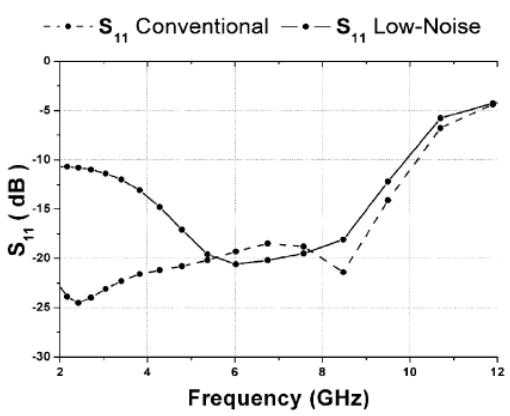

(b)

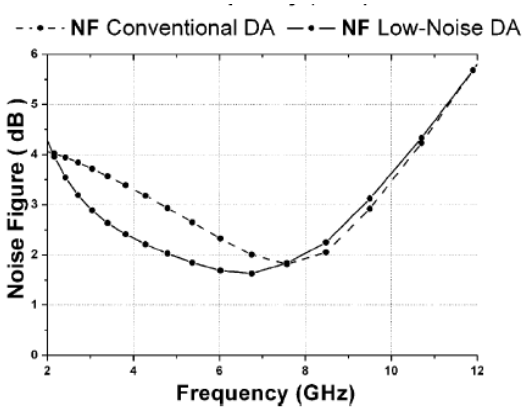

(c)

Figure 3.4 Frequency dependant passive termination from [39]. (a) Conceptual schematic, (b) matching comparison, and (c) noise figure comparison.

transmission line is employed to gradually increase the artificial transmission line impedance so that it can be fed by 50Ω at one end and terminated in 125Ω at the other end. This approach requires the trade off of gain and matching. In the tapered artificial

transmission line, shown in Figure 3.5(a), the capacitors can be as large as 0.20pF, but are tapered down in size while the inductors are tapered up to transform the impedance. The decrease in capacitance correlates with a decrease in transistor area (when this transmission line is applied to a DA) which will give a reduction in overall transconductance and thus total gain. I estimate that the demonstrated approach sacrifices 11% of possible gain due to tapering transistor size to values smaller than the largest possible for the given bandwidth. The increased skin effect loss from increased inductor size might have also shorted the optimal length of the amplifier, N_{max}.

Figure 3.5(b) reveals some other drawbacks to this method, beyond lost gain. The ripple in the transmission characteristic of the tapered line, while minor, will

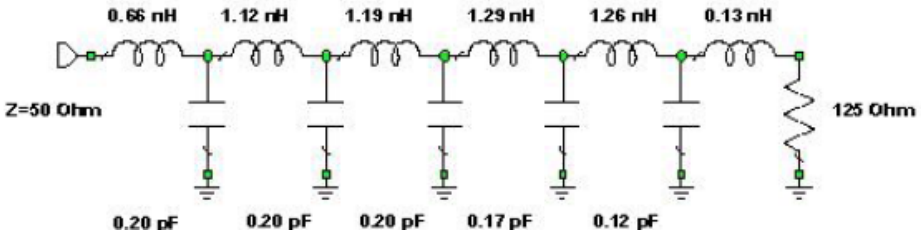

(a)

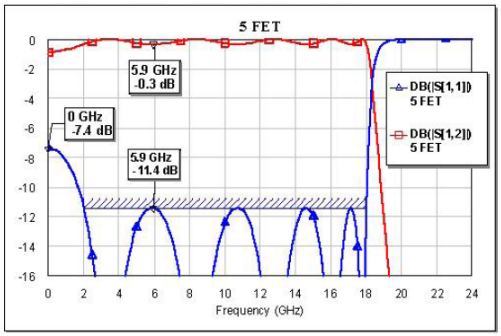

(b)

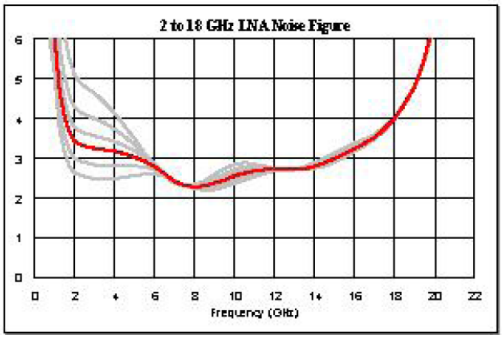

(c)

Figure 3.5 (a) Tapered transmission line (to be a building block of a DA), (b) transmission and matching characteristics, and (c) noise figure curves for terminations ranging from 50Ω to 250Ω, with 125Ω highlighted in red.

translate directly to gain ripple. Also, the impedance transformation of the tapered line doesn't work at low frequency where the inductors are essentially wires. Thus the low frequency matching is severely deteriorated. This may be acceptable in a limited number of applications, but does not provide a general, broadband solution. Figure 3.5 shows the effect of different termination resistors on noise figure, with 125Ω highlighted in red as an acceptable trade off of gain, matching, and noise. This confirms that the tapered line does reduce the low frequency noise figure, but because of gain ripple and matching considerations, the amount of noise reduction attainable is restricted.

3.1.2 New Proposed Solution

The new proposed approach to this problem is to use a hybrid of the active and frequency dependant approaches. While a simple diode connected MOSFET has a high noise temperature relative to room temperature, the shunt feedback amplifier can achieve quite low noise temperature as demonstrated by its use as both a broadband LNA and an optical receiver. The input impedance of the shunt feedback amplifier can be used as a low noise termination similar in concept to the COLFET (cold FET) [41] which uses the input impedance of an inductive degeneration LNA as a lower-than-room-temperature termination. Also like the COLFET, the frequency over which it will be a good termination is limited. At some frequency the real part of the impedance drops and over all frequencies it has non-zero imaginary impedance. However, a passive network can be placed in series which has the complimentary impedance profile, so that the combination sum up to 50Ω real and 0Ω imaginary for the full bandwidth of the distributed amplifier which it is to terminate. This circuit will have a blue-shifted noise spectrum, lower noise temperature at low frequency where the active circuit dominates and room temperature noise at higher frequencies where

the passive network dominates. For this reason, I have named it the Blue Noise Active Termination (BNAT).

3.2 Blue Noise Active Termination

The Blue Noise Active Termination (BNAT) is a hybrid approach, exploiting the frequency dependant noise contribution from the termination to the output. As depicted in Figure 3.6(a), it is composed of two distinct parts, an active section and a passive section.

3.2.1 Active Termination 1-port Network

The active portion of the proposed termination shown in Figure 3.6(a) resembles a shunt feedback amplifier which we will view as a 1-port network rather than an amplifier. To begin the impedance and noise analysis of this feedback network, we can express the components with generalized *y*-parameters as in Fig. 3.3(b), with the

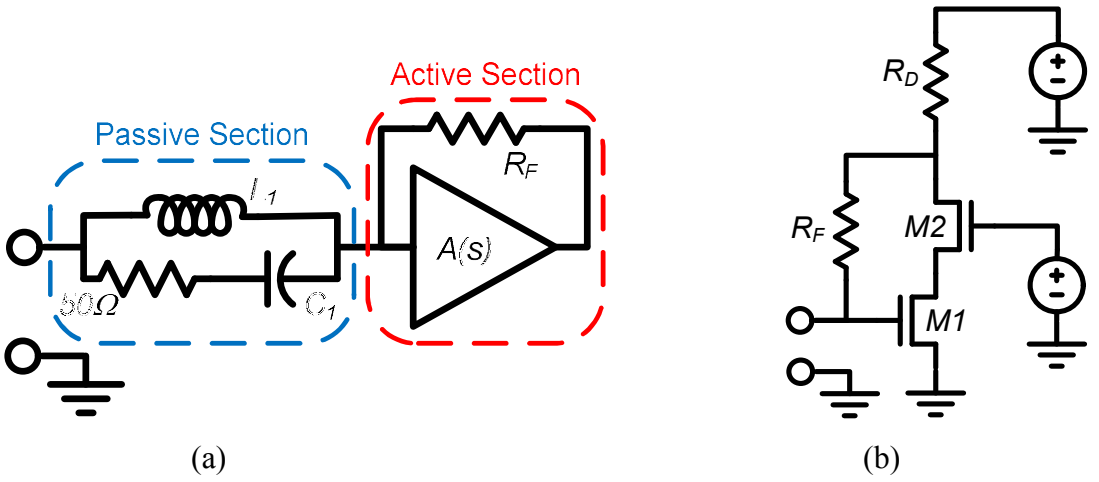

(a) (b)

Figure 3.6 (a) Blue noise active termination (BNAT) and (b) detailed active circuit

subscript *A* representing the forward amplifier and the subscript *F* representing the return feedback path, in this case a resistor. The individual *y*-parameters are shown on Fig. 3.3(b) and the combined *y*-parameters are

$$\begin{aligned} y_{11} &= \frac{1}{R_F} + sC_i & y_{21} &= g_{m1} \\ y_{12} &= -\frac{1}{R_F} & y_{22} &= \frac{1}{R_D} + sC_D \end{aligned} \tag{3.2}$$

if we assume that $R_F >> R_L$ and $g_m >> R_F$. The closed loop input impedance in *y*-parameters is given by

$$Z_{in,CL} = \frac{1}{y_{11}\left(1 - \frac{y_{12}y_{21}}{y_{11}y_{22}}\right)} \tag{3.3}$$

which, after substituting (3.2), becomes

$$Z_{in,CL} = \frac{R_F}{1+g_m R_D}\left[\frac{1+sR_DC_D}{1+s\frac{R_FC_G+R_DC_D}{1+g_mR_D}+s^2\frac{R_FC_GR_DC_D}{1+g_mR_D}}\right] \tag{3.4}$$

which is a second order function with two coupled poles and a zero. The poles are strictly coupled so the zero cannot be placed in any way to reduce the order. The real part of this impedance is designed to be 50Ω to provide the best real part matching

Figure 3.7 shows a simulation of the circuit. The real part of the impedance is 50Ω at DC and peaks a bit before decreasing toward zero. The peaking here is so that the circuit can tolerate the additional parasitic capacitance which will be introduced by the passive circuit it will be connected to. Also, we see the shape of the imaginary impedance that the passive section will need to provide the opposite of. The noise temperature of active termination is as low as 50K at 7GHz.

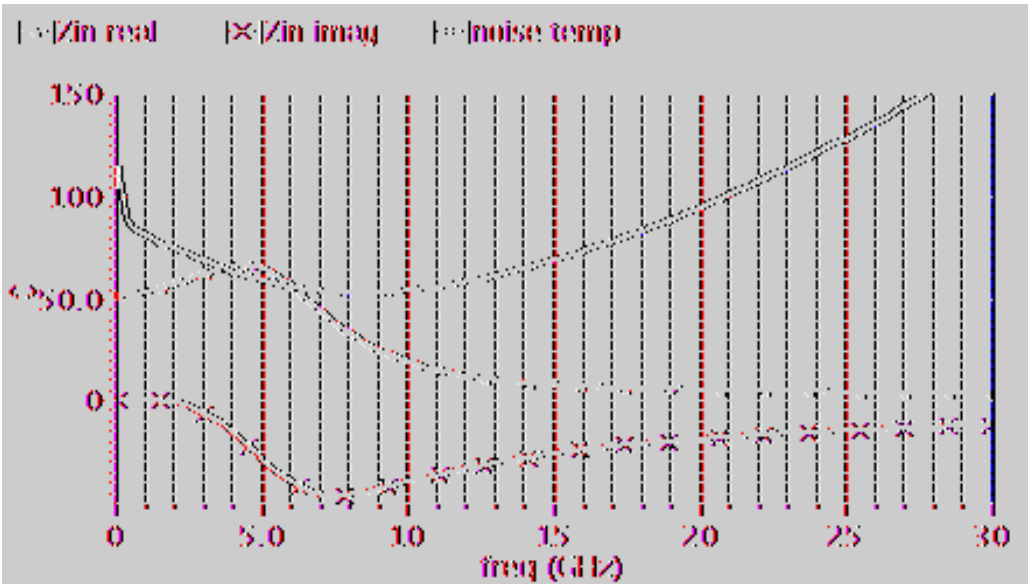

Figure 3.7 Simulation showing the real and imaginary impedance of the active termination as well as its apparent noise temperature.

Looking at this circuit from a noise perspective in Figure 3.6(c) can calculate its apparent noise temperature. We ignore induced gate noise current because the frequency is relatively low. Here the gain A is

$$A = -\left(g_{m1} - \frac{1}{R_F}\right) \cdot R_D \| R_F \approx -g_{m1} R_D \tag{3.5}$$

and the available noise power from this one-port is given by

$$P_{N,available} = kTB \cdot \frac{1 + \frac{1}{g_{m1} R_F} \cdot \left(\gamma - \frac{1}{A}\right)}{1 - A} \approx \frac{kTB}{1 - A} \tag{3.6}$$

where k is Boltzmann's constant, T is temperature, B is the bandwidth, and γ is the transistor excess noise coefficient. This is clearly an improvement if the gain is chosen to be as large as possible for the bandwidth of matching required. When the bandwidth of this termination circuit is exceeded it becomes a short to ground and no longer delivers noise power to the transmission line it terminates.

3.2.2 Passive 2-port Network

Above we have developed a 1-port termination which has 50Ω real impedance and a noise temperature below 290K at low frequency, but becomes a short at high frequency. We now must synthesize a 2-port passive network with a complementary impedance characteristic that will be placed in series with our termination to provide high frequency matching once the active circuit becomes an RF short. Figure 3.7 shows that the active termination impedance is second-order low-pass and Figure 3.8 has the requisite complementary impedance profile. Figure 3.6(a) shows the *LRC* circuit which implements this impedance profile. The inductor L_1 shorts the 50Ω resistor below the corner frequency of the active termination and becomes an open at higher frequencies. The capacitor C_1 is needed to create the second order shape that will complement the active termination. For frequencies where the resistor is contributing to the total impedance, it is also contributing noise power. In other words,

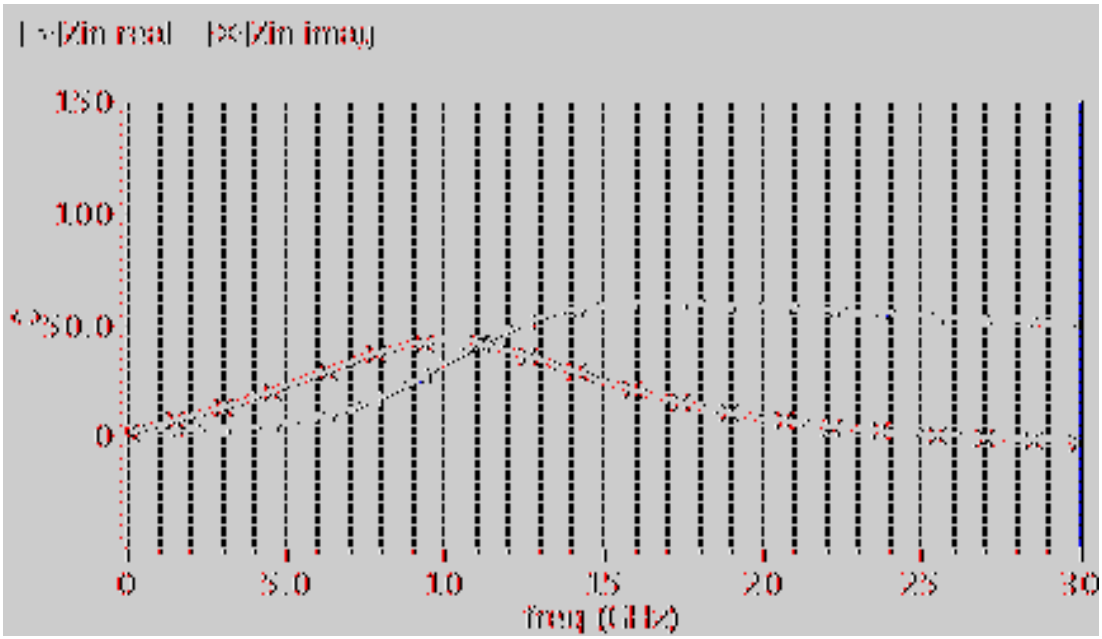

Figure 3.8 Simulation of *LRC* impedance. It is approximately complementary to the active section.

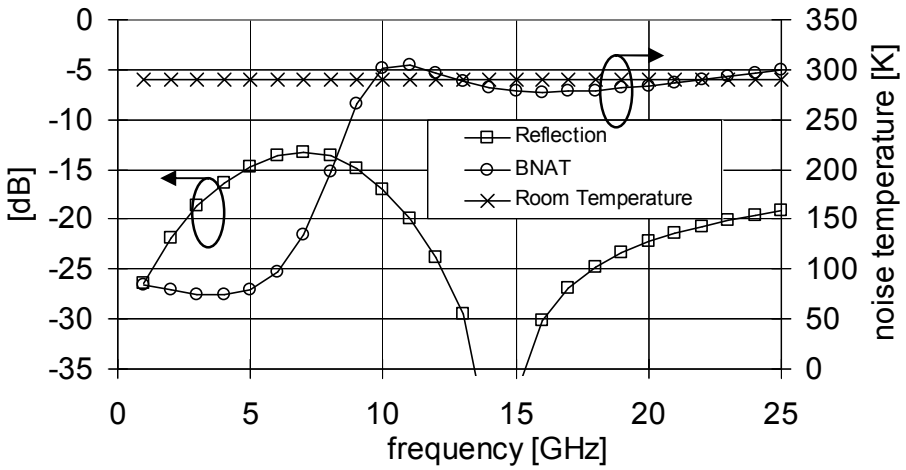

Figure 3.9 Simulated reflection coefficient and noise temperature of blue noise active termination (BNAT) in 180nm CMOS

at high frequencies the resistor is the dominant impedance and contributes the normal thermal noise of an ohmic resistor.

The simulation in Figure 3.9 shows that this combined active and passive termination matches 50Ω over a much broader bandwidth than the passive circuit alone and has a noise spectrum that is blue shifted rather than white. The noise temperature reaches a minimum of 73K at 4GHz, 75% less noise than an ohmic resistor, and levels off above 10GHz to very near room temperature.

3.3 Distributed Amplifier with Blue Noise Active Termination

Two distributed amplifiers were designed and fabricated in 180nm CMOS to demonstrate the effectiveness of this technique. Cascode gain cells are employed to reduce channel length modulation loss in the output transmission line. Transistors are 96μm/180nm, arranged into 24 fingers to reduce series gate resistance. A section of transmission line couples each common-source transistor's drain to the cascode's source. The cascode gates are biased through a 16Ω resistance which creates a small

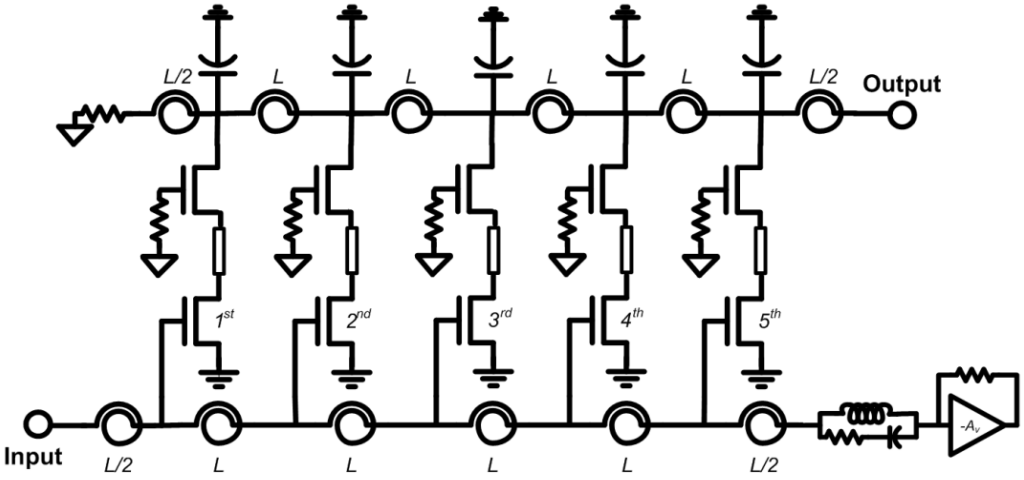

Figure 3.10 Schematic of a CMOS distributed amplifier with BNAT.

negative resistance to offset some of the input line loss. Five gain cells are interconnected by spiral inductors to form artificial transmission lines with the input line terminated in an ohmic resistor in the first amplifier and a blue noise active termination in the second amplifier. Figure 3.11 shows a die photo of the second distributed amplifier with the novel termination. The output line could have been terminated in a blue noise active termination as well, but since the noise from that termination sees no gain its relative contribution to total output noise is insignificant. Figure 3.12 shows an average gain of 12dB and bandwidth of 21.5GHz for both amplifiers. The circuit with our novel termination does not show any degradation of

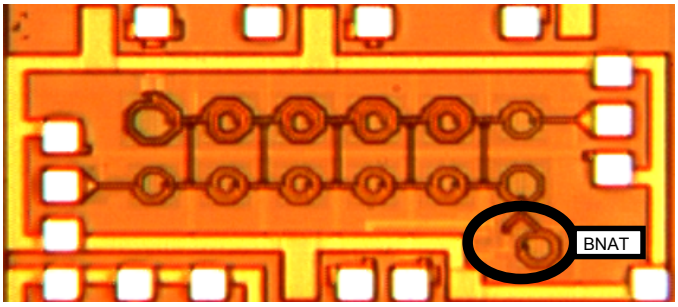

Figure 3.11 Die photo of CMOS distributed amplifier with BNAT circled

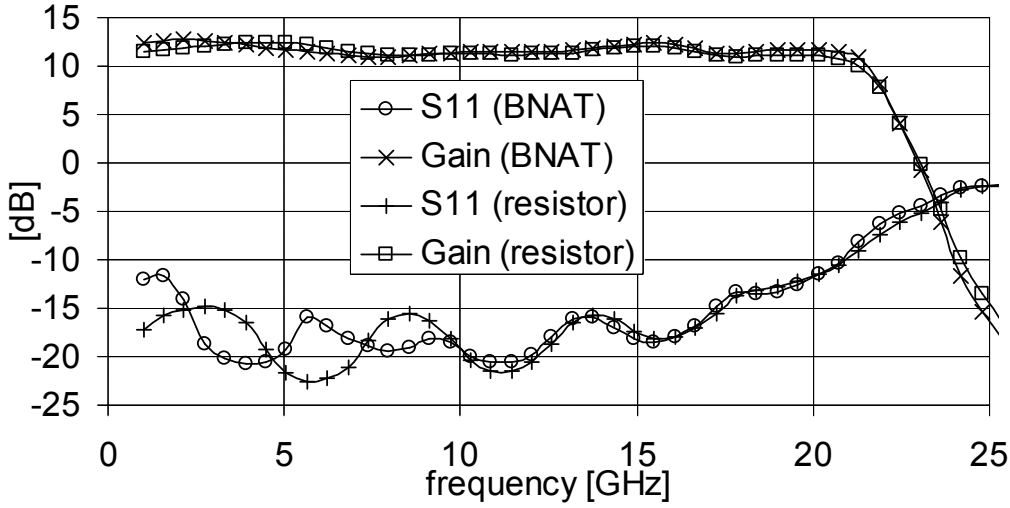

Figure 3.12 Comparison shows no significant impact on measured gain or matching

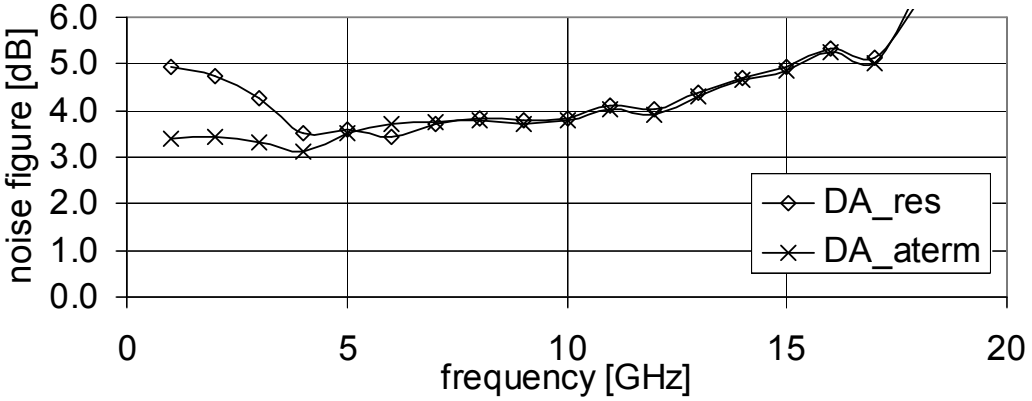

Figure 3.13 Measured noise figure shows significant improvement for low frequency and equal performance at higher frequencies

gain or matching over the full bandwidth of the amplifier. Figure 3.13 shows the noise figure of each amplifier. We clearly see the effect of our termination network as a noise figure reduction of up to 1.5dB (44% noise factor reduction) at 1GHz. The noise performance below 5GHz is improved with this type of termination; however noise performance at higher frequencies shows no difference as the amplifier noise figure

approaches the intrinsic noise figure of the gain cells. This agrees well with our theoretical prediction of noise improvement with this network. Total power dissipation in the gain cells of each amplifier is 160mW, while the BNAT consumes an additional 64mW.

3.4 Conclusion

In this chapter, I have developed the theory for, simulated, and experimentally measured a Blue Noise Active Termination circuit for terminating the input transmission line of a distributed amplifier. The topology makes active termination a viable noise reduction technique for CMOS distributed amplifiers and by extension can provide further improvement upon active termination techniques in GaAs and other microwave circuit technologies. By reducing the input termination noise contribution, the DA noise figure is dominated entirely by the transistor noise as well as the skin effect losses of the inductors.

Chapter 4

Distributed Amplifier as a Dispersive Delay Line

Thus far in this dissertation, I have discussed the distributed amplifier explicitly as an amplifier. In this chapter I will introduce the concept of dispersion, the DA's dispersion characteristic, and how a DA can be viewed as a dispersive delay line (DDL) and employed for analog signal processing.

Data conversion between the analog and digital domains is the primary bottleneck to employing more robust and flexible digital techniques and fewer analog circuits in communication systems such as software defined radio (SDR) [48]. Since the data conversion process and ultimately communication channels themselves are fundamentally analog, several analog techniques have the potential to support and augment the move to a more digital world. Specifically, the dispersive delay line (DDL) is a basic building block for many analog processors including time manipulation for ultra-wideband (UWB) signals, real-time spectrum analysis [60], compressive receivers [61], and temporal imaging/time-stretching [44][45], all of which support trends towards more heavily digital communication systems. The following several sections will introduce dispersion and an example of an analog signal processing system, followed by how the distributed amplifier topology can be manipulated into an effective DDL to enable such processors on the integrated circuit size scale.

4.1 What is Dispersion?

Dispersion has several different meanings, depending on the context. From a circuits and systems perspective, a dispersive system has a group delay that changes with frequency [51]. In other words, dispersion is a non-linear phase response. For a transfer function, $H(\omega)$, with a group delay function, $\tau_g(\omega)$, a dispersive system would have the property

$$\tau_g(\omega) = -\frac{\partial}{\partial\omega}\angle H(\omega) \neq \text{constant}. \tag{4.1}$$

Note that a non-linear phase response does not make the system non-linear in general. Dispersion is classified as linear distortion because its effects are not a function of signal amplitude and theoretically (though not always practically) can be reversed by a linear equalizer. In general, any circuit incorporating reactive elements will have a dispersive response. Dispersive delay line, or DLL, is simply a common name for a device or medium which has a dispersive propagation characteristic.

4.2 Consequences of Dispersion

Consider a hypothetical DDL with a flat amplitude response and a linear group delay, as described by the plots of Figure 4.1. An impulse, with many frequency components in a short time window, will be broadened in time by the dispersion. In the example of Figure 4.2, the high frequency components emerge from the system after a longer delay than the low frequency components. Ideally, a system with the same dispersion slope, but opposite sign, can recompress the broadened pulse back to the original narrow pulse. A second consequence of dispersion on pulses affects the amplitude. If we have a time limited pulse with energy, E, and spread that energy over a longer time period with dispersion, then conservation of energy dictates that the corresponding amplitude must be reduced. Even though the amplitude response of our dispersive

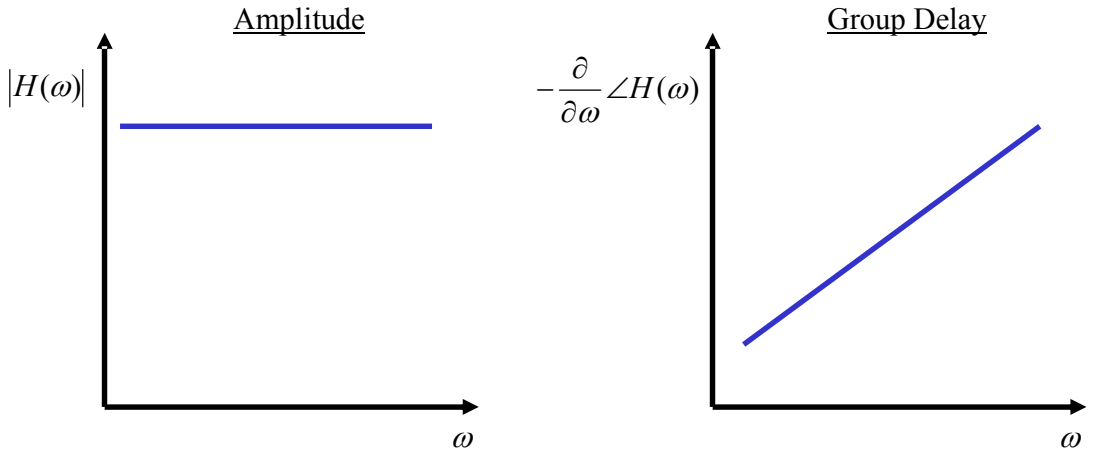

Figure 4.1 Ideal dispersive system.

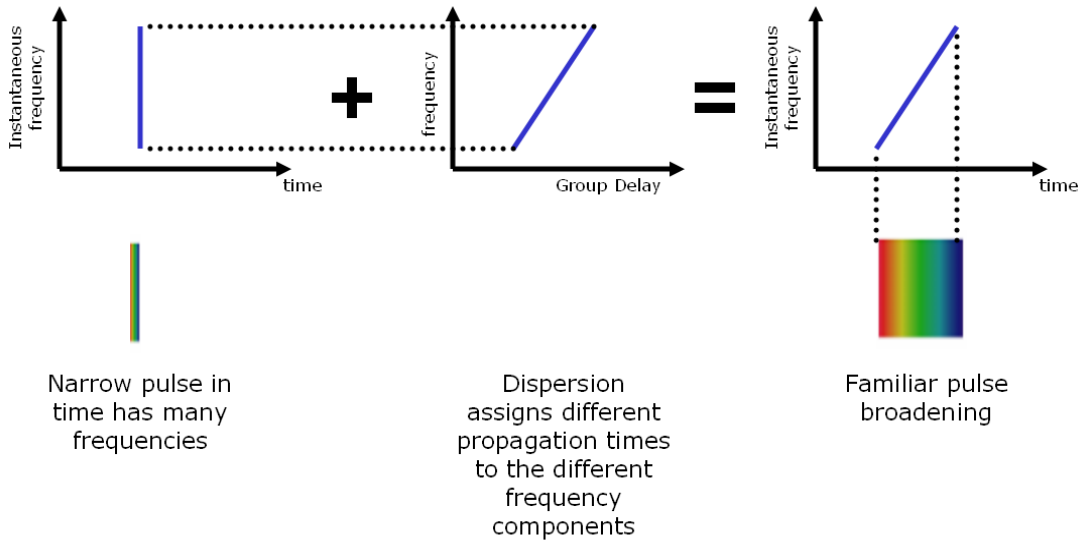

Figure 4.2 Effect of dispersion on a narrow impulse. The colors of the rainbow are used as a visual representation of frequency.

system is flat, the temporal amplitude of our signal can be changed while the magnitude of the power spectral density stays the same.

Having identified what dispersion and a DDL are, we should take a moment to look into an application. As noted above there are numerous applications for DDLs, but in the following section we will look specifically at temporal imaging in detail.

This introduction forms a foundation and motivation for the analysis to follow. Ultimately this chapter will conclude with a demonstration of a temporal imager employing a distributed amplifier based DDL.

4.3 Introduction to Temporal Imaging

The term "temporal imaging" refers to an analogy to optical imaging, illustrated in Figure 4.3. The same differential equations which govern paraxial optical imaging govern temporal imaging, through a space-time duality [42]. With temporal imaging we can stretch, compress, or reverse time signals similar to how optical lenses can magnify, shrink, or invert optical images.

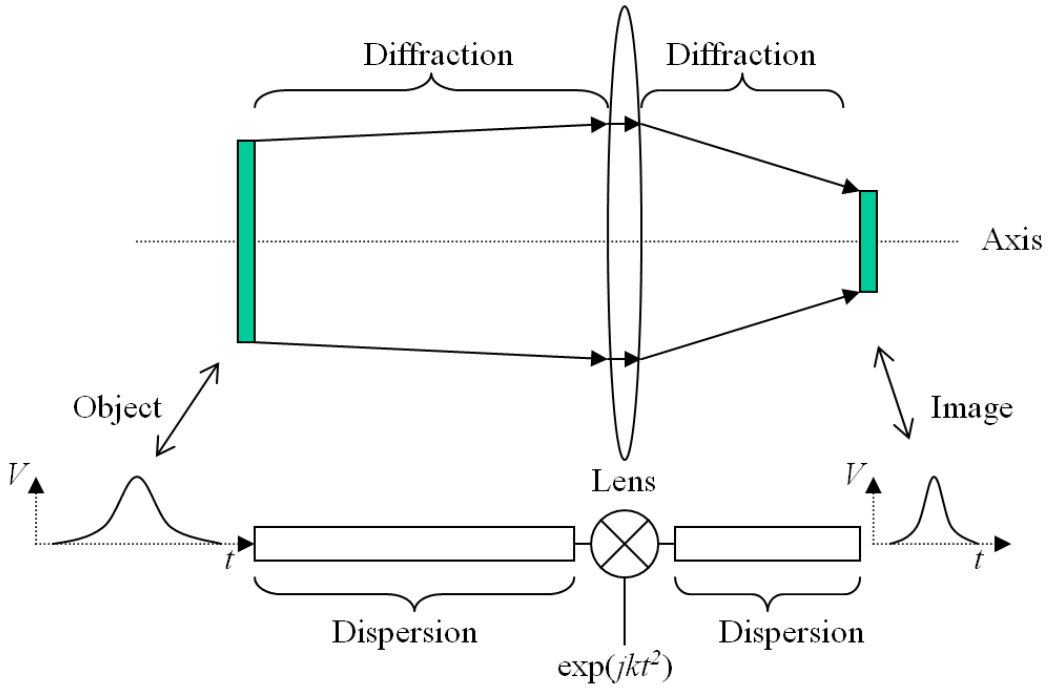

Figure 4.3 Analogy between paraxial optical imaging and temporal imaging. Dispersion plays the same role as diffraction. The "time lens" provides quadratic phase modulation, like a spherical lens in optics.

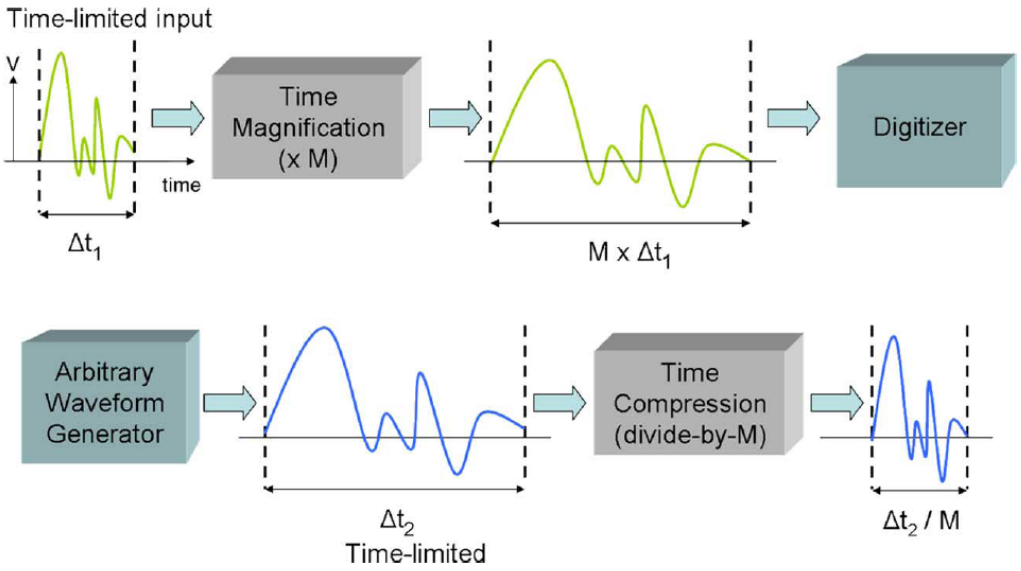

Figure 4.4 Temporal imaging is a way to manipulate the bandwidth of time-limited signals, extending the utility of relatively low frequency devices such as ADCs and AWGs into the microwave range.

Stretching and compressing signals is part of the bandwidth conversion process [43], shown in Figure 4.4. Bandwidth conversion enables the use of relatively low frequency signal processing systems at higher frequencies. For example, the ability to stretch or slow down a signal in time allows an analog-to-digital converter (ADC) to process signals originally containing frequencies much higher than its actual bandwidth and sampling frequency would normally allow [44]. Conversely, time compression allows precision generated waveforms from an arbitrary waveform generator (AWG) to be transferred up to the microwave frequency range [45]. Both of these elements, the ADC and AWG, will play critical roles in future ultra-wideband (UWB) radio and ranging systems [46], as well as the most ambitious software-defined radio (SDR) schemes [47][48]. Countless UWB and SDR systems are emerging which work with or around the shortcomings of modern ADCs and AWGs,

but temporal imaging has the potential to bridge the gap to high bandwidth and reconfigurable systems otherwise unimaginable today [48].

A complete theory of temporal imaging goes back to at least the 1970s [49], with basic pulse compression going back as far as World War II and the early days of radar. Temporal imaging has also been widely explored for the photonic ADC [44], producing conversion rates an order of magnitude higher than conventional electronic ADCs [50]. These high performance systems can afford the complexity, exotic materials, and high cost currently associated with performing temporal imaging functions. Their applications are thus limited primarily to high budget defense operations. However, UWB and SDR are targeted at much wider and ubiquitous markets including wireless communication, mobile handsets, sensor networks, and security/surveillance. Cost, size, and power are critical in such commercial and consumer applications leading to an interest in small, economical temporal imaging techniques as an enabling technology for UWB and SDR to achieve their fullest potential. A scheme for temporal imaging integrated on the same chip as the ADC or AWG would be a boon to realizing the most ambitious UWB and SDR systems.

In this chapter I will introduce the basic concepts of temporal imaging, particularly the role of dispersion. Developing a suitable dispersive medium (i.e. DDL) on-chip will be the first step towards an integrated CMOS temporal imager. I will review existing sources of dispersion and introduce the new, fully integrated dispersion-enhanced distributed amplifier as the highest dispersion-per-unit-length device in the microwave frequency range reported to date, a billion times stronger than common optical fiber. Using the dispersion-enhanced DA, I will demonstrate time stretching and compression of nanosecond pulses in a simplified, proof-of-concept single chip temporal imager.

4.3.1 Sources of Dispersion

There are several well known sources of dispersion, some of which are employed in the high performance temporal imagers mentioned in the above. However, none to date exist on the scale of a silicon chip. It is my goal to find one which has all the desirable properties of the existing sources but is also able to be integrated in a CMOS chip. To that end, we should first review the existing sources of dispersion as well as hypothesize about chip-scale candidate approaches.

In seeking a chip-scale dispersive medium, I will express dispersion, D, on a *per unit length* basis

$$D = \frac{\Delta\tau_g}{BW \cdot L} = \frac{\sigma}{L} \text{ [ns/GHz/m]} \tag{4.2}$$

where $\Delta\tau_g$ is the group delay variation in nanoseconds, BW is the bandwidth in gigahertz, and L is the propagation length or device size in meters. The dispersion rate, σ, is the slope of the group delay vs. frequency curve. This is similar to how dispersion is expressed for optical fiber (a well known dispersive medium) though in different units. This per unit length metric will facilitate comparison of the relative strength of a chip-scale dispersive medium to more familiar, but physically larger sources of dispersion.

4.3.1.13 Dispersion in Optical Fiber

Perhaps one of the best known sources of dispersion is optical fiber [52]. Optical communication is based on sending relatively short optical pulses down very low loss, but very long fibers. Optical fiber is an excellent approximation of the hypothetical dispersive system used as an example in section 4.2.

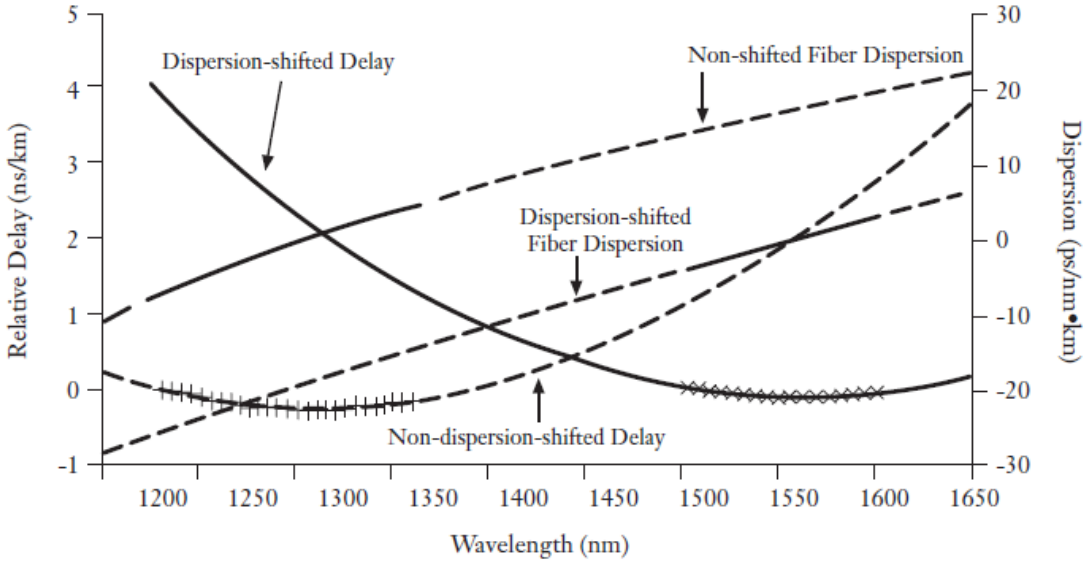

Figure 4.5 Dispersion of typical optical fiber. Material dispersion and waveguide dispersion both contribute to the total chromatic dispersion [20].

Figure 4.5 shows a common dispersion profile for single mode optical fiber. The dispersion has a non-constant, but gentle grade over a very wide optical bandwidth. When optical pulses are sent down the fiber, this dispersion causes a slow broadening of the optical pulses, which can ultimately cause inter-symbol interference where one pulse stretches until it overlaps with the pulse behind it in the fiber. It takes several kilometers for dispersion on the order of nanoseconds to accumulate, but the loss is still very low over such distances. Optical dispersion is expressed as ps/nm-km, though I would like to compare it to other dispersions in units of ns/GHz/m. Selecting 1300nm from Figure 4.5, the dispersion is -20ps/nm-km in common units which translates to approximately $1x10^{-7}$ns/GHz/m in my selected units.

This optical dispersion has been used specifically for time stretching in the photonic ADC [44]. In these systems, light serves as a carrier for the microwave signals being manipulated. The combination of low loss and dispersion allow for nice

temporal imaging effects. However, photonic ADC systems are quite large compared to an integrated circuit since they employ temperature controlled lasers, $LiNbO_3$ modulators, and the stretching happens in spools of fiber several kilometers long. Even though they achieve unparalleled performance, the large size and cost of these systems ultimately relegates their applications to the research laboratory.

4.3.1.14 Chirped Bragg Gratings

A chirped fiber Bragg grating (FBG) is a special type of optical fiber used specifically to generate high dispersion [53]. The refractive index of the fiber is alternated quasi-periodically, with the period increasing as a function of distance (called chirp). Figure 4.6 illustrates that as waves propagate, they will reflect off of the index discontinuities. Where the grading period corresponds to constructive interference for a particular wavelength, that wavelength will be reflected back toward the input of fiber. Since the grating is chirped, different wavelengths travel different distances before being reflected back. This creates dispersion, because different wavelengths experience different round-trip travel times. Calculating from the numbers in Table 4., the dispersion of a chirped FBG is on the order of $5x10^{-4}$ ns/GHz/m [43]. This generates

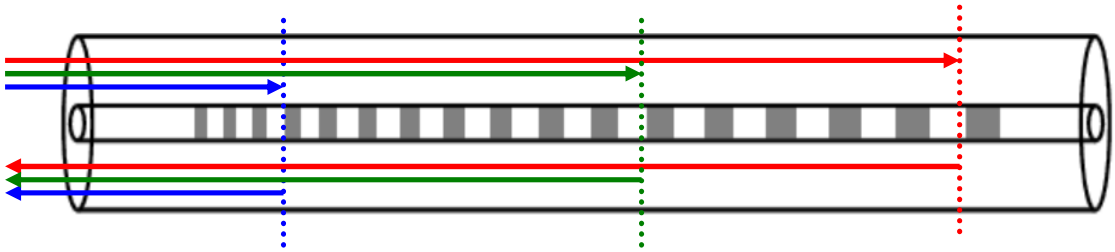

Figure 4.6 Chirped Fiber Bragg Grating. Different wavelengths experience different travel times, creating strong dispersion. An optical circulator is used to isolate the incoming and outgoing waves.

Table 4.1
Comparison of Commonly Chirped Structures [43]

Device/Criteria	Medium	Typical Delay Slopes	Typical Bandwidths (center frequency)	Dimensions	Typical Insertion Loss
Chirped Fiber Bragg Grating	Optical	100 ps / nm	THz (optical regime - hundreds of THz)	~10 cm / ns delay	~ 3 dB (includes optical circulator)
Chirped Surface Acoustic Wave	Electrical / Acoustic	10 – 40 μs / MHz	Up to ~ 1 GHz (~ 1 GHz)	1-2 mm^2	~ 20 dB
Chirped EBG	Electrical	0.1-2 ns / GHz	Up to 15 GHz (5 - 15 GHz)	~10 cm / ns delay	~ 7 dB (includes 6 dB coupler)

substantial improvement over conventional fiber, a factor of about 5000, reducing the fiber length from kilometers to meters. Obviously though, this still involves large optical components and electro-optic transduction.

It is even better for microwave signal processing to keep everything in the microwave regime. Figure 4.7 shows a chirped electronic Bragg grating (EBG) [43]. This structure is inspired by the chirped FBG, except here the characteristic impedance of a transmission line is quasi-periodically chirped so that microwave frequencies reflect from different distances into the structure. This chirped EBG was used in the first demonstration of an all electronic temporal imaging system [2]. The removal of all optical components is a great reduction in complexity and the dispersion is very high at 1.8ns/GHz/m. Unfortunately this device is based on travelling wave principles which cannot be scaled down to the chip-scale. The wavelengths involved are simply too large. For example, the low end of the UWB range is 3.1GHz with a wavelength of nearly 10cm, an order of magnitude longer than practical chip sizes. In addition, since it is a reflected wave device, a circulator must be used to separate the output signal from the input of the device.

Finally on the topic of chirped structures, it bears noting that the chirped surface acoustic wave (SAW) device achieves extremely high dispersion, on the order of 10,000ns/GHz/m. SAW devices are well understood for many pulse manipulation

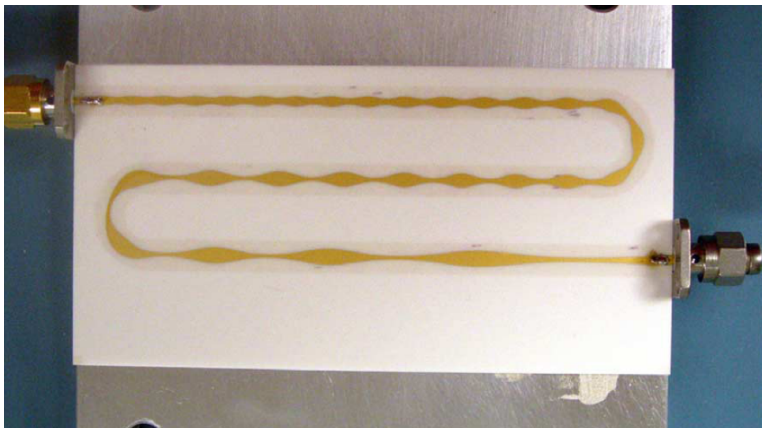

(a)

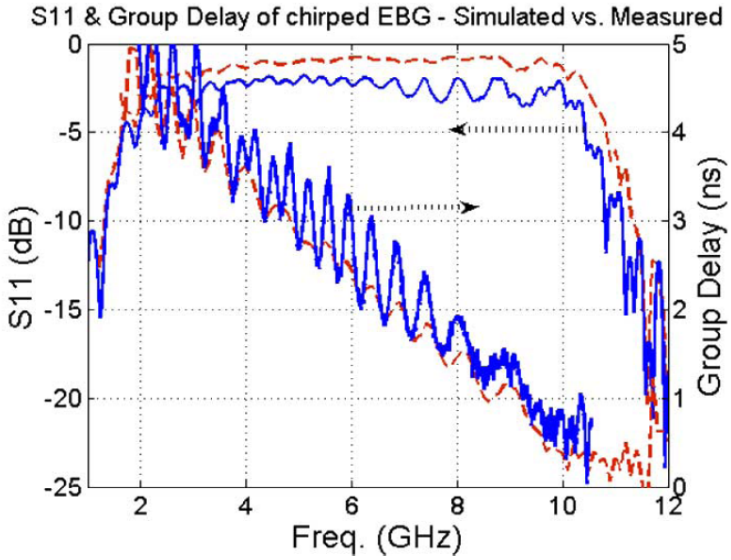

(b)

Figure 4.7 The (a) chirped electronic Bragg grating (EBG) produces a strong (b) dispersion curve in the UWB band [43].

functions [55], however such devices only work in the MHz range [56]. This severely restricts their applicability to temporal imaging of microwave signals.

4.3.1.15 Resonators

Resonators of all kinds are dispersive, although designers and engineers don't necessarily speak of them in those specific terms. One way to characterize resonance

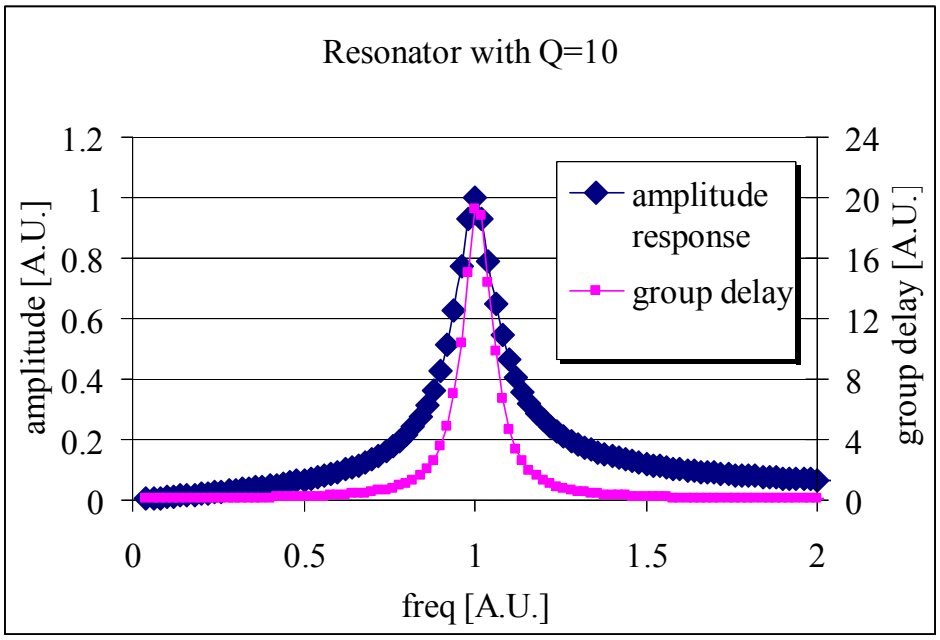

Figure 4.8 Typical resonator with Q =10. The amplitude response is as strong a function as the group delay, making a poor dispersive medium.

is with a "lifetime" which carries slightly different meaning in different contexts. Generally, the concept of lifetime is the time it takes for energy to escape from an excited resonator. Since resonators hold energy at one frequency better than at others, we can infer that the group delay should be much longer at the resonant frequency than at other frequencies. The group delay at the resonant frequency, ω_0, is Q/ω_0

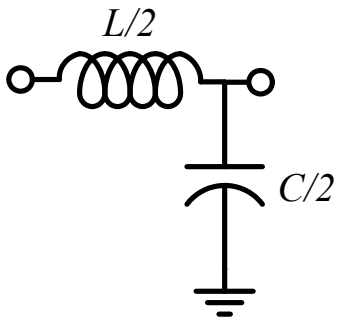

Figure 4.9 The L-section low-pass filter, the foundation for most artificial transmission lines.

where Q it is the quality factor of the resonator and decays rapidly around resonance as in Figure 4.8. This strong dispersive characteristic is attractive, but the amplitude response of a resonator is nearly as strong a function of frequency as the group delay. Resonant circuits might be well characterized on the chip scale, but they cannot produce dispersion without strong amplitude distortion as well, rendering them unsatisfactory as dispersive media. Harnessing the dispersive properties of resonators while mitigating the strong amplitude response would seem an attractive avenue.

4.3.1.16 Artificial Transmission Line

My prior experience with the distributed amplifier led me to investigate the artificial transmission line (ATL) as a chip scale source of dispersion. As discussed in Chapter 2, an ATL is composed of a ladder network of inductors and capacitors. The group delay of an "L" section, the half-section basis of both the "T" and "π" sections, can readily be calculated as

$$\tau_g(\omega) = \frac{\frac{1}{\omega_C}}{\sqrt{1-\left(\frac{\omega}{\omega_c}\right)^2}} \tag{4.3}$$

where ω_c is the cutoff frequency defined as

$$\omega_C = \frac{2}{\sqrt{LC}}. \tag{4.4}$$

The group delay approaches infinity as the frequency approaches cutoff. This equation assumes the lossless case and naturally losses in the reactive elements limit the peak to some finite value. In any case, the transmission theoretically goes to zero at cutoff anyway, so the useful region must be limited to some bandwidth approaching, but still below the cutoff frequency.

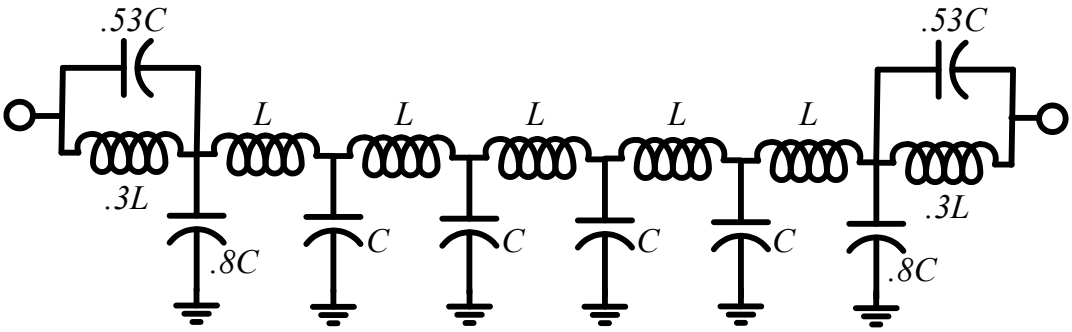

(a)

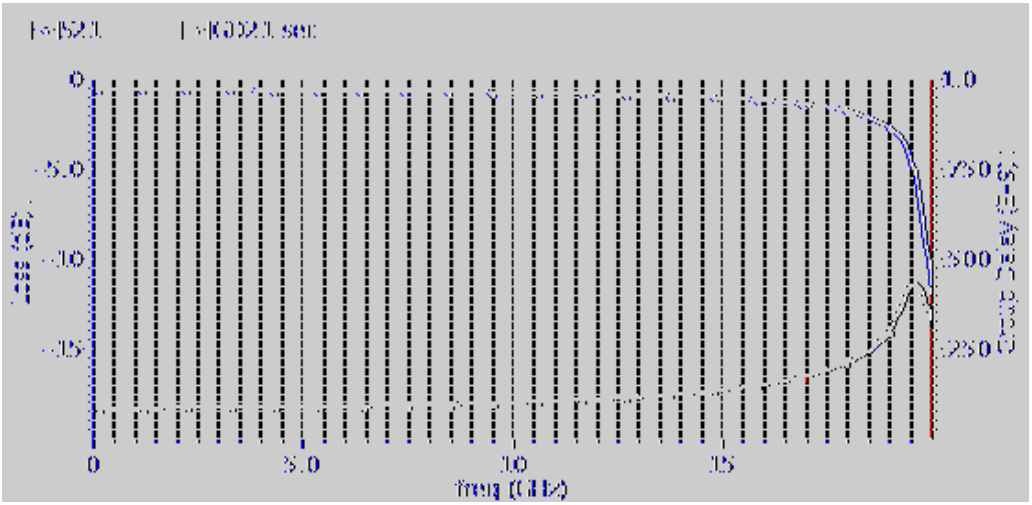

(b)

Figure 4.10 (a) An artificial transmission line and (b) its transmission (S_{21}) and group delay properties including modest and realistic losses.

Figure 4.10 depicts an artificial transmission line, formed of alternating L-sections and terminated with π-type m-derived terminations, as was discussed in detail in Chapter 2. This model includes modest and realistic losses, observable by the gradual degradation of transmission due to skin effect and the finite peak in group delay near the cutoff frequency of 20GHz. This example, with the equivalent of 12 half sections, shows only a modest group delay differential of about 250ps in the range of 15-19GHz, but the small size of integrated spiral inductors means this dispersion is achieved in a very small distance. Estimating 100μm inductor diameter, with a 100μm

pitch from one inductor to the next, the circuit of Figure 4.10(a) is only 1.3mm long and the dispersion is 48ns/GHz/m. This is over 8 orders of magnitude stronger than optical fiber and is implementable in low cost silicon. In the following section, I will introduce an enhancement for this dispersion to increase the dispersion even further.

4.4 Dispersion-Enhanced Distributed Amplifier

We have just observed that the artificial transmission line (ATL) is a good candidate for a chip scale dispersive medium. In this section, I will introduce a dispersion enhancement technique and also show that two ATLs coupled into a DA is superior to a single ATL.

4.4.1 Dispersion Enhancement

A typical ATL is formed of inductors and capacitors in a repeated ladder formation. Far from the cutoff frequency, the ratio of inductance to capacitance is a measure of the impedance of the ATL via the relation

$$Z = \sqrt{\frac{L}{C}} \tag{4.5}$$

and their product is a measure of the group delay though each repeated section

$$\tau_g = \frac{\sqrt{LC}}{2}. \tag{4.6}$$

A frequency dependent inductance and capacitance would allow relatively constant impedance (retain the same ratio) and as well as a frequency dependant group delay (varying product). We see next that resonant tank circuits provide just that.

The impedance of a lossless parallel tank, or resonator, is

$$Z(\omega) = j\omega \frac{L}{1 - \left(\frac{\omega}{\omega_{parallel}}\right)^2} = j\omega L_{eff}(\omega) \tag{4.7}$$

where $\omega_{parallel}$ is the resonant frequency of the series tank. At low frequency the circuit is completely dominated by the inductor. Near to, but still below ω_{series} this impedance is positive imaginary, but increases super-linearly. Similarly, a series tank has the admittance

$$Y(\omega) = j\omega \frac{C}{1 - \left(\frac{\omega}{\omega_{series}}\right)^2} = j\omega C_{eff}(\omega) \tag{4.8}$$

which is positive imaginary and increases super-linearly up to ω_{series}. These circuits give the frequency dependant inductance and capacitance which ought to be able to provide dispersion enhancement. We simply need to replace all inductors in the ATL with a parallel tank and all capacitors with a series tank to create the dispersion-enhanced ATL of Figure 4.11. We can manipulate the resonant frequencies to find

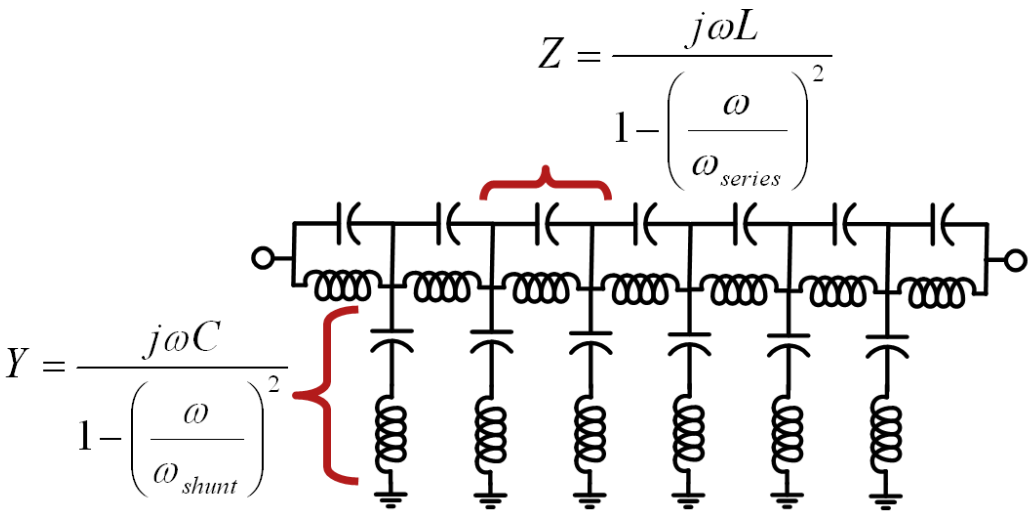

Figure 4.11 Dispersion-enhanced ATL, constructed of tank circuits with resonant frequencies above the cutoff frequency of the ATL.

values where the impedance matching and transmission ripple are acceptable and the dispersion curve is steeper than for a plain ATL.

The group delay function of one L-section of the dispersion-enhanced ATL is given by

$$\tau_g(\omega) = \frac{\frac{\sqrt{LC}}{2}\left(1-\left(\frac{\omega^2}{\omega_{parallel}\omega_{series}}\right)^2\right)}{\left(1-\left(\frac{\omega}{\omega_{parallel}}\right)^2\right)\left(1-\left(\frac{\omega}{\omega_{series}}\right)^2\right)\sqrt{1-\frac{\frac{LC}{4}\omega^2}{\left(1-\left(\frac{\omega}{\omega_{parallel}}\right)^2\right)\left(1-\left(\frac{\omega}{\omega_{series}}\right)^2\right)}}}. \tag{4.9}$$

The pole caused by the expression under the radical occurs at the lowest frequency of all the other poles and zeros and thus determines the cutoff frequency of the ATL. Comparing (4.3) and (4.9), we see that the radical approaches zero (and the group delay approaches infinity) with a higher order function of frequency in (4.6), thus the dispersion curve is steeper.

The only remaining challenge is to select the resonant frequencies. Taking an analytical approach is of limited value, as the derivative of (4.9) is cumbersome. Simulation and optimization proved to be the best approach to select the resonant frequencies. As a starting point, I made the resonant frequencies equal to each other ($1.6\omega_c$) which produces the dispersion curve of Figure 4.12. We can see clearly see that the dispersion in enhanced over that shown in Figure 4.10(b), though it has some ripple and is not smooth. Optimization, by increasing one and decreasing the other resonant frequency while maintaining the same cutoff, led to values of

$$\begin{aligned} \omega_{parallel} &= 1.15\omega_c \\ \omega_{series} &= 2.3\omega_c \end{aligned} \tag{4.10}$$

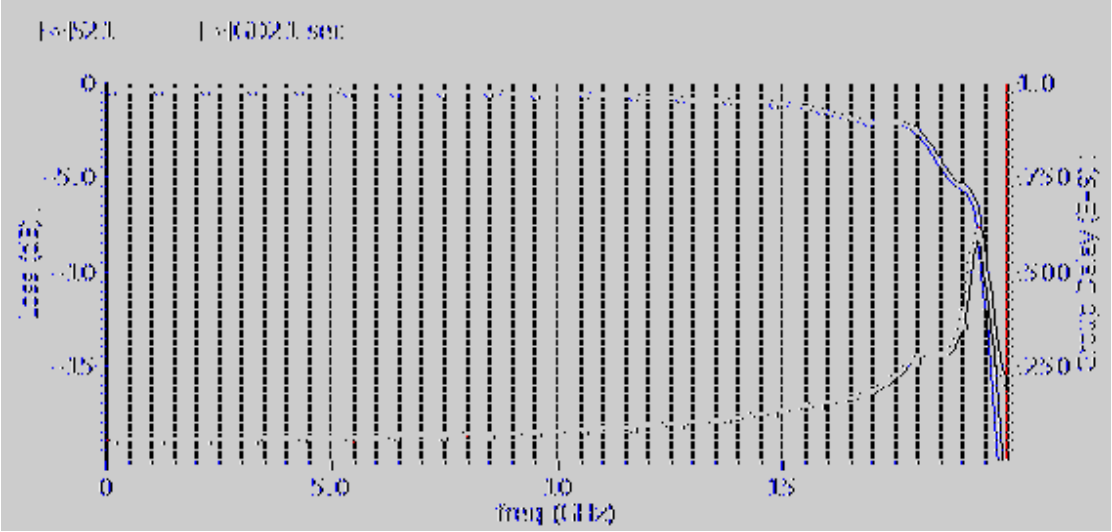

Figure 4.12 Transmission (S21) and dispersion of a dispersion-enhanced ATL with resonant frequencies $\omega_{parallel} = \omega_{series} = 1.6\omega_c$.

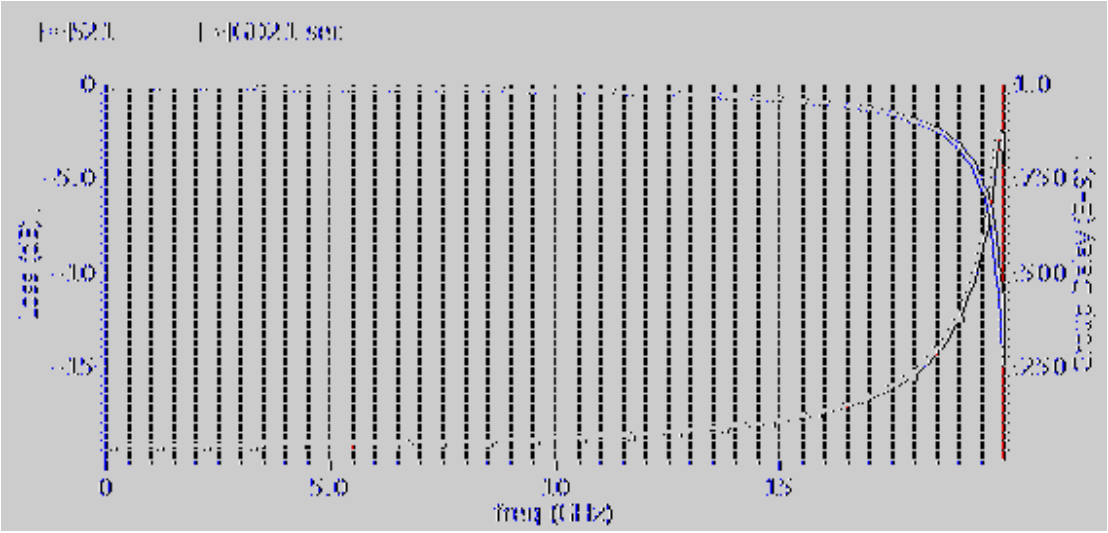

Figure 4.13 Transmission (S21) and dispersion of a dispersion-enhanced ATL with resonant frequencies $\omega_{parallel} = 1.15\omega_c$ and $\omega_{series} = 2.3\omega_c$.

which produce the curve in Figure 4.13. Here we see the dispersion is greatly enhanced over the basic ATL and the gain and dispersion are both smooth. The dispersion is 96ns/GHz/m, double that of a regular ATL. Also, since ω_{series} is so much

greater than ω_c or $\omega_{parallel}$, it really doesn't contribute much to the behavior below cutoff. This allows us to reduce the series tank to just a capacitor with minimal impact on performance.

4.4.2 Dispersion Enhanced Distributed Amplifier

Up to this point, I have only discussed dispersion enhancement in terms of ATLs. However, it is greatly beneficial to use dispersion-enhanced ATLs to build a DA rather than on their own. Figure 4.13 shows that skin effect losses in the ATL cause the transmission to roll off quite rapidly at higher frequencies. This drastically limits the number of sections which can be used before the signal-to-noise ratio (SNR) degrades beyond reasonable usability (~20dB). To counteract this, amplifiers can be periodically incorporated along the ATL or they can simply be built right into the structure in the form of a DA. With the right balance of gain and noise figure, such dispersion enhanced DAs can be cascaded nearly indefinitely, allowing arbitrarily large dispersion at the cost of power and area. An additional feature of the DA configuration is that several peaking techniques exist to combat high frequency losses [57]. Thus the gain can be made much flatter for a DA than an ATL alone. Flat gain prevents unwanted distortion of the signals passing through the dispersion.

4.5 Chirped Pulses

In Section 4.3, I described the analogy between temporal imagining and optical imaging. Thus far, I have only discussed dispersion, the dual of diffraction. We also need a time lens to serve the same role as an optical lens. An ideal time lens is simply a quadratic phase modulator. Since the end goal is to demonstrate the distributed amplifier as a dispersive delay line, I will somewhat simplify the rest of the temporal

imaging system. Instead of following the analogy in Figure 4.3 exactly, I will lump the primary dispersion and time lens into a single block – the chirped pulse generator. In this section I will describe the properties of chirped pulses and explain how they fulfill the role of a time lens in my temporal imaging demonstration.

4.5.1 Chirped Pulses

A chirped pulse is one in which the instantaneous frequency changes monotonically as a function of time. It is essentially a pulse shaped amplitude modulation of a continuously changing, high frequency carrier. A general chirped pulse, *p(t)*, has the form

$$p(t) = A(t)\exp\left(j\phi(t)\right). \tag{4.11}$$

where *A(t)* is the slowly varying pulse envelope and $\phi(t)$ is the strictly non-linear phase function. The instantaneous frequency, $\omega(t)$, is a function of time

$$\omega(t) = \frac{\partial\phi}{\partial t} = \phi'(t). \tag{4.12}$$

The spectrum of this pulse is calculated from the Fourier Transform

$$\begin{aligned} P(\omega) &= \int_{-\infty}^{\infty} p(t)\exp(-j\omega t)dt = \int_{-\infty}^{\infty} A(t)\exp\left[j\left(\phi(t)-\omega t\right)\right]dt \\ &= \int_{-\infty}^{\infty} A(t)\exp\left[j\psi(t)\right]dt \end{aligned} \tag{4.13}$$

which is not trivial to evaluate. We must apply the principle of stationary phase [21], which states that a signal of rapidly changing phase and slowly changing amplitude vanishes from an integral, so we need only integrate where the phase doesn't change. We find the stationary point, $t_0(\omega)$, by setting the rate of change of the total phase of the integrand in (4.13) to zero

$$\psi'(t)\big|_{t=t_0} = \frac{\partial}{\partial t}\left(\phi(t)-\omega t\right)\Big|_{t=t_0} = 0 \tag{4.14}$$

and solving for $t_0(\omega)$. We can then Taylor expand $\psi(t)$ around $t_0(\omega)$ to the second order as

$$\psi(t) = \psi(t_0) + \psi'(t_0)(t - t_0) + \frac{1}{2}\psi''(t_0)(t - t_0)^2 + \cdots \tag{4.15}$$

which by (4.14) reduces to

$$\psi(t) = \psi(t_0) + \frac{1}{2}\psi''(t_0)(t - t_0)^2 + \cdots. \tag{4.16}$$

With this, we can evaluate the spectrum from (4.13) in the vicinity of t_0 as

$$\begin{aligned} P(\omega) &= A(t_0)\exp\left(j\psi(t_0)\right)\int_{-\infty}^{\infty}\exp\left(j\frac{1}{2}\psi''(t_0)(t - t_0)^2\right)dt \\ &= \sqrt{\frac{2\pi}{\psi''\left(t_0(\omega)\right)}}A\left(t_0(\omega)\right)\exp\left(j\psi\left(t_0(\omega)\right)\right) \end{aligned}. \tag{4.17}$$

4.5.2 Linear Chirp and Linear Dispersion

Now, let us plug in a common example of a chirped pulse and see its spectrum. A linear chirp has a constant chirp rate, k, giving a linear change in frequency over time. The phase of a linear chirp, $\phi(t)$, is therefore quadratic

$$\phi(t) = \frac{1}{2}kt^2 \tag{4.18}$$

and the total phase of the transform is

$$\psi(t) = \frac{1}{2}kt^2 - \omega t\,. \tag{4.19}$$

Using (4.14) to find the stationary point, we have

$$t_0(\omega) = \frac{\omega}{k} \tag{4.20}$$

which we can then use to evaluate the final transform in (4.17) as

$$P_1(\omega) = \sqrt{\frac{2\pi}{k}} A\left(\frac{\omega}{k}\right) \exp\left(-j\frac{1}{2k}\omega^2\right). \tag{4.21}$$

There are two remarkable properties of this result. First, the shape of the spectrum (vs. frequency) is the same as the temporal envelope. This means that a chirped pulse with a triangular envelope has a triangular spectrum, a raised-cosine envelope has a raised-cosine spectrum, and so on. Second, the spectral phase is quadratic, just as the temporal phase was quadratic.

Now we would like to pass this pulse through a hypothetical dispersive filter, *H(ω)*, defined as

$$H(\omega) = \exp\left(-j\frac{1}{2\sigma}\omega^2\right) \tag{4.22}$$

where σ is the group delay slope or dispersion rate, to see the effect of pure linear dispersion on this linearly chirped pulse. The new spectrum is simply

$$P_2(\omega) = P_1(\omega)\cdot H(\omega) = \sqrt{\frac{2\pi}{k}} A\left(\frac{\omega}{k}\right) \exp\left(-j\frac{1}{2}\left(\frac{1}{k}+\frac{1}{\sigma}\right)\omega^2\right) \tag{4.23}$$

which has the same bandwidth and shape as $P_1(\omega)$. Since (4.23) has essentially the same form as (4.11), only in the frequency domain instead of the time domain, we can use the same stationary phase method to calculate the Inverse Fourier Transform. Following this procedure yields

$$\begin{aligned} p_2(t) &= \sqrt{\frac{\sigma}{k+\sigma}} A\left(\frac{\sigma}{k+\sigma}t\right) \exp\left(-j\frac{k}{2}\left(\frac{\sigma}{k+\sigma}\right)t^2\right) \\ &= \sqrt{\frac{1}{M}} A\left(\frac{t}{M}\right) \exp\left(-j\frac{1}{2}\frac{k}{M}t^2\right) \end{aligned} \tag{4.24}$$

with the scale factor, *M*, defined as

$$M = \frac{k+\sigma}{\sigma}. \tag{4.25}$$

We can quickly observe the two primary effects of the dispersion mentioned at the beginning of this chapter. The duration of the temporal envelope has been scaled by the factor M. Also, the amplitude is scaled by the square root of M. Since energy is the square of the amplitude, energy is conserved. The same amount of energy is redistributed over a different period of time, but maintaining the same *envelope shape*. Thus we have imaged the *envelope* of the pulse. If k and σ have same sign ($M>1$) the envelope will be stretched. If they have opposite sign, the envelope will either be compressed ($0<M<1$) or reversed in time ($M<0$). A scale factor of zero would ideally produce a transform limited pulse.

4.5.3 Compensating for Non-Linear Dispersion

Non-linear chirp or dispersion is analogous to aberration in the optical imaging [58]. Unlike optics, in temporal imaging we have the unique ability to manipulate the time lens (chirp rate) and/or the dispersion to compensate aberration in the other. We can handle non-linear chirps and dispersions by applying the above methods in a piecewise linear fashion. Let's assume we have a known non-linear dispersion (non-constant dispersion rate $\sigma(\omega)$) and a particular envelope to time-stretch. We need to select the appropriate chirped carrier to stretch our envelope without distortion. To do so, we can break up the frequency dependant dispersion rate, $\sigma(\omega)$, into N subsections which can each be approximated by a slope, σ_n. Then find each subsection's required chirp rate, k_n, by setting the stretch factor

$$\frac{\sigma_n}{k_n + \sigma_n}. \tag{4.26}$$

to the desired value. If the same stretch factor is chosen for each subsection, then the envelope will be stretched with minimal distortion.

4.5.4 Qualitative Evaluation of Dispersion and Chirped Pulses

Following such intensive mathematics, a visual aid may be helpful. The following series of figures illustrates the results of various permutations of dispersion rate and chirp rate. A rainbow of color is used to depict the many frequencies of the chirped pulse, in analogy to the different wavelengths (frequencies) of visible light. Also, it should be pointed out that a rectangular pulse is not a good candidate for temporal imaging because it violates the assumptions of the PSP analysis above, but it provides for easy visualization.

Figure 4.14 shows dispersion free propagation of an impulse and Figure 4.16 similarly for a chirped pulse. Obviously these pulses are undisturbed. Figure 4.15 shows what happens when dispersion is introduced – we see the familiar pulse broadening effect from optical communications. Figure 4.17 illustrates chirped pulse stretching. The dispersion acts to exaggerate and enhance the chirp of the pulse. Figure 4.18 shows pulse compression where the dispersion acts in opposition to the original chirp, realigning the frequency components into a more narrow time window.

Figure 4.16

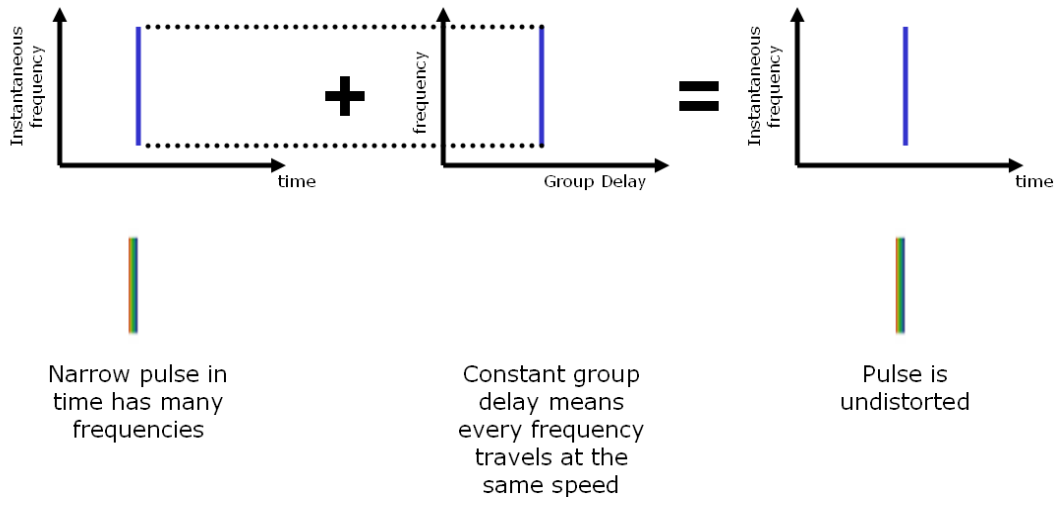

Figure 4.14 Impulse propagation without dispersion

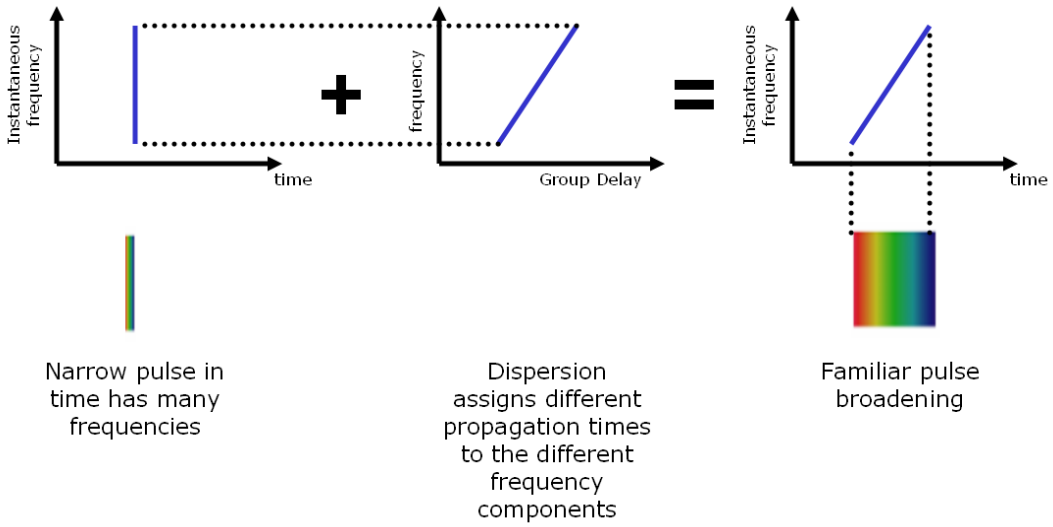

Figure 4.15 Impulse propagation with Dispersion

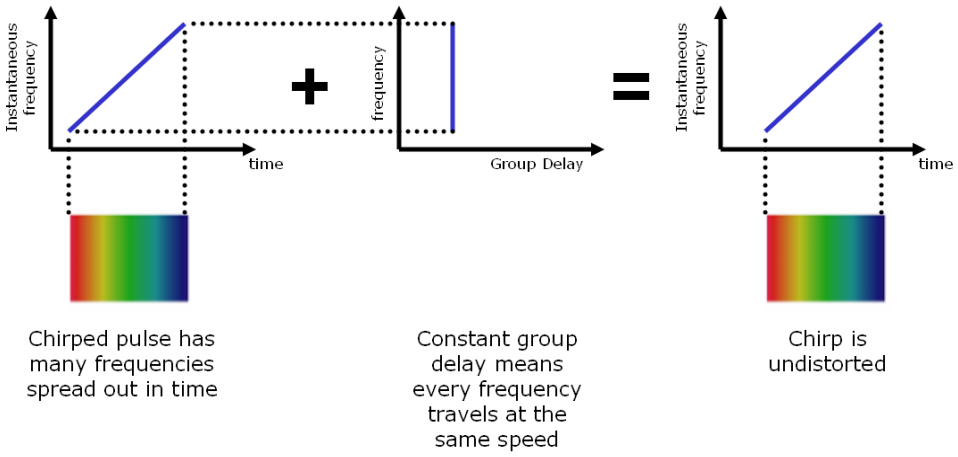

Figure 4.16 Chirp propagation without dispersion

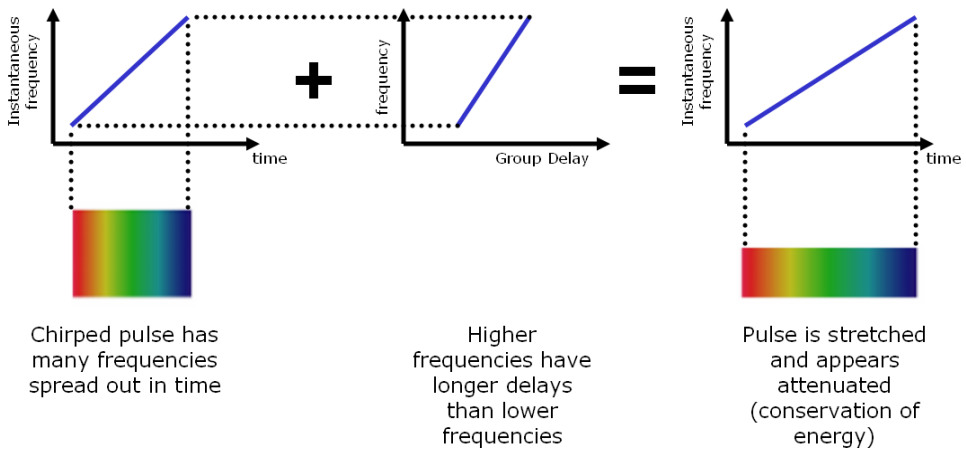

Figure 4.17 Pulse stretching

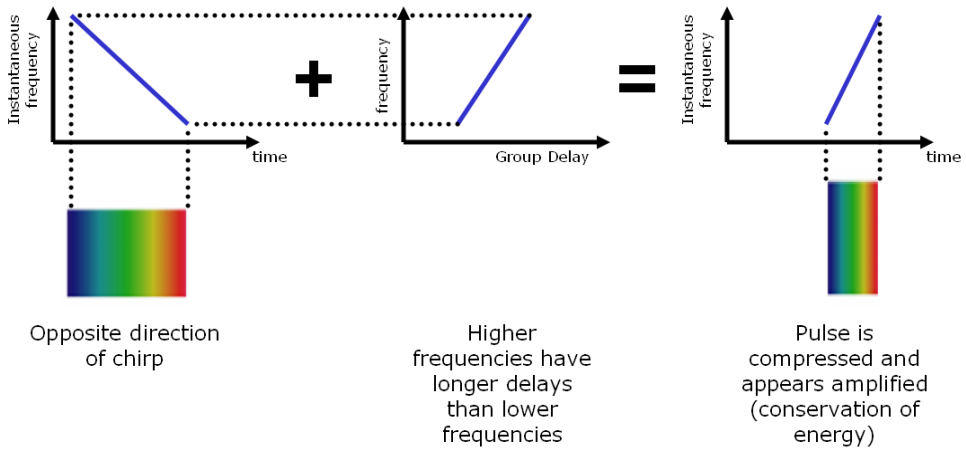

Figure 4.18 Pulse compression

In addition to recognizing the cases we expect to find, it is important to identify sources of false confirmation of these cases. Since the DA is both a traveling wave structure and contains dozens of resonators, ringing at high frequency is a distinct possibility. This could produce a false-positive stretch as in Figure 4.19. If the DA roll-off at high frequency is fast enough, it could simply truncate a pulse giving the appearance of compression. Luckily, these most likely false-positive results are mutually exclusive. The DA cannot both ring at high frequency and over attenuate high frequencies. Thus, if a single DA, without modification, can both stretch and

compress pulses with the same frequency components then we may conclude that temporal imaging is in fact occurring and not some other process.

Another way to aid confirmation is to observe the Fourier transform of the pulses, as was calculated in section 4.5.1. There are 2 ways to do this. The first would be to Nyquist sample the pulse and perform the actual transform on the data. This is not an option as we do not presently have the capability to Nyquist sample the pulse. The other possibility is to observe a chain of pulses on a spectrum analyzer. However, the repetition of the pulses causes the spectrum to become a series of discrete peaks, rather than the proper continuum. These peaks ideally trace the outline of the continuous spectrum, but low power levels and wide peak spacing makes this measurement impractical. Temporal measurements will have to suffice.

4.6 Design and Measurement

In order to demonstrate temporal imaging on a single silicon chip, I designed a dispersion enhanced DA and an analog chirp generation circuit. In this section, I will discuss the design and operation of each.

Figure 4.19 Potential false confirmation scenarios.

4.6.1 Chirp Generator

The chirp generation circuit can produce chirped pulse in the frequency range from 11-16GHz. The frequency range selected does not correspond with UWB or any other major communication band, but was selected because a simple wide tuning VCO could be readily designed in that range. More sophisticated chirp generation could be employed in a different frequency range, but the focus of this work was the dispersive DA so a low-risk approach to chirp generation was preferred.

The chirp generator of Figure 4.20 is a fairly simple circuit. At its core is a cross-coupled voltage controlled oscillator (VCO) with a low quality factor, *Q*. This condition achieves two goals: very wide tuning range (11-16GHz) and fast tuning response. This wide tuning range was achieved with single turn inductors and many-fingered MOSCAP varactors. The signal from the VCO then passes though a mixer to create the desired envelope shape, in this case a raised-cosine. A digital clock signal is included to override the envelope signal and quench the mixer output. Finally, the

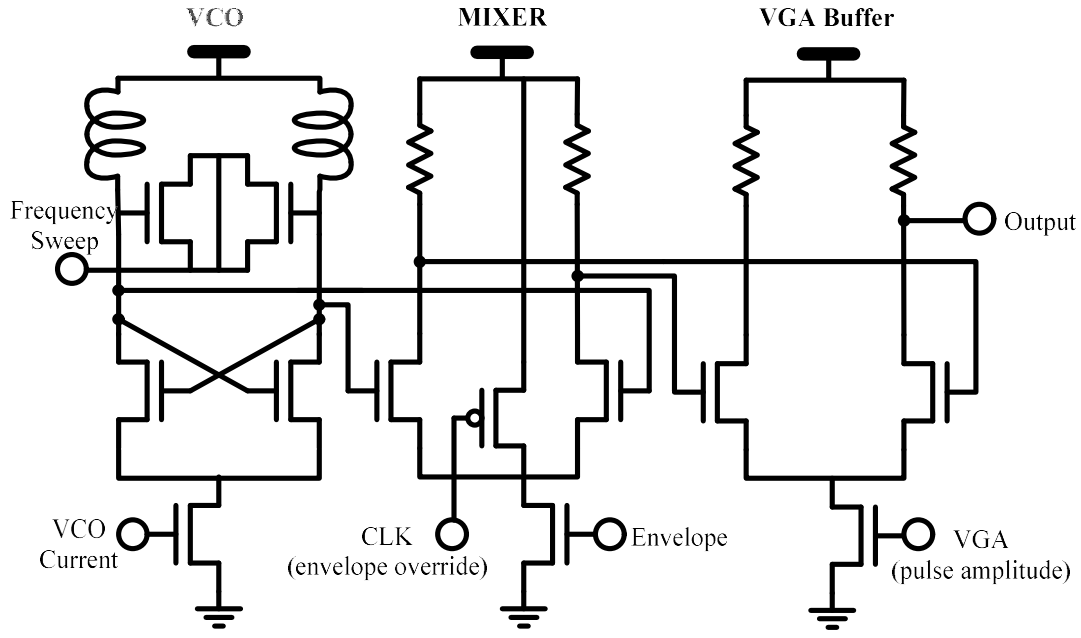

Figure 4.20 Chirp generator, consisting of a VCO, mixer, and VGA buffer.

chirped pulse emerging from the mixer is buffered by a variable gain amplifier (VGA) to allow control of the pulse amplitude.

The VCO control voltage is directly driven by an off-chip voltage source. Ideally, an arbitrary waveform generator could be used to compensate for the non-ideality of the DA dispersion as described in section 4.5.3. Unfortunately, the only source available capable of sweeping the control voltage on the nanosecond time scale required was a sinusoidal RF generator. The linear portion of the sinusoid proved adequate for this demonstration.

A similar sinusoidal RF generator, synchronized to the first, was used to drive the mixer. This creates the raised-cosine envelope. In addition, a digitally clocked dump-switch was used to extinguish the mixer output after generating a single pulse. This prevents the next pulse from occurring on the next period of the sinusoidal envelope signal, allowing further separation in time of successive chirped pulses.

4.6.2 Dispersion Enhanced Distributed Amplifier

The dispersion-enhanced DA in Figure 4.21 is constructed along the guidelines derived in section 4.4 for a cutoff frequency of 16GHz. The parallel tank consists of a spiral inductor and an inter-digitated metal capacitor with resonant frequency at 18.5GHz. The series tank is reduced to just a capacitor, implemented by a common-source MOSFET with 10x6μm fingers. The drain of this transistor is connected to the source of a common-gate transistor by a straight-line inductor, providing modest peaking to compensate roll-off near cutoff. Four section DAs are used, and cascaded drain-line to gate-line three times for a total of 12 sections.

Bias current for the transistors is delivered by a 1.2V supply through a large 1.5nH spiral inductor. This large inductor is in parallel with a 50Ω resistor which

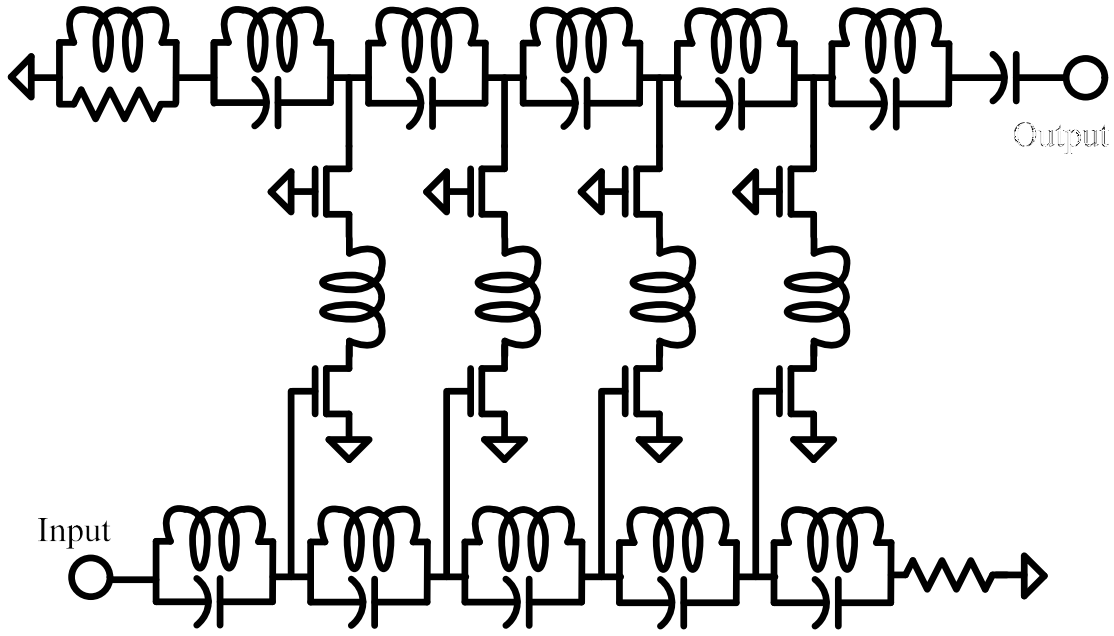

Figure 4.21 Dispersion-enhanced DA. Three of these amplifiers were cascaded to achieve almost 1ns group delay difference over a 4GHz bandwidth.

provides proper termination in the range where gain and dispersion are required. The transistors are biased at a linear operating point to minimize non-linear amplitude distortion.

The gain and dispersion curve of this DA, measured on a vector network analyzer, is shown in Figure 4.22. The peak group delay occurs at 15GHz, with a steep and reasonably linear slope extending back to 11GHz. Given the 2.7mm total length of the DA, the dispersion for this circuit is 83ns/GHz/m, higher than any of the other dispersion sources reviewed in section 4.3.1. The gain peaking however, was not sufficient to completely smooth out the roll-off near cutoff and we see 20dB of attenuation at the peak group delay. We will thus expect to see some distortion of the high frequency portions of the imaged pulses and will not be able to harness the entire 4GHz of dispersive bandwidth.

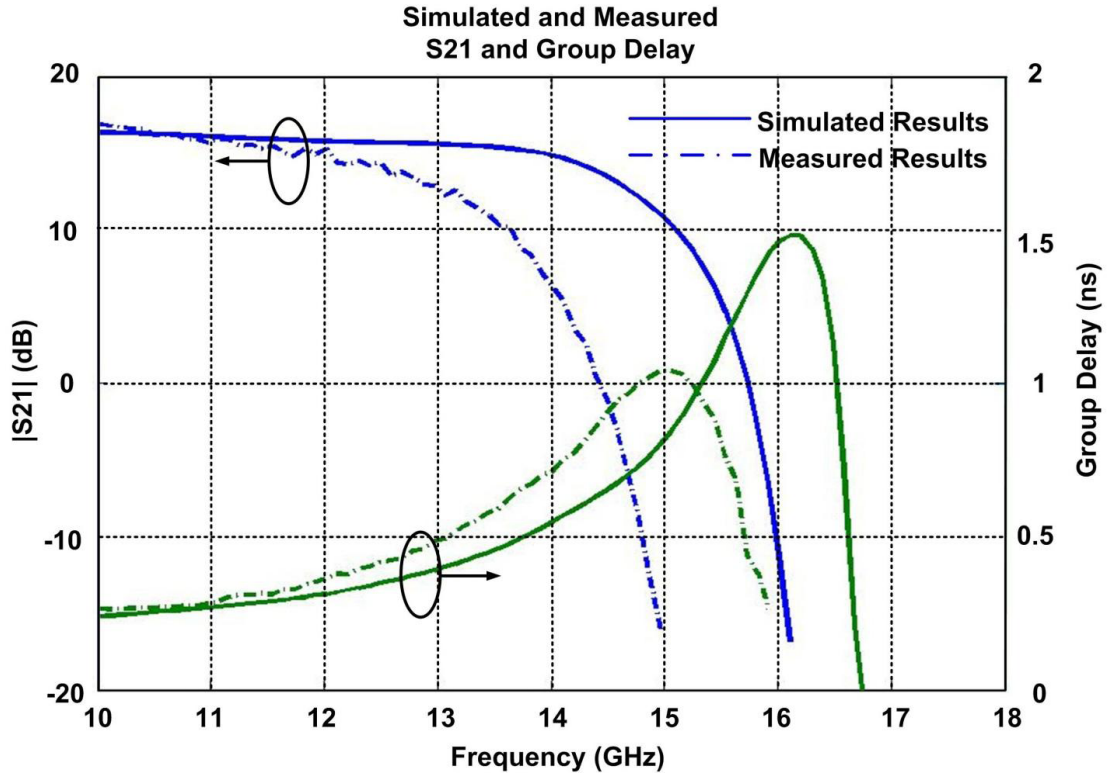

Figure 4.22 Measured gain and dispersion of the dispersion-enhanced DA.

Figure 4.23 shows the die photo of the entire temporal imager as fabricated in 130nm CMOS. The chirp generator and 3 DAs are clearly visible. The GSG pads on the left side are for the digital clock input and the GSG pads on the right are where the pulse exits the chip. DC biases, frequency sweep, and envelope shaping signals are input from the pads along the top and bottom.

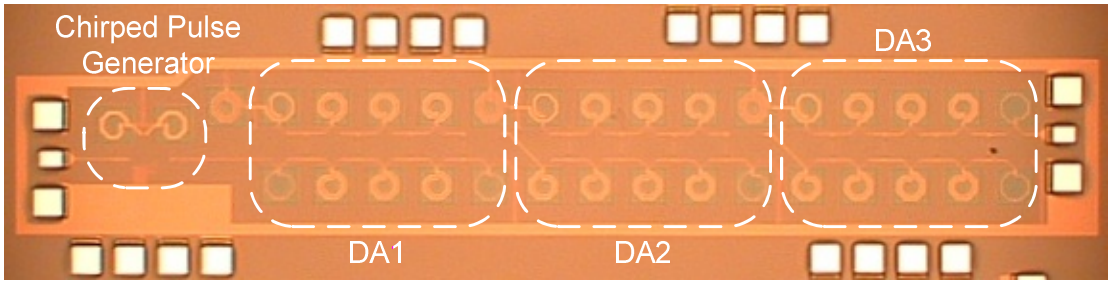

Figure 4.23 Die Photo of complete temporal imaging circuit.

4.6.3 Temporal Imaging Demonstration

Four total cases were experimentally evaluated – stretching and compression both on single pulses and on '101' bit patterns. Since only approximately 0.9ns of group delay difference is produced by the DA, this is the most we can change the duration of a pulse or pattern by. Measurements were performed by observing pulse shapes on a 20GHz digital storage oscilloscope (DSO). A real-time oscilloscope would be preferable, to capture the high frequency carrier signals, but one was not available. Instead, the oscilloscope was triggered with the period of the *envelope* and several pulses were overlaid like an eye-diagram such that the envelope shape was accurately detected but carrier information was lost.

To demonstrate stretching and compression on individual pulses, we sent identical pulses with no chirp, positive chirp, and negative chirp through the dispersive DA. Figure 4.24(a) shows the original un-chirped 1ns pulses. The un-chirped carrier frequency is approximately 13GHz in the middle of the dispersion curve. Figure 4.24(b) shows the positive and negatively chirped pulses on the left and right, respectively. The positive chirp sweeps from approximately 11-15GHz while the negative chirp sweeps from 15-11GHz. The stretched pulse on the left is extended to approximately 1.75ns, with a slight reduction in amplitude. Its envelope is also distorted by the gain shape of the DA, with later components (higher frequencies) showing additional attenuation. The compressed pulse on the right of Figure 4.24(b) has duration of 0.5ns and is also distorted by the DA gain. In this case, the higher, attenuated frequencies occur earlier making the pulse asymmetric around the peak.

The original '101' series of bits was generated at 1Gbps on a 13GHz carrier, so that the total pattern has duration of 3ns as in Figure 4.25. Positively chirping this whole pattern, from 11GHz to 15GHz over the entire 3ns, produces the stretched pattern in Figure 4.25(b). The entire pattern is elongated to approximately 3.75ns. Reversing the

(a)

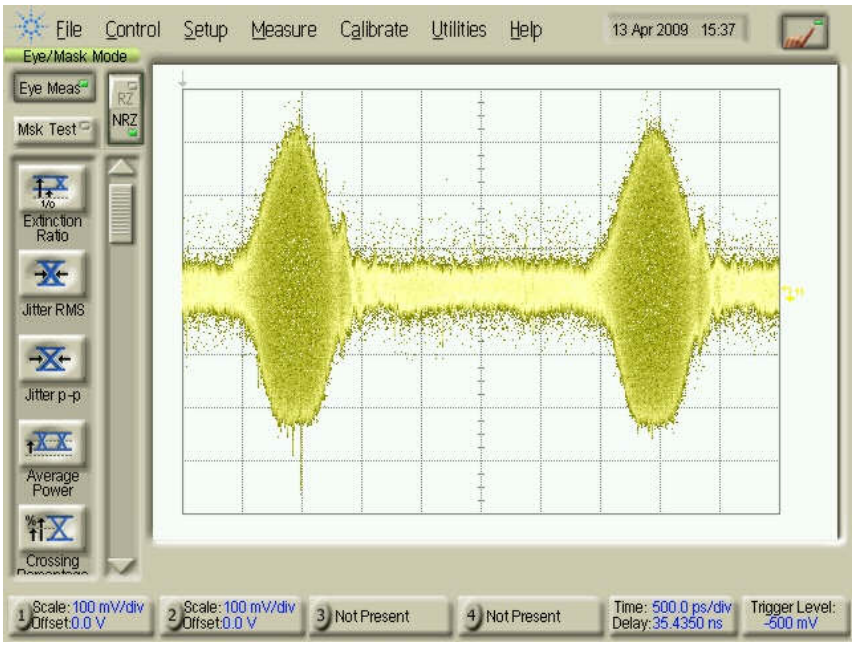

(b)

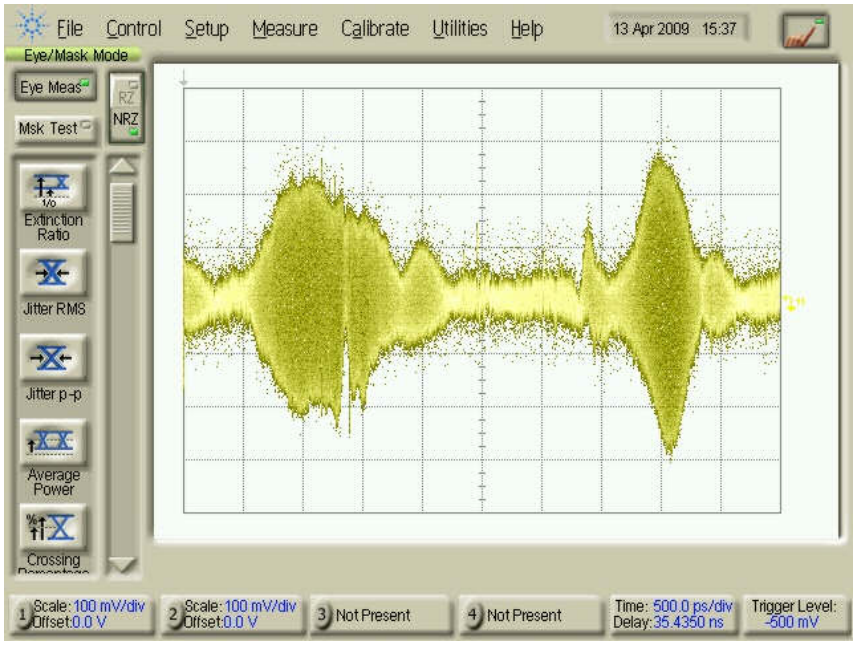

Figure 4.24 (a) Un-chirped pulses and (b) chirped pulses after dispersion. The left pulse receives positive chirp and is stretched while the right pulse receives negative chirp and is compressed.

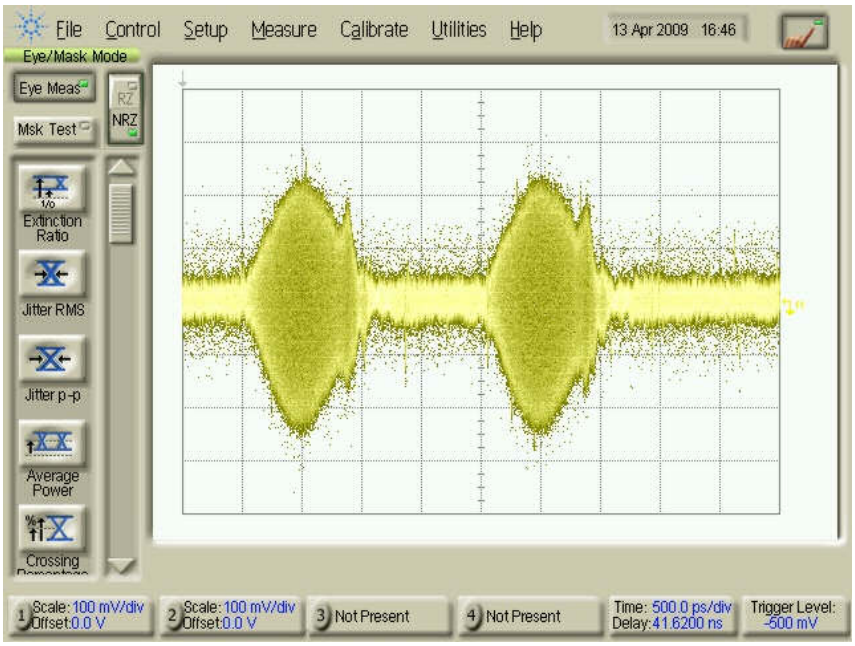

(a)

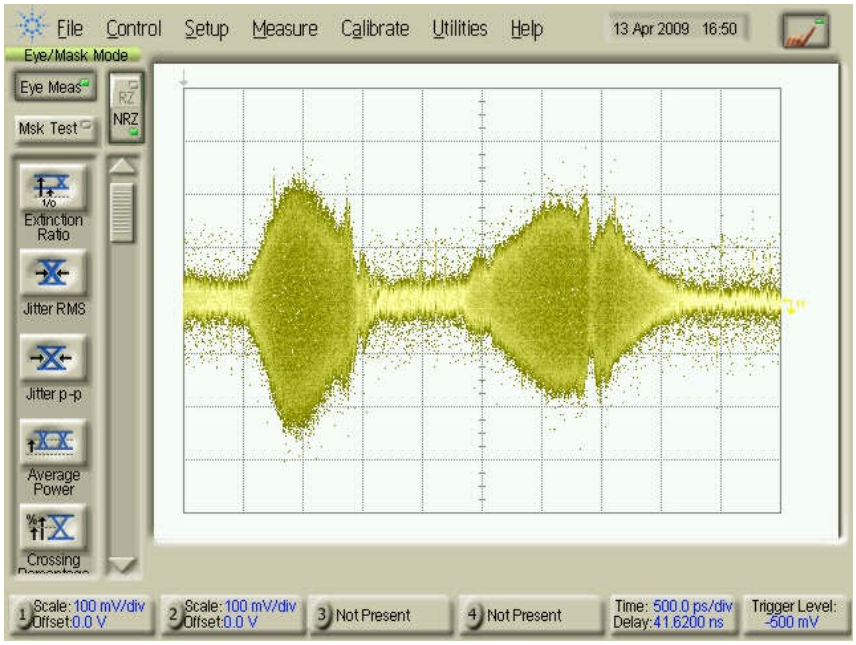

(b)

Figure 4.25 (a) Original '101' bit pattern, (b) stretched, and (c) compressed.

Figure 4.25 (continued)

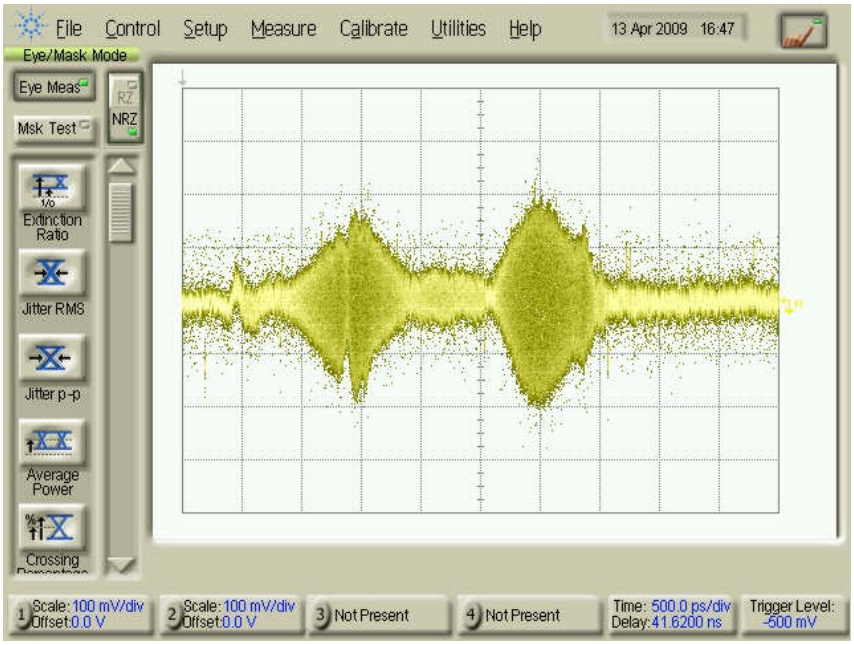

(c)

chirp in Figure 4.25(c) reduces the pattern length to 2.5ns. These stretching and compressing values are the same as for the individual pulses.

4.7 Conclusion

The experimental measurements of section 4.6 show that the dispersion-enhanced DA presented in this chapter, implemented on a single CMOS chip, has a highly dispersive character which can be used to stretch and compress chirped (time-lensed) pulses. The measured dispersion is 83ns/GHz/m, stronger than any other reported dispersive system in the microwave range and approximately a billion times stronger than optical fiber. The actual imaging system shown here is only a modest demonstration, showing 75% stretching and 50% compression, but it is the first system of its kind on a single chip.

This successful proof of concept is encouraging for further development of the dispersion enhanced distributed amplifier. Lower loss processes, compact layout, custom resonator (as opposed to design kit supplied), and advanced DA bandwidth extension techniques can all contribute to even higher dispersion values for this circuit. Also more advanced chirp generation techniques, both analog and digital, will be needed to make a temporal imaging system with real world applications such as UWB/impulse radio/ranging.

Perhaps the ultimate limitation of using the dispersion-enhanced distributed amplifier, or indeed any active circuit, to achieve large dispersion is dynamic range. Since the distributed amplifier has gain and a sharp frequency cutoff, many amplifiers can be cascaded to achieve large dispersion while maintaining large bandwidth. Each such amplifier contributes some noise which will accumulate for long cascades. Such noise can be masked by making the gain large, but there is of course a limitation on the largest signals an active circuit can handle while maintaining linearity. It will be a challenge for future work to explore the trade space of loss, gain, noise, and linearity to achieve the maximum usable dispersion.

APPENDIX

A.1 Common-Gate Amplifier Noise

The noise figure of the common-gate amplifier, Figure 1.6(a), may be derived by referring each noise source to the output and dividing by the contribution from the input source impedance. The noise sources in this circuit include the input source resistance, the transistor channel noise, and the load resistance noise. The voltage gain from the gate to drain of the transistor is approximately $-g_m R_L$ and so the output noise from the source is

$$kTR_s\left(g_m R_L\right)^2 . \tag{A.27}$$

The transistor channel squared current noise is well known as

$$4kT\gamma g_m \tag{4.28}$$

which gives a squared voltage at the output of

$$kT\gamma g_m {R_L}^2 \tag{4.29}$$

with the notably missing factor of 4 due to current division with the input source. The squared voltage noise from the load is already present at the output as

$$4kTR_L . \tag{4.30}$$

Adding these uncorrected sources yields a total output noise

$$v_{n,out}^2 = kTR_s\left(g_m R_L\right)^2 + kT\gamma g_m {R_L}^2 + 4kTR_L \tag{4.31}$$

The fundamental definition of noise figure is the total noise at the circuit output, divided by the fraction cause by the input source resistance. Thus, we divide (4.31) by (A.27) giving

$$F_{CG} = 1 + \frac{\gamma}{g_m R_s} + \frac{4}{{g_m}^2 R_s R_L} . \tag{4.32}$$

Applying the matching condition R_s=1/g_m and following the assumptions of (1.4) we finally arrive at the same expression in (1.5).

A.2 Shunt Feedback Amplifier Noise

Setting up similar conditions for the shunt feedback amplifier of Figure 1.7, the gain is assumed the same so that the contribution of the source resistance to the output is the as in (A.27). Assuming the feedback resistor, R_F, is large compared to R_L and R_s, the squared noise current from R_F is

$$\frac{4kT}{R_F}. \tag{4.33}$$

driving the input only, the terminal of that resistors noise generator is assumed to see low impedance approximately ground. From the matching condition at the input, this generator develops a square voltage noise of

$$\frac{kTR_s^2}{R_F} \tag{4.34}$$

which sees the voltage gain of the amplifier and thus contributes to the output as

$$\frac{kTR_s^2\left(g_mR_L\right)^2}{R_F}. \tag{4.35}$$

Applying the matching condition yet again, this time noting that

$$R_F = R_s\left(g_mR_L\right), \tag{4.36}$$

then (4.35) becomes

$$kTR_sg_mR_L. \tag{4.37}$$

The FET and load resistor contributions are similar to the common-gate case, but this time the FET source is grounded and the factor of 4 absent in (4.30) remains such that the total squared noise voltage at the output is

$$v_{n,out}^2 = kTR_s\left(g_m R_L\right)^2 + kTR_s g_m R_L + 4kT\gamma g_m R_L^{\ 2} + 4kTR_L \tag{4.38}$$

and thus the noise figure is

$$F_{FB} = 1 + \frac{1}{g_m R_L} + \frac{4\gamma}{g_m R_s} + \frac{4}{g_m^{\ 2} R_s R_L}. \tag{4.39}$$

Again using (1.4) and the definition of f_T this reduces to

$$F_{FB} = 1 + \frac{1}{2}\left(\frac{BW}{f_T}\right) + 6\gamma\left(\frac{BW}{f_T}\right) + 3\left(\frac{BW}{f_T}\right)^2. \tag{4.40}$$

A.3 Distributed Amplifier Noise

Referring to Figure 1.9, we can quickly approximate the noise figure of a distributed amplifier with N equal sized transistors, each with transconductance g_m. Since there are N individual FETs, the noise from the source times the amplifier gain is

$$kTR_s\left(Ng_m R_L\right)^2. \tag{4.41}$$

The noise from the input line termination resistor, at the right hand side of Figure 1.9, is amplified by all N transistors, but since the path length to the output through each is different, they will add *uncorrelated* at the output so that the contribution is only

$$kTR_s\left(Ng_m R_L\right). \tag{4.42}$$

The squared current noise from each FET is the same as in (4.28), but loses a factor of 4 due to being split equally between the left hand termination and the right hand output load, and each is uncorrelated such that the total contribution at the output is

$$kT\gamma g_m N R_L^{\ 2}. \tag{4.43}$$

Finally, the left hand termination and load each contribute equal noise, assuming lossless propagation, for a combined noise of

$$8kTR_L. \tag{4.44}$$

Similar to the previous two sections, we now sum all noise contributors at the output

$$v_{n,out}^2 = kTR_s\left(Ng_mR_L\right)^2 + kTR_s\left(Ng_mR_L\right) + kT\gamma g_m N{R_L}^2 + 8kTR_L \tag{4.45}$$

normalize

$$F_{DA} = 1 + \frac{1}{Ng_mR_L} + \frac{\gamma}{Ng_m} + \frac{8}{\left(Ng_m\right)^2 R_L} \tag{4.46}$$

and substitute

$$F_{DA} = 1 + \frac{1}{N} + \frac{4\gamma}{N}\left(\frac{BW}{f_T}\right) + \frac{2}{N^2}\left(\frac{BW}{f_T}\right)^2. \tag{4.47}$$

REFERENCES

[1] T. Lee, The Design of CMOS Radio Frequency Integrated Circuits, Cambridge University Press, 2003.

[2] G. R. Aiello and G. D. Rogerson, "Ultra-wideband wireless systems", Microwave Magazine, IEEE , vol. 4, issue 2, pp. 36-47, June 2003.

[3] E. Hamidi, M. Mohammad-Taheri, and G. Moradi, "Improvements in the Noise Theory of the MMIC Distributed Amplifiers," *IEEE Trans. on Microwave Theory and Tech.*, vol. 56, no. 8, Aug. 2008.

[4] K. Moez and M. I. Elmasry, "A Low-Noise CMOS Distributed Amplifier for Ultra-Wide-Band Applications," *IEEE Trans. on Circuits and Systems II*, vol. 55, no. 2, pp. 126-130, Feb. 2008.

[5] D. E. Meharry and W. Kong, "Reduction of Noise in Wideband Distributed Amplifiers" in *IEEE Int. Microwave Sym.*, pp. 2099-2103, Jun. 2007.

[6] Y. Wang and A. Hajimiri, "A Compact Low-Noise Weighted Distributed Amplifier in CMOS," in *IEEE ISSCC Dig. Tech. Papers*, San Francisco, CA, 8-12 Feb. 2009.

[7] E. L. Ginzton, W. R. Hewlett, J. H. Jasberg, and J. D. Noe, "Distributed amplification," *Proc. IRE*, pp. 956–969, Aug. 1948.

[8] J. A. Archer, F. A. Petz, and H. P. Weidlich, "GaAs FET Distributed Amplifier," Electronic Letters, vol. 17, p. 433, 1981.

[9] Y. Ayasli, J. L. Vorhaus, R. Mozzi, and L. Reynolds, "Monolithic GaAs Travelling-wave Amplifier," vol. 17, pp. 12-13, 1981.

[10] B. Ballweber, R. Gupta, and D. J. Allstot, "Fully-integrated CMOS RF amplifiers," in *IEEE ISSCC Dig. Tech Papers*, pp. 72–73, 1999.

[11] International Technology Roadmap for Semiconductors, 2007, see http://public.itrs.net/

[12] J. Kim, J. Plouchart, N. Zamdmer et al., "A 12dBm 320GHz GBW distributed amplifier in a 0.12μm SOI CMOS," in *IEEE ISSCC Dig. Tech. Papers*, pp. 478-479, Feb. 2004.

[13] J. Chien and L. Lu, " 40Gb/s High-Gain Distributed Amplifiers with Cascaded Gain Stages in 0.18μm CMOS," in *IEEE ISSCC Dig. Tech. Papers*, San Francisco, CA, Feb. 2007.

[14] A. Arbabian and A. M. Niknejad, "A Broadband Distributed Amplifier with Internal Feedback Providing 660GHz GBW in 90nm CMOS," in *IEEE ISSCC Dig. Tech. Papers*, San Francisco, CA, Feb. 2008.

[15] J. Mitola, III, "Cognitive radio for flexible mobile multimedia communications", in *Proc. IEEE Mobile Multimedia Commun. Conf. (MoMuC)*, New York, Nov. 1999.

[16] A. A. Abidi, "The Path to the Software-Defined Radio Receiver," *IEEE J. of Solid-State Circuits,* vol. 42, no. 5, May 2007.

[17] F. Bruccoleri, E. A. M. Klumperink, and B. Nauta, "Wide-Band CMOS Low-Noise Amplifier Exploiting Thermal Noise Canceling," *IEEE J. of Solid State Circuits*, vol. 39, no. 2, Feb. 2004.

[18] S. Chehrazi, A. Mirzaei, R. Bagheri and A. A. Abidi, "A 6.5 GHz Wideband CMOS Low Noise Amplifier for Multi-Band Use," in *Proc. of IEEE Custom Integrated Circuits Conf.*, San Jose, CA, Sep. 2005.

[19] C. M. Soer, E. A. M. Klumperink, Z. Ru, F. E. van Vliet, B. Nauta, " A 0.2-to-2.0GHz 65nm CMOS Receiver Without LNA Achieving >11dBm IIP3 and <6.5 dB NF," in *IEEE ISSCC Dig. Tech. Papers*, San Francisco, CA, 8-12 Feb. 2009.

[20] S.C. Blaakmeer, E. Klumperink, D. M. W. Leenaerts, and B. Nauta, "The Blixer, a Wideband Balun-LNA-I/Q-Mixer Topology," *IEEE J. of Solid State Circuits*, vol. 43, no. 12, Dec. 2008.

[21] M. K. Chirala, X. Guan, and Cam Nguyen, "Integrated Multilayered On-Chip Inductors for Compact CMOS RFICs and Their Use in a Miniature Distributed Low-Noise-Amplifier Design for Ultra-Wideband Applications," *IEEE Trans. on Microwave Theory and Techniques,* vol. 56, no. 8, Aug. 2008.

[22] C. S. Aitchison, "Intrinsic Noise Figure of the MESFET Distributed Amplifier," *IEEE Microwave Theory and Tech*., vol. MTT-33, pp. 460-466, Jun. 1985.

[23] J. D. Kraus, Radio Astronomy, McGraw-Hill, 1966.

[24] J. Michel, J.F. Liu, D.H. Ahn, D. Sparacin, C.Y. Hong, W. Giziewicz, M. Beals, L.C. Kimerling, A. Kopa, A.B. Apsel, M.S. Rasras, D.M. Gill, S.S. Patel, K.Y. Tu, Y.K. Chen, A.E. White, A. Pomerene, D. Carothers, and M.J. Grove, "Advances in Fully CMOS Integrated Photonic Devices," Invited Paper, in *Proc. of SPIE Photonics West*, vol. 6477, Jan. 2007.

[25] X. Y. Wang and A. B. Apsel, "Pulse Coupled Oscillator Synchronization for Low Power UWB Wireless Transceivers," in *IEEE Midwest Sym. on Circuits and Systems*, pp. 1524 – 1527, 5-8 Aug. 2007.

[26] E. L. Ginzton, W. R. Hewlett, J. H. Jasberg, and J. D. Noe, "Distributed amplification," *Proc. IRE*, pp. 956–969, Aug. 1948.

[27] B. Ballweber, R. Gupta, and D. J. Allstot, "Fully-integrated CMOS RF amplifiers," in *IEEE ISSCC Dig. Tech Papers*, pp. 72–73, 1999.

[28] M. K. Chirala, X. Guan, and C. Nguyen, "Integrated Multilayered On-Chip Inductors for Compact CMOS RFICs and Their Use in a Miniature Distributed

Low-Noise-Amplifier Design for Ultra-Wideband Applications," *IEEE Microwave Theory and Tech.*, vol. MTT-56, pp. 1783-1789, Aug. 2008.

[29] A. Arbabian and A. M. Niknejad, "A Broadband Distributed Amplifier with Internal Feedback Providing 660GHz GBW in 90nm CMOS," in *IEEE ISSCC Dig. Tech Papers*, pp. 196–197, 2008.

[30] P. Heydari, "Design and Analysis of a Performance-Optimized CMOS UWB Distributed LNA," *IEEE J. of Solid State Circuits*, vol. 42, no. 9, pp. 1892-1905, Sep. 2007.

[31] Y. J. Wang and A. Hajimiri, "A Compact Low-Noise Weighted Distributed Amplifier in CMOS," in *IEEE ISSCC Dig. Tech. Papers*, pp. 220-221, 2009.

[32] T. T. Y. Wong, *Fundamentals of Distributed Amplification*, Artech House, Boston, 1993.

[33] C. S. Aitchison, "Intrinsic Noise Figure of the MESFET Distributed Amplifier," *IEEE Microwave Theory and Tech*., vol. MTT-33, pp. 460-466, Jun. 1985.

[34] A. Arbabian and A. M. Niknejad, "A Tapered Cascaded Multi-stage Distributed Amplifier with 370GHz GBW in 90nm CMOS," in *IEEE RFIC Symposium Dig. Papers*, pp. 57–60, 2008.

[35] J. C. Chien and L. H. Lu, "40-Gb/s High-Gain Distributed Amplifiers With Cascaded Gain Stages in 0.18-μm CMOS," *IEEE J. of Solid State Circuits*, vol. 42, no. 12, pp. 2715-2725, Dec. 2007.

[36] C. S. Aitchison, "Intrinsic Noise Figure of the MESFET Distributed Amplifier," *IEEE Microwave Theory and Tech.,* vol. MTT-33, pp. 460-466, Jun. 1985.

[37] P. K. Ikalainen, "Low-Noise Distributed Amplifier with Active Load," *IEEE Microwave and Guided Wave Letters,* vol. 6, pp. 7-9, Jan. 1996.

[38] Y. Cheng, M. J. Deen, and C. H. Chen, "MOSFET Modeling for RF IC Design," *IEEE Trans. On Elec. Devices*, vol. 52, pp. 1286-1303, Jul. 2005.

[39] K. Moez and M. I. Elmasry, "A Low-Noise CMOS Distributed Amplifier for Ultra-Wide-Band Applications," *IEEE Trans. on Circuits and Systems II*, vol. 55, no. 2, pp. 126-130, Feb. 2008.

[40] D. E. Meharry and W. Kong, "Reduction of Noise in Wideband Distributed Amplifiers" in *IEEE Int. Microwave Sym.*, pp. 2099-2103, Jun. 2007.

[41] R. H. Frater and D. R. Williams, "An Active 'Cold' Noise Source," *IEEE Trans. on Microwave Theory and Tech.,* vol. MTT-29, no. 4, pp. 344-347, Apr. 1981.

[42] B. H. Kilner, "Space-Time Duality and the Theory of Temporal Imaging," *IEEE J. of Quantum Electronics,* vol. 30, no. 8, Aug. 1994.

[43] J. D. Schwartz, J. Azana, and D. V. Plant, "A Fully Electronic System for the Time Magnification of Ultra-Wideband Signals," *IEEE Trans. on Microwave Theory and Tech.*, vol. 55, no. 2, Feb. 2007.

[44] F. Coppinger, A. S. Bhushan, and B. Jalali, "Photonic Time Stretch and its Application to Analog-to-Digital Conversion," *IEEE Trans. on Microwave Theory and Tech.,* vol. 47, no. 7, Jul. 1999.

[45] J. L. Blanton, "Cued Medium-PRF Air-to-Air Radar Using Stretch Range Compression" in *Proc. of IEEE Nation Radar Conference*, Ann Arbor, MI, 13-16 May 1996.

[46] J. D. McKinney, D. Peroulis, and A. M. Weiner, "Dispersion Limitations of Ultra-Wideband Wireless Links and Their Compensations Via Photonically Enabled Arbitrary Waveform Generation" *IEEE Trans. on Microwave Theory and Tech.,* vol. 56, no. 3. Mar, 2008.

[47] J. Mitola, III, "Cognitive radio for flexible mobile multimedia communications", in *Proc. IEEE Mobile Multimedia Commun. Conf. (MoMuC)*, New York, Nov. 1999.

[48] A. A. Abidi, "The Path to the Software-Defined Radio Receiver," *IEEE J. of Solid-State Circuits,* vol. 42, no. 5, May 2007.

[49] W. J. Caputi, Jr., "Stretch: A Time-Transformation Technique," *IEEE Trans. on Aerospace and Electronic Systems*, Mar. 1971.

[50] A. S. Bhushan, P. V. Kelkar, B. Jalali, O. Boyraz, M. Islam, "130Gsample/s Photonic Analog to Digital Converter," at *IEEE Int. Topical Meeting on Microwave Photonics*, 7-9 Jan. 2002.

[51] D. M. Pozar, *Microwave Engineering,* 3rd edition, 2005.

[52] C. Pollack and M. Lipson, *Integrated Photonics*, 2003.

[53] G. C. Valley, G. A. Sefler, J. Chou, and B. Jalali, "Continuous Time Realization of Time-Stretch ADC," at *IEEE Int. Topical Meeting on Microwave Photonics*, 22-27 May 2005.

[54] S. W. Y. Mung and W. S. Chan, "Novel Active Quasi-Circulator with Phase Compensation Technique," *IEEE Microwave and Wireless Components Letters,* vol. 18, no. 12, Dec. 2008.

[55] M. A. Jack, P. M. Grant, and J. H. Collins, "The Theory, Design, and Applications of Surface Acoustic Wave Fourier-Transform Processors," *Proc. of the IEEE*, vol. 68, no. 4, Apr. 1980.

[56] G. L. Villanueva, P. Hartogh, and L. M. Reindl, "A Digital Dispersive Matching Network in Chirp Transform Spectrometers," *IEEE Trans. on Microwave Theory and Tech.*, vol. 54, no. 4, Apr. 2006.

[57] K. Moez and M. Elmasry, "A New Loss Compensation Technique for CMOS Distributed Amplifiers," *IEEE Trans. on Circuits and Systems II,* vol. 56, no. 3, Mar. 2009.

[58] C. V. Bennet and B. H. Kolner, "Aberrations in Temporal Imaging," *IEEE J. of Quantum Electronics,* vol. 37, no. 1, Jan. 2001.

[59] M. A. G. Laso, T. Lopetegi, M. J. Erro, D. Benito, M. J. Garde, M. A. Muriel, M. Sorolla, M. Guglielmi, "Real-Time Spectrum Analysis in Microstrip Technology," *IEEE Trans. Microwave Theory and Tech*., vol. 51, no. 3, pp. 705-717, Mar. 2003.

[60] Samer Abielmona, Shulabh Gupta, Christophe Caloz, "Compressive Receiver Using a CRLH-Based Dispersive Delay Line for Analog Signal Processing" IEEE Trans.Microw. Theory Tech., vol. 57, no. 11, pp. 2617-2626, Nov. 2009.

[61] "Single Mode Dispersion," www.corning.com/opticalfiber.

[62] N. Bleistein and R. Handelsman, Asymptotic Expansions of Integrals, Dover, New York, 1975.